

The Influence of Endothelial Panx3/Bcl6 Interactions on Blood Pressure Regulation

Abigail Grace Wolpe

Sandwich, Massachusetts

Bachelor of Arts, Smith College, 2015

A Dissertation presented to the Graduate Faculty of the University of Virginia

in Candidacy for the Degree of Doctor of Philosophy

Department of Cell Biology

University of Virginia, May 2023

Abstract

Complex regulatory mechanisms control the abundance and localization of transcription factors due to the broad impact their transcriptional activity can have on cell, tissue and organism physiology. The activity of transcriptional repressor B cell lymphoma 6 (Bcl6), which has been well studied for its roles in immune cell specification and lymphonogenesis, is largely regulated by its targeted degradation. However, outside of tumor-related angiogenesis, a role for Bcl6 in the vasculature has yet to be defined. Bcl6 has been reported to interact with Pannexin 3 (Panx3) channels in other cell types, though the product of this interaction has yet to be described. Here, we report that Bcl6 interacts with Golgi-localized Panx3 in endothelial cells, and demonstrate that Panx3-Bcl6 interactions modulate the endothelial transcriptional landscape by shielding the transcriptional repressor from targeted degradation. We show genetic deletion of Panx3 from endothelium induced spontaneous hypertension, aligning with human data, but did not result in any tested channelopathies. When Panx3 was deleted from endothelium, there was significantly decreased Bcl6 protein, but not *Bcl6* mRNA, hinting Panx3 may stabilize Bcl6. In the absence of Panx3, Bcl6-protected oxidative genes Nox4 and NFκB were significantly increased. The result was H₂O₂-specific oxidative damage throughout the vasculature and circulation. Pharmacological inhibition of the Panx3-Bcl6 interaction recapitulated an increase in Nox4 and blood pressure. These data elucidate a channel-independent function of Panx3 wherein interactions with perinuclear Bcl6 can dictate transcriptional repression and protect against oxidative stress. Our next study aimed to determine if Panx3-Bcl6 interactions would alter communication between endothelium and inflammatory cells. Unexpectedly, we found that loss of endothelial Panx3 was associated with a significant increase in the expression of IL4 receptors on endothelium and concomitant increase in IL4 in bone marrow. Because activation of IL4 has been reported to drive expression of Bcl6 in other cell types, we considered the potential for vascular-immune signaling to contribute to blood pressure regulation. To this end, genetic deletion of endothelial Panx3 was associated with a significantly increased population of circulating basophils, a primary source of IL4. Preliminary studies involving expansion or depletion of the circulating basophil population were

shown to reduce or augment systemic blood pressure, respectively. These data elucidate a novel Golgi-localized oxidative signaling pathway in endothelium with a potential basophil-derived negative feedback loop for the purpose of homeostatic blood pressure control.

Table of Contents

| | |
|--|----|
| <i>Abstract</i> | 2 |
| <i>List of Figures</i> | 6 |
| <i>Dedication</i> | 8 |
| <i>Chapter 1: General Introduction</i> | 11 |
| 1.1: Blood pressure regulation and vascular oxidative stress | 11 |
| 1.2: Pannexin channels | 14 |
| 1.3: Transcriptional Repressor Bcl6..... | 20 |
| <i>Chapter 2: Materials and Methods</i> | 24 |
| <i>Chapter 3: Endothelial Panx3 – BCL6 Interactions Protect Against Oxidative Stress</i> | 36 |
| 3.1: Abstract..... | 36 |
| 3.2: Introduction | 38 |
| 3.3: Results | 40 |
| 3.4: Discussion | 71 |
| <i>Chapter 4: A potential role for basophils in blood pressure regulation</i> | 78 |
| 4.1: Abstract..... | 78 |
| 4.2: Introduction | 80 |
| 4.3: Results | 84 |
| 4.4: Discussion | 96 |
| <i>Chapter 5: General Discussion and Future Directions</i> | 99 |

| | |
|---|-------------------|
| 5.1: Elucidate the impact of endothelial Panx3/Bcl6 interactions on angiogenesis | 101 |
| 5.2: Evaluate the use of our novel BCLiP peptide as a therapeutic Bcl6 inhibitor..... | 103 |
| 5.3: Uncover the mechanism by which the subcellular distribution of Panx3 is regulated by shear stress | 105 |
| 5.4: Effects of hydrogen peroxide exposure on SK/IK channels..... | 108 |
| <i>Chapter 7: References</i> | <i>113</i> |

List of Figures

Figure 1: Hypertensive humans exhibit significantly reduced expression of Panx3. 46

Figure 2: Murine vascular Panx3 is attenuated by hypertension. 47

Figure 3: Endogenous Panx3 expression in vascular endothelium. 48

Figure 4: Endothelial Panx3 localizes to the Golgi Apparatus of intact endothelium, unlike Panx1. 50

Figure 5: Subcellular distribution of endothelial Panx3 is regulated by shear stress. 51

Figure 6: Generation of an inducible, endothelial cell-specific Panx3 knockout mouse (EC Panx3^{ΔA}). 53

Figure 7: EC Panx3^{ΔA} mice exhibit unremarkable gross anatomy, blood lipids, heart and kidney functions, and splenic B cell development. 54

Figure 8: Genetic deletion of endothelial Panx3 impairs peripheral resistance and induces spontaneous hypertension. 55

Figure 9: Renal infiltration by macrophages and T_{reg} cells is unchanged by genetic deletion of endothelial Panx3. 57

Figure 10: Channel-independent association of Panx3 and transcriptional repressor Bcl6 in intact endothelium. 58

Figure 11: EC Panx3^{ΔA} mice exhibit increased endothelial TRPV4 activity. 60

Figure 12: Genetic deletion of endothelial Panx3 does not alter Golgi pH but does ablate interaction of Panx3/Bcl6 in intact endothelium. 61

Figure 13: Genetic deletion of endothelial Panx3 is associated with decreased Bcl6 protein, increased NFκB activity and the specific upregulation of Nox4, which can be predicted by evidence of Bcl6 transcriptional activity. 62

Figure 14: Endothelial Panx3 protects against H₂O₂-induced oxidative stress and prevents endothelial-mediated vascular dysfunction in resistance arteries. 63

Figure 15: Evidence of Oxidative Stress in the aortic vascular wall in EC Panx3^{ΔA} mice. 65

Figure 16: Assessment of other potential sources of oxidative stress following genetic deletion of endothelial Panx3. 66

Figure 17: Inhibition of the Panx3/BCL6 interaction via BCLiP peptide phenocopies genetic deletion of endothelial Panx3. 69

| | |
|---|------------|
| <i>Figure 18: Schematic of endothelial Panx3/Bcl6 interactions.....</i> | <i>70</i> |
| <i>Figure 19: Splenic B Lymphocytes are unchanged by endothelial Panx3 expression.....</i> | <i>87</i> |
| <i>Figure 20: Endothelial Panx3 expression has no effect on cytokine production by splenic T cells.</i> | <i>88</i> |
| <i>Figure 21: Loss of endothelial Panx3 results in increased myeloid IL4 and increased IL4 receptor expression.....</i> | <i>89</i> |
| <i>Figure 22: Circulating basophils are uniquely increased following Panx3 deletion from endothelium.....</i> | <i>90</i> |
| <i>Figure 23: Circulating levels of IL33 are unaffected by endothelial Panx3 expression.</i> | <i>91</i> |
| <i>Figure 24: Scavenging hydrogen peroxide in vivo may attenuate the circulating basophil population.</i> | <i>92</i> |
| <i>Figure 25: In vivo basophil expansion relieves blood pressure elevation following loss of endothelial Panx3.</i> | <i>93</i> |
| <i>Figure 26: Stimulation of basophilic IL4 release with IPSE in EC Panx3^{Δ/Δ} mice.</i> | <i>94</i> |
| <i>Figure 27: Basophil depletion significantly elevates systemic blood pressure.</i> | <i>95</i> |
| <i>Figure 28: Perinatal genetic deletion of endothelial Panx3 may impair angiogenesis.</i> | <i>111</i> |
| <i>Figure 29: Endothelial Panx3 expression may promote venous specification through modulation of repression by Bcl6.....</i> | <i>112</i> |

Dedication

This document is the culmination of a lot of time, and a lot of growth. There are so many people who have helped, pushed, or inspired me along the way.

First, to Jake, my husband, my closest friend, my confidante, my idea bouncer, and my very favorite collaborator: I am so lucky to have gone through this graduate program with you by my side. It turns out you were right, dating another scientist is the best. Thank you for believing in me when I needed it most. Thank you for the countless hours we've spent talking through frustrations of failed experiments. Thank you for the times I needed your guidance and also for the times I just needed you to listen while I talk myself through the problem. Thank you for your partnership, your commiseration, your brilliance and your patience. I can't wait to take our next steps together and see what our life becomes.

For my family, my mom, Christine, my dad, Paul, and for my sisters and their families, Hillary, Guido and G3, and Danielle, Matt, Chloe and Taylor: Thank you for your support and the packages you sent with beautiful artwork and delicious treats. Thank you for your patience as I figured out how to balance adult responsibilities along with family connections. To Hillary especially, thank you for always making sure I stayed close despite living too far away. Thank you for letting me complain and helping me remember the challenge at hand is just an opportunity to overcome. Without your support and generosity, I'm not sure I would be here today.

I also have an overabundance of gratitude for the folks I've met here in the program. I've been so fortunate to have a plethora of mentors who have sculpted the scientist I have become. To Brant, thank you for taking a chance on me when I was a late stage student needing to start a new dissertation project. I am so grateful for your mentorship. You met me where I was and helped me see the path towards growing into a better scientist and a better thinker. You showed me how to approach research with humility and humor. You taught me to see the story through the numbers and how to effectively share my story with others. I

appreciate every time you could direct my next step, though I might be most grateful for the time the best you could offer was simply “Did you think it was supposed to be easy?”

To Miranda and Scott, I am so grateful for the time I had to learn from you before you moved on. Thank you for showing me the kind of scientist I aspire to be: rigorous, meticulous, creative, and resilient with limitless generosity and an intact sense of humor. Thank you also for sharing your protocols, I treat them like gospel and they have never let me down. Miranda, you taught me almost every marketable skill I have, and you also taught me how to organize my experiments without sacrificing my life. You calmed my fears, and wiped some tears. Your generosity with your time, knowledge and friendship has left a lasting impact on the person I am today. Thank you. Scott, you were the first person to treat me like a professional, even before I saw myself that way. Thank you for the time you spent teaching me, and for the thoughtful edits on the drafts of my grant proposals. Your revisions and edits changed the way I think about academic writing.

To Melissa, thank you for keeping me sane with our morning chats. Your friendship is such an instrumental part of my support system, especially because you are always willing to call me out. Thank you for the countless hours we've spent troubleshooting my experiments and yours. Thank you for the months you've spent working on experiments for my paper. Thank you for always striving for excellence, seeing you running circles around me in lab has always been a good source of motivation. To Angie, thank you for everything you do to keep the lab running and for always being willing to share dog stories. To Luke, thank you for your willingness to brainstorm and your thoughtful contributions to my experiments and my writing. Thank you also for teaching me statistics, especially because I probably should have known some of that already. To Zuzanna, Wyatt and Skylar, thank you for your fresh takes and positive attitude. Your time in the lab has only just begun, but I can't wait to see what you make of it. To the previous members of the lab, to Claire, Steven, Leon, Isola, Alex and Yang, thank you for your friendship, for introducing me to new fields of research and the good times we shared over too many cups of coffee. To Lauren Biwer, who

graduated from the lab just a few years before I joined, thank you for connecting me to your professional network and for sharing so much wisdom. You are everything I could have hoped for in a science-crush. Thank you also to the friends I've made along the way. To Xavier and Laura, our monthly family dinners have been such a wonderful source of support and connection. Thank you for your friendship and for everything we've shared together. To Faith, thank you for commiserating and for always being able to pick up right where we left off, no matter how long it had been since we last connected.

Chapter 1: General Introduction

1.1: Blood pressure regulation and vascular oxidative stress

Blood pressure is an important indicator of health, as hypertension is the foremost risk factor for global mortality.¹ Operating as a closed loop system, blood pressure is a dynamic parameter that is influenced by the cardiac output and vascular resistance, with each determinant governed by its own intricate regulatory mechanisms. Vascular resistance is the force exerted by the vasculature in opposition to blood flow. In Poiseuille's Law, vascular resistance is calculated by accounting for vessel length and blood viscosity over the vessel radius raised to the fourth power, which highlights how alterations of vessel diameter, in the form of constriction and dilation, is a major determinant of vascular resistance. Changes in vessel diameter are a function of smooth muscle contractility, though the endothelium is more than a passive barrier to the circulation. At the interface with the circulation, the endothelium is a flat, largely continuous monolayer which participates in heterocellular communication, regulating constriction and relaxation of smooth muscle through the release of vasoactive factors. While all arteries are composed of endothelium and overlaying smooth muscle, their unique characteristics determine how they contribute to total peripheral resistance.

Resistance arteries are anatomically and functionally distinct from larger conduit arteries. Characterized by their small diameter ($<200\mu\text{m}$) and the presence of only 1-2 layers of smooth muscle cells (SMC), resistance arteries have been reported to generate 80-90% of vascular resistance in skeletal muscle tissue.² In comparison, large conduit arteries such as the aorta or carotid are characterized by a thick vascular wall composed of several layers of smooth muscle and elastin-rich extracellular matrix to contend with and dampen pulsatile flow. The myoendothelial junction (MEJ) is another anatomical feature unique to resistance arteries. First described in 1957, MEJs are endothelial protrusions through fenestrations in the extracellular matrix. These protrusions directly connect endothelial cells (EC) and SMC, thereby promoting heterocellular communication.³ To this end, the MEJ is a signaling microenvironment, enriched with cation

channels and gap junctions to facilitate EC-SMC signaling through membrane hyperpolarization and the sharing of cytoplasmic contents, respectively. However, in large arteries, the internal elastic lamina (IEL) forms a continuous matrix which physically separates SMC from EC. In order to dilate large arteries, endothelium signaling to SMC is mediated in large part by nitric oxide (NO) signaling.

Capable of diffusing through cell membranes and matrices, NO is a reactive nitrogen species and potent vasodilatory signal. Endothelium generates NO mainly through the activation of endothelial nitric oxide synthase (eNOS) which catalyzes a reaction between L-arginine and oxygen to generate L-citrulline and NO.⁴ In SMC, NO directly binds soluble guanylate cyclase (sGC), inducing cyclic guanine monophosphate production (cGMP) and downstream relaxation of the smooth muscle cells. Following muscarinic activation, changes in intracellular calcium can drive eNOS interaction with calmodulin and activate NO generation. Alternatively, eNOS can be activated by phosphorylation at Ser1177 downstream of PKA or Akt activation, following a stimulus such as shear stress. The essential role for NO in regulating vascular hemodynamics became obvious from animal studies. Inhibition of eNOS activity via global genetic knockout⁵ or pharmacological inhibitors⁶ results in dramatic hypertension. Under normal conditions, eNOS exists as a homodimer. However, in pathological conditions such as aging or diabetes, eNOS can become physically uncoupled. Unregulated electron transport of uncoupled eNOS can favor the generation of superoxide (O_2^-) over nitric oxide and ultimately induce endothelial dysfunction.^{7,8} Furthermore, NO and superoxide can react to form peroxynitrite ($ONOO^-$), which reduces the bioavailability of NO and drives endothelial dysfunction in obesity and pulmonary hypertension.^{9,10}

Similar to reactive nitrogen species, reactive oxygen species (ROS) are naturally produced as a consequence of oxygen metabolism, and can often be neutralized by cellular antioxidant defenses. During periods of ROS overproduction and imbalance, ROS can damage nucleic acids, proteins and lipids indiscriminately. Transcriptional alterations can impact expression of antioxidant systems as well as oxidant generating systems. For instance, NF κ B activation can drive vascular NADPH Oxidase isoforms (Nox1, Nox2, Nox4,

Nox5) resulting in ROS overproduction and oxidative stress.¹¹⁻¹³ Endothelial cells are at a significantly greater risk for oxidative damage from ROS production because of their highly metabolic nature.¹⁴ In endothelium, activation of NFκB produces proinflammatory cytokines that have been shown to cause a significant increase in blood pressure,¹⁵ and can drive vascular oxidative stress.¹⁶⁻¹⁸ The pathological connection between vascular ROS and cardiovascular diseases has been well-documented. Indeed, many experimental models of hypertension rely on the generation of ROS to induce hypertensive phenotypes, including: angiotensin-II,¹⁹ aldosterone,^{20, 21} high-fat diet,^{22, 23} high salt diet,^{24, 25} and DOCA-salt.^{26, 27} Furthermore, hypertensive patients reproducibly exhibit increased oxidative stress and decreased antioxidant capacity as compared to normotensive participants.²⁸⁻³⁰ In spite of their causal connection, clinical trials specifically testing antihypertensive effects of antioxidative agents are relatively rare.^{29, 31-37} Antioxidant administration was shown to decrease blood pressure in hypertensive patients within a selection of randomized double-blind placebo-controlled studies.^{29, 32} However, other clinical studies suggest that antioxidants augment^{36, 37} or have no effect^{33, 34} on hypertension. Altogether, these clinical studies have been heavily criticized, citing choice of antioxidant agents, duration of treatment and lenient patient exclusion criteria as possible confounding variables.^{29, 38, 39} It is also possible antioxidant administration has been ineffective at controlling hypertension due to interference with nascent oxidative signaling.

While historically ROS have been perceived as health burdens due to their potential to damage cellular components, many in the field view ROS as another means of cellular signaling. Nox4 was recently reported to act as a *bona fide* oxygen sensor due to its unusually high binding affinity for O₂ (K_m 18%).⁴⁰ While Nox4 is generally considered to be constitutively active, careful analyses revealed that the rate of hydrogen peroxide (H₂O₂) generation by Nox4 is determined by tissue oxygenation.⁴⁰ Vascular tissue oxygenation can range from 4-14%,^{41, 42} which would result in more than 300% increase in Nox4 activity.⁴⁰ Taken together with reports that vascular Nox4 expression is driven under both hypoxic^{43, 44} and hyperoxic^{45, 46} conditions, this poses Nox4 as an important adaptation to oxidative stress with the ability to finely tune H₂O₂ production in response to cellular stimuli. Altogether, this highlights the importance of considering

the different sources of ROS and their mechanisms of action in understanding their impact on cellular physiology.

H₂O₂ can also directly impact arterial constriction and dilation. Its small nonpolar nature coupled with its ability to diffuse across membranes makes this specific ROS a key signaling molecule that can arise from endothelium.^{47, 48} H₂O₂ can be directly generated by Nox4, or through the dismutation of superoxide. Like NO, H₂O₂ can diffuse through membranes, though H₂O₂ has a much longer half-life which may permit long-range downstream effects. Endogenous H₂O₂ participates in the generation of myogenic tone,⁴⁹ a defining feature of small arteries in which smooth muscle cells constrict respond to sustained increased in intramural pressure. Along those lines, exposure to mild doses of H₂O₂ induces constriction of smooth muscle cells through activation of cyclooxygenase enzymes^{50, 51} and resultant activation of the smooth muscle thromboxane receptor.⁵² Paradoxically, supraphysiological doses of H₂O₂ induce a rapid and dramatic dilation of small arteries which involves NO generation and hyperpolarization of endothelium and smooth muscle through the activation of potassium channels.⁵² To this end, overexpression of Nox4 in endothelium has been reported to induce systemic hypotension.⁵³

1.2: Pannexin channels

The concept of cellular topology is central to research on large pore channel proteins like pannexins. A transmembrane channel fated for the plasma membrane is constructed in the endoplasmic reticulum (ER) and processed through the Golgi Apparatus, trafficking through the organelles in vesicles, before reaching its final destination. Upon translation, intracellular domains of the protein are delivered to and maintained in the cytoplasm; the 'extracellular' domains will be exposed to the lumens of the organelles and vesicles before emerging to the extracellular space when the protein is delivered to the plasma membrane. In an additional level of complexity, each of these compartments will have distinct electrochemical gradients; as such, a channel opening on the plasma membrane will trigger distinct downstream signaling events than the same channel opening on each organelle. To this end, the transient receptor potential vanilloid 1

(TRPV1) channels are best known for their roles as plasma membrane channels transducing sensation of heat and acidity in nociceptive neurons through influx of extracellular calcium ions;⁵⁴ however, in microglia, TRPV1 preferentially localizes to mitochondrial membranes, and its activation increases mitochondrial calcium content rather than cytoplasmic calcium, ultimately promoting cellular migration.⁵⁵ The topology and localization of a channel determines the functional consequence of the channel's activation.

The current study aims to elucidate how the transmembrane channel Pannexin 3 (Panx3) contributes to endothelial physiology and development. Due to a dearth of relevant literature, it was necessary to additionally assess many foundational channel properties of Panx3, including its subcellular distribution and oligomeric state. Thus, a multiscale approach enabled assessment of both (1) basic channel properties of endogenously expressed Panx3 and (2) organism-scale physiological effects of its conditional, inducible deletion from endothelium.

The pannexin family of glycoproteins consists of three isoforms (Panx1, 2, 3). Topologically similar to connexins, the vertebrate gap junction proteins, each pannexin monomer contains a four transmembrane domains, two extracellular loops, with the N-terminus, one loop and the C-terminus restricted to the cytoplasm.⁵⁶ The transmembrane channel is formed when six or more of the monomers oligomerize together. A gap junction is formed when the extracellular domains of two connexin oligomers expressed on the membrane of two adjacent cells bind, bringing the abutting membranes in close apposition. Opening a gap junction effectively connects the cytoplasmic contents of the neighboring cells, enabling the passage of second messengers, ions, and electrical impulses in an efficient mechanism of localized intercellular communication.

Because of these structural similarities, initial investigations hypothesized pannexin channels would form functional gap junctions,⁵⁷ like connexins. However, attempts to detect gap junction activity through dye

transfer or dual voltage clamp assays have largely failed to demonstrate Panx3-dependent intercellular communication.⁵⁷⁻⁵⁹ Glycosylation of the extracellular loops of Panx1 and Panx3, which promote their trafficking to the plasma membrane,⁵⁸⁻⁶⁰ would likely sterically hinder the close apposition of pannexins in a gap junction complex. To this end, gap junctional current associated with Panx1 was detected in xenopus oocyte pairs only following treatment with an extracellular deglycosylation enzyme,⁶¹ further indicating nascent glycosylation inhibits the formation of pannexin gap junctions. In contrast, pannexin-associated gap junctional current was reported in a single study led by Dr. Amal Kanti Bera in 2014 using HeLa cells stably expressing rat Panx3 or rat Panx1; though their attempts to reproduce their findings failed in a murine neuroblastoma line (N2A) as well as a rat adrenal medulla line (PC-12). Interestingly, assessments of glycosylation status revealed the majority of Panx1 is glycosylated in N2A and PC-12 cells, but not HeLa cells, and the lack of extracellular glycosylation may permit the formation of Panx1 gap junctions. Unfortunately, assessment of Panx3 glycosylation was not included in the study. It is also worth noting that the HeLa cells used in the Bera study endogenously express Panx1 as well as several connexin isoforms (Cx26, Cx31.1, Cx45).⁶² It is possible that transiently expressed Panx3 could form chimeric assemblies with novel channel properties, confounding interpretation of their results. To this end, another independent study failed to demonstrate pannexin gap junction activity in HeLa cells deficient for gap junctional intercellular communication, and noting Panx3 distribution to intracellular membranes as well as the plasma membrane in this condition.⁵⁹ This suggests that while the transcripts for endogenous Cx26, Cx31.1, Cx45 and Panx1 were unchanged by overexpression of Panx1 or Panx3,⁶² their expression may have contributed to junctional current generation. Altogether, a mounting body of evidence suggests pannexins operate as single membrane channels unable to function as gap junctions in most mammalian cells.

As channel proteins enable permeant diffusion across membranes, their localization is integral to their function. Panx1, the most-studied pannexin isoform, has consistently been localized to the plasma membrane where it has been reported to facilitate purinergic signaling.^{59, 63} Though various reports also note intracellular localization.^{59, 64} In contrast, Panx2 has largely been observed on intracellular membranes

(including endoplasmic reticulum and Golgi Apparatus, but excluded from endosomal system or mitochondria^{65, 66}), though some reports note additional minimal distribution to the plasma membrane.^{66, 67} However, the subcellular distribution of Panx3 appears to be more variable than for the other pannexin isoforms. Human embryonic kidney (HEK293T) cells overexpressing Panx3 exhibit a preference for its localization to intracellular membranes which is exaggerated in a glycosylation-resistant mutant (Panx3^{N71Q}), indicating that glycosylation of Panx3 likely promotes plasmalemmal distribution. In both transient and stable expression systems, Panx3 is most frequently reported at the plasma membrane,^{58, 59, 62, 68-71} though some reports note a preference for intracellular distribution^{59, 72-74} and others observe the protein at both locations.^{59, 60, 75-78} However, endogenously expressed Panx3 has been observed on intracellular membranes (in human epidermal samples,^{58, 79} including keratinocytes, sebaceous and eccrine glands, as well as the vascular wall;⁷⁹ in cultured MC3T3-E1 osteoblast cells⁶⁰). Exogenous expression systems have been reported to result in mislocalization and supraphysiologic abundance of the target protein,^{80, 81} which may contribute to this disparity. The distribution of Panx3 can also be perturbed through protein tagging. In normal rat kidney (NRK) cells, the presence of a green fluorescent protein (GFP) tag impairs trafficking of transiently expressed Panx3, resulting in its restriction to the endoplasmic reticulum while untagged Panx3 distributes to the plasma membrane. In the same study, Panx1 and Panx1-GFP both localize to the plasmalemmal membrane,⁵⁸ further demonstrating distinct regulation of Panx1 and Panx3 trafficking. Tagged fusion proteins have been reported to mislocalize other membrane bound proteins,⁸² including caveolins,⁸³ though the mechanism of why this phenomena occurs has yet to be described. Altogether, the localization of Panx3 appears to be easily perturbed, varying with post translational modifications, expression systems, protein tagging and cell type.

As a protein family, pannexins exhibit notable variability in their oligomeric status. Panx1 was originally reported as a hexamer via chemical crosslinking,⁸⁴ wherein protein lysates are treated with a homobifunctional compound that nonspecifically reacts with free amines, tethering proximal proteins and subunits together for analysis of macromolecular weight. However, recent work has reproducibly

demonstrated heptameric Panx1 assemblies using cryogenic electron microscopy to visualize the structures with up to 2.8Å resolution.^{70, 85-88} In contrast, crosslinking of Panx2 has revealed octameric structures,⁶⁷ indicating potential plasticity in the pannexin multimeric assemblies, though this has yet to be confirmed with more precise techniques. The oligomeric structure of Panx3 has yet to be described, though many assume Panx3 would adopt heptameric assemblies, like Panx1, due to their high degree of sequence similarity. However, if the Panx3 multimeric assemblies follow the pattern of Panx3 subcellular distribution, then the oligomeric status may vary based on cell type and expression system. While unconventional, channel assemblies with different stoichiometries has been reported for other large pore channels. Indeed, calcium homeostasis modulator (CALHM) channels have been reported to assemble decameric, undecameric and dodecameric oligomers.⁸⁹ Canonically, the size of multimeric assemblies is determined by energetically favorable oligomeric conformations. As such, multimeric plasticity indicates the energetic requirements to incorporate additional monomers is insignificant enough to permit variable assemblies.

While Panx3 is incapable of functioning as a gap junction, it may operate as a single membrane channel under permissive circumstances. Indeed, several in vitro studies report increased dye uptake,^{58, 59, 90} intracellular calcium flux,^{73, 91, 92} or ATP release^{68, 69, 78, 90, 91, 93} associated with Panx3 expression, using mechanical stimulation,⁶⁰ ATP^{69, 73, 91, 92} or membrane depolarization facilitated by exposure to high concentrations of potassium^{68, 72, 78, 91} to activate the channel. Some reports include treatment with carbenoxolone, a nonspecific Panx1 inhibitor, in attempts to demonstrate Panx3 channel function.^{78, 92, 93} Carbenoxolone is a nonspecific inhibitor, known to block Panx1 in addition to connexins,⁹⁴ voltage-gated calcium channels,⁹⁵ and N+/K+ ATPase.⁹⁶ It is possible that the carbenoxolone-sensitive current associated with Panx3 expression may actually represent the activity of an unnamed channel whose expression is altered with Panx3 induction. Furthermore, each of these studies relied on exogenous expression systems in cultured cells, which can augment protein abundance and localization.^{80, 81} However, an elegant study by Michalski and Kawate in 2016 brings into question whether Panx3 may exhibit a distinct response to

carbenoxolone. Here, electrophysiology was used to assess conductance through Panx1, Panx3 and novel chimeras. Panx3 expression alone was insufficient to generate channel conductance at baseline, unlike Panx1, which produced an outwardly rectifying, carbenoxolone-sensitive current. However, a Panx1 chimeric mutant, containing the residue sequence of the first extracellular loop of Panx3 instead of the nascent Panx1 loop, supported channel conductance at baseline, and intriguingly, exhibited a dramatic dose-dependent increase in conduction through the channel following exposure to carbenoxolone.⁹⁷ Carbenoxolone interacts with Trp74 in the first extracellular loop of Panx1 to allosterically inhibit channel activity.^{70,97} Despite a high degree of conservation in this domain, in Panx3, this residue is replaced with isoleucine,⁹⁷ a much smaller hydrophobic moiety which may not support the same interactions with small molecules such as carbenoxolone. To this end, there is a gap in the field's understanding of Panx3 channel functionality in the skin, bone and vasculature.

Because channel proteins can exhibit channel-independent functions, their biological functions are not limited to channel activation. The role of Connexin 50 (Cx50) in the developing eye lens is an elegant example of these noncanonical functions. Global Cx50 knockout mice exhibit developmental impairments in the eye^{98,99} due to reduced proliferation of lens epithelium,⁹⁹⁻¹⁰¹ indicating a role for Cx50 in cell cycle progression. However, attempts to recapitulate this phenotype through expression of dominant negative Cx50 orthologues were unsuccessful. The Cx50 mutant orthologues paradoxically promoted epithelial proliferation and differentiation, despite their inability to form functional gap junctions.¹⁰² Indeed, later work identified an alpha helix in the Cx50 C-tail which facilitates interactions between Cx50 and the E3 ubiquitin ligase Skp2.^{103,104} The product of this interaction promotes degradation of Skp2. In the absence of Cx50, Skp2 translocates into the nucleus and efficiently degrades cell cycle regulator p27, ultimately promoting premature quiescence of the lens epithelium and impairing eye development.¹⁰³ Similarly, Panx1 has been shown to inhibit progression of rhabdomyosarcoma, an aggressive pediatric soft tissue sarcoma. Exogenous Panx1 expression reduced cell proliferation and migration in embryonic and alveolar cell lines derived from rhabdomyosarcoma patients. The effect was maintained despite exposure to Panx1 channel

inhibitors, implicating a noncanonical role of the channel protein inhibiting tumorigenesis.¹⁰⁵ Empirical interactome analyses uncovered a novel interaction between Panx1 and the scaffolding protein AHNAK. Indeed, loss of AHNAK abrogated the protective effects of Panx1 expression on proliferation and migration of the patient derived cell lines, though a complete mechanism of this effect has yet to be described.¹⁰⁶ While the functional effects of channel proteins are often linked to their canonical pore gating behavior, channel-independent functions exerted through protein-protein interactions can also impact cellular physiology.

While it has yet to be described in the literature, it is possible that Panx3 also functions through protein-protein interactions instead of, or in addition to, its potential channel functionality. To this end, Panx3 has been implicated in interactions with RecQ-like protein 4 (RECQL4),¹⁰⁷ a component of nuclear and mitochondrial RecQ helicases, and transcriptional repressor B cell lymphoma 6 (Bcl6)¹⁰⁸ through affinity capture-mass spectroscopy. With Panx3 localizing to endoplasmic reticulum, Golgi Apparatus or the plasma membrane, one may assume that neither of these interactions would occur under normal physiological conditions due to spatial restrictions. However, while Bcl6 is mainly localized to the nucleus, though independent protein localization descriptions⁷² and validated protein interactions with Golgi-resident proteins^{109, 110} demonstrate the Golgi Apparatus as a secondary localization site for Bcl6. Panx3 and Bcl6 may prove to interact under physiological conditions, though the product of this interaction is not yet known.

1.3: Transcriptional Repressor Bcl6

Bcl6 is a transcription factor with well-documented roles in immune specification. As its name would suggest, Bcl6 is required for normal development of B lymphocytes and its dysregulation is associated with many forms of human lymphoma.¹¹¹⁻¹¹³ Transcriptional activity of Bcl6 is required to promote B cell survival against an onslaught of genotoxic stress during the somatic hypermutation and class switch recombination process from which a diverse repertoire of immunoglobulin genes arise.¹¹⁴⁻¹¹⁹ Because

repression by Bcl6 can promote proliferation and survival in spite of DNA damage and cellular stress, it is a gene frequently dysregulated in lymphomas and other cancers. Indeed, chromosomal rearrangements of the Bcl6 gene are observed in nearly half of the cases of Diffuse Large B Cell Lymphoma (DLBCL),¹²⁰ the most common form of non-Hodgkin's lymphomas. However, global knockout mice deficient for Bcl6 suffer from neonatal cardiovascular death due to myocarditis and pulmonary vasculitis by mechanisms that still are not understood,¹²¹ suggesting that Bcl6 may also exert important functions in the cardiovascular system and immune interactions with the vasculature.

Despite this, there has been little formal investigation of the impact on transcriptional repression by Bcl6 in the vasculature. During angiogenesis, Bcl6 is required to promote endothelial stalk phenotype through regulation of Notch related genes including Hes1, Hey1 and Dll4.¹²² Because Bcl6 activity has been shown to promote proliferation of other cell types,^{123, 124} Bcl6 activation may also promote the proliferation of stalk cells required for elongation and maturation of developing blood vessels. Similarly, Bcl6-associated-Zinc-Finger protein (BAZF), a close homolog of Bcl6 which has been shown to bind the same DNA elements^{125, 126} and even form heterodimers with Bcl6,¹²⁷ was identified in a screen of molecules that mediate VEGF signaling through downregulation of Notch signaling.¹²⁸ However, there is little known about the functions of endothelial Bcl6 outside of development. In vitro studies suggest Bcl6 can repress expression of adhesion molecules that facilitate leukocyte rolling and extravasation,¹²⁹ suggesting anti-inflammatory effects of endothelial Bcl6 activation. Endothelial Bcl6 promotes angiogenesis, though its role in mature vascular tissue and its potential to mediate immune interactions have yet to be described.

Structurally, Bcl6 contains an N-terminal BTB domain,^{114, 130} a central unstructured domain which includes several PEST sequences,¹³¹ and a C-terminal domain with six Kruppel-type Zinc Finger (ZF) domains to facilitate DNA binding.^{132, 133} The BTB domain, named after transcription factors originally identified in drosophila (Broad Complex, tramtrack, bric à brac), is a highly conserved region which facilitates protein-protein interactions. Through the BTB domain, Bcl6 interacts with corepressors including but not limited

to silencing mediator for retinoid or thyroid hormone receptor (SMRT),¹³⁴⁻¹³⁷ nuclear receptor corepressor 1 (N-CoR1),¹³⁶ BCL6 corepressor (BcoR),¹³⁸ and Histone deacetylase 1 (HDAC1).¹³⁵ Differential binding of corepressors can affect the transcriptional effects of Bcl6 activation. The PEST sequences confer an additional means of regulation, phosphorylation of the PEST sequences, particularly at Ser333 and Ser343, promote proteasomal degradation of Bcl6 to effectively inhibit its transcriptional activity.^{124, 139}

In addition to DNA binding, the ZF domain of Bcl6 can directly interact with the Rel homology domains of many NFκB subunits,¹⁴⁰ which has been suggested as one manner in which Bcl6 can repress NFκB. However, the mutually antagonistic relationship of Bcl6 and NFκB extends further than direct interaction. The primary mechanism of Bcl6 antagonism is transcriptional repression of NFκB promoter sites. Nearly half of the BCL-6 binding sites on the human genome are within 200 base pairs of an NFκB binding site.¹⁴¹ ChIP-Seq analysis of LPS-stimulated DLBCL cells demonstrate a switch from Bcl6 binding during quiescence to NFκB binding following activation.¹⁴¹ Similarly, Bcl6 inhibition of NFκB has been shown to regulate immune activation and tissue remodeling during atherosclerosis progression. Adoptive transfer of Bcl6 deficient bone marrow cells resulted in a dramatic increase in plaque coverage at the aortic root and along the length of the aorta in a cholesterol-mediated model of atherosclerosis.¹⁴² While this study identifies Bcl6 activation in inflammatory cells as an important regulator of atherosclerosis, it drives curiosity as to whether Bcl6 activation in smooth muscle and endothelial cells would also contribute to the progression of atherosclerosis and other cardiovascular diseases.

The current study seeks to understand the physiological impact of interactions between Panx3 channels and transcriptional repressor Bcl6 in the vasculature. Our data suggest that Panx3 and Bcl6 interact in endothelium, which shields Bcl6 from degradation and protects against vascular oxidative stress. Using a conditional, inducible genetic knockout of Panx3 from endothelium, we demonstrate increased Bcl6 degradation, loss of Bcl6 transcriptional activity and consequent upregulation of H₂O₂-producing Nox4. In

this condition, we observe a proinflammatory, pro-oxidant vascular environment which facilitates the development of spontaneous systemic hypertension through H₂O₂-induced impairments in endothelial-mediated vasodilation of resistance arteries. Special care has been taken to assess immune activation in the context of genetic deletion of endothelial Panx3, with largely unremarkable results. However, we uncover a potential basophil-endothelial signaling axis and accumulate evidence to suggest a role for basophil-derived IL4 to drive endothelial expression of Bcl6 and contribute to systemic blood pressure regulation.

Chapter 2: Materials and Methods

Human Samples

The collection and use of human adipose tissue biopsies were approved by the University of Virginia's Institutional Review Board for Health Sciences Research (Study 17194). Human volunteers with resistant hypertension (elevated blood pressure above 140 mmHg systolic) and healthy controls had an approximate 40 mm×20 mm biopsy of adipose tissue removed from the abdomen (no additional procedures were performed), which was immediately placed in ice-cold KREBS buffer and arterioles dissected manually within 30 minutes of removal. Samples collected for immunostaining were placed in 4% paraformaldehyde, and paraffin embedded. Samples collected for mRNA quantification were collected in Trizol and frozen at -80C. All subjects were males (N = 4). Hypertensive participants had an average age of 47.75±/4.23 years, with a body mass index of 36.75±/5.24.

Cell Culture

Human aortic endothelial cells (HAoEC, PromoCell, C-12271, Lot#431Z013.5) and human coronary artery endothelial cells (HCAEC, Cell Applications, 300-05a, Lot#3159) were cultured in Endothelial Cell Growth Medium 2 with the manufacturer's recommended supplements (PromoCell, C-39211). For golgi neutralization, HCAEC were plated on fibronectin-coated coverslips (Sigma, FC0105) and exposed to 2.5mM ammonium chloride (Sigma, A9434) or vehicle (deionized water) for 48 hours prior to fixation in 4% paraformaldehyde. For overexpression studies: HEK293T were cultured in DMEM, high glucose (Gibco, 11965-092) supplemented with 1mM sodium pyruvate, 1% Pen-Strep (Gibco, 15140122), 10% FBS (Avantor, 97068-085).

Animals

All mice were mixed sex, 10–20 weeks of age, on a C57Bl/6 genetic background, and were cared for under the provisions of the University of Virginia Animal Care and Use Committee and followed the National

Institutes of Health guidelines for the care and use of laboratory animals. C57Bl/6n mice were purchased from Taconic. The inducible, EC-specific Panx3 knockout mice (VECAdER^{T2+}/Panx3^{fl/fl}) were generated by crossing VECAdER^{T2+}/Panx3^{wt/wt} mice (a kind gift from Dr Ralf Adams, Max Plank Institute, Germany) with VECAdER^{T2-}/Panx3^{fl/fl} mice.¹⁴³ To conditionally induce Panx3 deletion in the vascular endothelium, VECAdER^{T2+}/Panx1^{fl/fl} (EC Panx3^{Δ/Δ}) and VECAdER^{T2-}/Panx1^{fl/fl} (Panx1^{fl/fl}) littermates received intraperitoneal (I.P.) injections of Tamoxifen (1 mg in 0.1 ml peanut oil) at six weeks of age for 10 consecutive days. All animal experiments were performed at least 14 days from the final injection with tamoxifen. The global Panx3 knockout mice were generated by crossing B6.Cg-Edil3^{Tg(Sox2-cre)1Amc/J}/Panx3^{wt/wt} mice (Jackson, #008454) with B6.Cg-Edil3^{Tg(Sox2-cre)1Amc/J}/Panx3^{fl/fl} mice.¹⁴³ All experiments were performed on a minimum of three mice. For all assessments of blood, blood was collected via terminal cardiac puncture using a syringe fitted with 25G needle, coated with EGTA to prevent clotting. To assess plasma renin levels, ~100uL of whole blood was collected via tail vein into gold microtainers two hours into the dark/active time period. Following centrifugation, renin concentration was assessed in isolated plasma using a Mouse Renin 1 ELISA (Ray BioTech, ELM-Renin1-1). To assess circulating hydrogen peroxide concentration, plasma was isolated from whole blood and passed through deproteinization columns within 30 minutes of collection (Abcam, ab93349). Deproteinized plasma was processed using the Hydrogen Peroxide Assay Kit (Abcam, ab102500). Cardiac MRI data was collected from anesthetized mice using a black blood sequence following imaging in the 7T ClinScan MRI. For catalase dosing, pegylated-catalase (40,000U/kg) were injected retro-orbitally in alternating eyes for five days. Assessment of IL33 was determined from blood plasma using commercial ELISA kit (Thermo Fisher Scientific) as per manufacturer's instructions. Plasma was isolated from whole blood by centrifugation at 5000xg for 10 minutes at 4C in gold microtainers (BD, 365967). Cytokine concentrations in the plasma lysate were normalized to total protein content measured by BCA Assay (Thermo Fisher Scientific).

Western blotting

Cell and tissue lysates were generated in RIPA (50mM Tris-HCL, 150mM NaCl, 5mM EDTA, 1% deoxycholate, 1% Triton-X100) in PBS and pH adjusted to 7.4) supplemented with protease inhibitor cocktail (Sigma). Lysates were rocked at 4°C for 30-60 min to solubilize proteins, sonicated briefly, and centrifuged for 15 min at 12,000 rpm to pellet cell debris. Protein concentration was determined using the BCA method (Pierce). 30µg of total protein was loaded into each sample well. For crosslinking studies, mesenteric vascular and aortic lysates were made in non-amine lysis buffer (137mM NaCl, 5.4mM KCl, 0.34mM Na₂HPO₄, 0.35mM KH₂PO₄, 0.8mM MgSO₄, 2.7mM CaCl₂, 1mM NaF, 250mM sucrose, 20mM Hepes, 10% glycerol). 100 µg of mesenteric vascular and aortic protein was incubated with 0.5 or 2.5mM bis-sulfosuccinimidyl-suberate (BS³) at room temperature prior to inactivation with Tris HCl pH 7.5. Samples were subjected to SDS gel electrophoresis using 8% Bis-Tris gels (Invitrogen) and transferred to PVDF (when blotting for Panx3) or nitrocellulose membranes for immunoblotting. Membranes were blocked for 1 hour at room temperature in a solution containing 3% milk (for visualization of Panx3) in phosphate buffered saline or 3% BSA in Tris buffered saline, then incubated overnight at 4°C with primary antibodies against Panx3 (Thermo Fisher, 433270; 1:500), eNOS (BD Biosciences, 610297; Cell Signaling Tech, 9572S), peNOS Thr495 (BD Biosciences, 612706), Bcl6 (BD Bioscience 561520, Cell Signaling Tech, 5650S), Panx1 (Cell Signaling Tech, 91127S), GAPDH (Santa Cruz, sc-51907), Nox4 (Abcam, ab109225), p22^{phox} (Santa Cruz, sc-271968), 3-nitrotyrosine (Millipore, 06-284), Flag (Sigma, F3165). Membranes were washed and incubated in LiCOR IR Dye secondary antibodies (1:10,000) for 1 hour and viewed/quantified using the LiCOR Odyssey CLx with Image Studio software. Licor Total Protein stain or GAPDH was used for loading normalization. Representative western blot images have been cropped for presentation.

Real-time quantitative PCR

Total RNA was extracted from mouse tissues using the Aurum Total RNA Fatty and Fibrous Tissue Extraction kit (Bio-Rad, #732-6870). RNA concentration was measured using the Nanodrop1000 spectrophotometer (Thermo Fisher Scientific). RNA was stored at -80°C before reverse transcription with

SuperScript III First-Strand Synthesis system (Thermo Fisher Scientific, #18080051) using random hexamer primers on 1 µg of template RNA. Real-time quantitative PCR was performed using TaqMan Gene Expression Master Mix (Thermo Fisher, 4369016) and TaqMan Real-Time PCR assays in MGB-FAM for Pannexin 3/Panx3 (Hs00364808_m1; Mm00552586_m1), Pannexin 1/Panx1 (Hs00209790_m1; Mm00450900_m1), B-Cell Lymphoma-6/BCL6 (Hs00153368_m1; Mm00477633_m1), v-rel reticuloendotheliosis viral oncogene homolog B/RelB (Mm00485664_m1), Nuclear factor κB p100 subunit/Nfkb2 (Mm00479807), nuclear factor of kappa light polypeptide gene enhancer in B-cells inhibitor, alpha (IkBα)/Nfkb1a (Mm00477798_m1), NADPH Oxidase-2/Cybb (Mm01287743_m1), NADPH Oxidase-4/Nox4 (Mm00479246_m1), and were normalized to β-2-microglobulin/B2M in VIC-PL (Hs00364808_m1; Mm00437762_m1). Reactions were run in a CFX Real-Time Detection System (Applied BioSystems) and threshold cycle number (CT) was used as part of the $2^{-\Delta\Delta CT}$ method to calculate fold change from control.

Immunohistochemistry, histology & Microscopy

Vascular tissues (aortae, third-order mesenteric resistance arteries and veins) were collected and fixed in 4% paraformaldehyde or ice-cold acetone-methanol. For en face preparation, arteries were cut longitudinally with microdissection scissors and pinned open on polymerized Sylgard 184 (Electron Microscopy Sciences) using tungsten wire (0.0005", ElectronTubeStore). Vessels prepared en face were then permeabilized in 0.2% NP-40 in PBS for 30 minutes at room temperature, blocked in 1% bovine serum albumin, Fraction V (BSA, Sigma) in 0.2%NP40/PBS and stained with primary antibodies overnight at 4°C in 0.1% BSA in 0.2%NP40/PBS. For paraffin sections, 5 µm tissue sections were deparaffinized with heat (1 hour at 65°C) and histoclear (National Diagnostics, 5989-27-5). Following rehydration, tissues were blocked in 5%BSA, Fraction V, 0.05% fish skin gelatin (Sigma, G7765), and 0.2% Triton-X100 for 1 hour at room temperature in a humidified chamber. Primary antibodies include Panx3 (Thermo Fisher, 433270; 1:50), Panx3 CT-379^{58, 60, 144}, BCL6 (Invitrogen #14-9887-82), PECAM (Santa Cruz, sc-376764, 1:50),

calnexin (Abcam, #ab219644, 1:100), eNOS (BD Transduction, 610297, 1:100), GM130 (R&D Systems, AF8199), Claudin 5 (Invitrogen, 35-2500), B4GALT1 (Invitrogen, PA5-106617, 1:50), MGAT1 (Invitrogen, PA5-121001), Panx1 (Cell Signaling Tech, 91137S), PrxSo3 (Abcam, ab16830), 3-nitrotyrosine (Millipore Sigma, 06-28), 4-hydroxynonenal (Invitrogen, MA5-27570). Samples were incubated with secondary antibodies at 1:500 for 1-2 hours at room temperature. Nuclear staining was achieved with a brief incubation with DAPI (Invitrogen, D1306, final concentration 0.1 μ g/mL) in addition to mounting with Prolong Gold Antifade Mountant (Invitrogen, P36930). Images of endothelium were collected on LSM 880 with Airyscan or Olympus FV1000 and post processing was completed using Fiji. For colocalization analyses, images were assessed in Fiji using the Coloc 2 plugin following rolling ball background subtraction.

Blood Pressure Assessments via Radiotelemetry

Blood pressure was measured using telemetry equipment (Data Sciences International, DSI) as previously described.¹⁴⁵ Mice were surgically implanted with radiotelemetry units (PA-C10 or HD-X10). Briefly, while under isoflurane anesthesia, the catheter of a radiotelemetry unit was placed in the left carotid artery and positioned such that the probe reached the aortic arch. The radiotransmitter was placed in a subcutaneous pouch at the right flank. Buprenorphine was used as an analgesic. Mice were allowed to recover for seven days prior to the initiation of recordings. Mice that were injected with tamoxifen underwent implantation at least 10 days after the last injection. Baseline blood pressure measurements, including systolic pressure, diastolic pressure, mean arterial pressure (MAP) and heart rate, were recorded every minute for a continuous period of 5 days using Dataquest A.R.T. 20 software (DSI). Change in MAP (Δ MAP) was calculated by subtracting the average baseline MAP to the MAP after treatment administration. Diurnal (inactive period) MAP was measured during animal's light cycle: 6:00 a.m. to 5:59 p.m., and nocturnal (active period) MAP was measured during the animal's dark cycle: 6:00 p.m. to 5:59 a.m. To assess blood pressure during in vivo basophil depletion, mice were given twice daily I.P. injections

with MAR1 functional grade monoclonal antibody (Thermo Fisher, 16-5898-95; 5µg in sterile saline per injection) for three consecutive days¹⁴⁶ and blood pressure was monitored over the following 10 days. For blood pressure assessments in the context of basophil expansion, following two days of baseline recordings, blood pressure was monitored for 10 days following intravenous administration of murine IL-3 (Peprotech, 213-13; 10µg) and monoclonal antibodies against IL-3 (BD Biosciences, 554379; 5µg).¹⁴⁷

Pressure Myography

Freshly isolated third-order mesenteric arteries were placed into ice-cold Krebs-HEPES buffer (containing 118.4mM NaCl, 4.7mM KCl, 1.2mM MgSO₄, 4mM NaHCO₃, 1.2mM KH₂PO₄, 2mM CaCl₂, 10mM HEPES, 6mM glucose; pH 7.40-7.42). The vessels were then mounted in a pressure arteriograph (Danish MyoTechnology, DMT) with the lumen and bath filled with Krebs-HEPES buffer as previously described.^{145, 148-151} The vessels were equilibrated for 30 min at 80 mmHg and 37°C. Increasing concentrations of acetylcholine (ACh) were added into the bath to examine the endothelial-dependent vasodilation of these vessels. Full ACh curves were obtained for each vessel under a given treatment condition. Smooth muscle cell health was verified by constriction to KCl. Next, arteries were exposed to NS309 (small- and intermediate-conductance calcium activated potassium channel agonist). The vessels were then washed with a Ca²⁺-free Krebs-HEPES solution supplemented with 1mM Ethyleneglycol-O,O'-bis(2-aminoethyl)-N,N,N',N'- tetraacetic acid and 10µM sodium nitroprusside to obtain maximal passive diameter of the vessels. Internal diameter was measured at each step using the DMT MyoVIEW software. Vasodilation to ACh or NS309 was calculated as a % relaxation: $\% \text{ relaxation} = ((D_{\text{ACh}} - D_{\text{Tone}}) * 100) / (D_{\text{max}} - D_{\text{Tone}})$, where D_{Tone} was the diameter of the artery after the establishment of stable basal tone, D_{ACh} was the diameter after application of a given dose of ACh, and D_{max} was the maximal diameter measured at the end of experiment.

Immunogold Labeling and Electron Microscopy

Third-order mesenteric resistance arteries were collected in cellulose capillary tubes (Leica Microsystems, Vienna, Austria) with an inner diameter of 200 μ m. The tissues were transferred within the capillary tube to membrane carriers and cryo-immobilized using an EM ICE high-pressure freezer (Leica Microsystems, Vienna, Austria).^{152,153} Freeze substitution was performed over 2-3 days at -90C using an automatic freeze substitution machine (EM AFS Leica Microsystems). Samples were embedded in LR White (Electron Microscopy Sciences, 14380) and polymerized at 65°C. Semithick sections (200nm) were collected on pioloform-coated nickel grids (Electron microscopy sciences, EMS300-NI). Immunostaining was completed using the grid-on-drop technique in humidified chambers. All staining solutions were passed through a 0.2 μ m syringe filter prior to use. Briefly, grids were washed with PBS followed by 0.1% glycine/PBS. Blocking solutions contained 0.1% cold-water fish skin gelatin (Sigma, G7765), 5% BSA, 5% goat serum and were incubated with samples for 1 hour at room temperature. Primary antibodies were diluted to 1:20 in blocking solution diluted 1:1 in PBS and incubated with sample for one hour at room temperature. Samples were briefly washed in diluted blocking solution prior to secondary antibody incubated for 2 hours at room temperature (Electron Microscopy Sciences, 15-25nm, 1:20, #25116 and #25133). Samples underwent 10 washes in filtered diH₂O to remove salts. Contrast staining was achieved by brief incubation in 4% uranyl acetate followed by incubations in 0.4% lead citrate. Electron micrographs were collected on a TECNAI F20 transmission electron microscope (Thermo-Fisher, formerly FEI) operated at 200kV and recorded on a Gatan US4000 (4000 px \times 4000 px) CCD or a Teitz TVIPS XF416 camera.

Immunoprecipitation

HEK293T were cultured in DMEM, high glucose (Gibco, 11965-092) supplemented with 1mM sodium pyruvate, 1% Pen-Strep (Gibco, 15140122), 10% FBS (Avantor, 97068-085). Cells were transfected with pcDNA3.1-3xFlag-hPANX3 (NovoPro, 74275501, accession #: NM_052959) and pCMV6-AC-GFP-hBCL6 (Origene, RG226102, accession#: NM_001130845) using Lipofectamine 3000 (Thermo Fisher, L3000001). For BCLiP treated samples, 50 μ M BCLiP was introduced to the cells 6 hours after transfection.

Lysates were collected in IP RIPA (125mM NaCl, 5mM EDTA, 1% sodium deoxycholate, 0.5% Triton-x 100 in phosphate buffered saline supplemented with 10 μ M AEBSF, 10mM NaF, 10mM NEM, 500 μ M Na₃VO₄ and protease inhibitor cocktail (P1, Sigma, P8340). M-280 Sheep anti-mouse IgG Dynabeads (Invitrogen, 11201D) were washed in a blocking solution containing 0.5% BSA, 0.2% fish skin gelatin in PBS prior to incubation with Flag antibody (Sigma, F3165). Beads were mixed with 800 μ g HEK lysate in IP RIPA for three hours at 4C with gentle agitation prior to elution in 5x Lamelli buffer (0.5M TrisHCl pH6.8, 5% SDS, 0.5% Bromophenol blue, 12.5% β -mercaptoethanol) prior to assessment by western blot.

Calcium imaging

Ca²⁺ imaging studies were performed as described previously.^{10, 154} Third-order mesenteric arteries (~100 μ m) were cut open and pinned down *en face* on Sylgard blocks. Mesenteric arteries were then incubated with fluo-4 AM (10 μ M) and pluronic acid (0.04%) at 30°C for 45 minutes. Ca²⁺ images were acquired at 30 frames per second using Andor Revolution WD (with Borealis) spinning-disk confocal imaging system (Andor Technology, Belfast, UK) comprising of an upright Nikon microscope with a 60X water dipping objective (numerical aperture 1.0) and an electron multiplying charge coupled device camera. Mesenteric arteries were superfused with physiological salt solution (PSS; 119mM NaCl, 4.7mM KCl, 1.2mM KH₂PO₄, 1.2mM MgCl₂ 160 hexahydrate, 2.5mM CaCl₂ dihydrate, 7mM dextrose, and 24mM NaHCO₃) bubbled with 21% O₂ and 5% CO₂ to maintain the pH at 7.4. All the experiments were performed at 37°C. Fluo-4 was excited using a 488 nm solid-state laser and emitted fluorescence was captured using a 525/36 nm band-pass filter. Ca²⁺ images were analyzed using a custom-designed SparkAn software (developed by Dr. Adrian Bonev, University of Vermont) as described previously (<https://github.com/vesselman/SparkAn>).¹²³ Calcium transients were automatically detected using an ROI of 5 x 5 pixels, and a threshold of 1.25 F/F₀. The number of calcium transients per field before or after 10 μ M carbachol (CCh) stimulation was determined, and the numbers were averaged for each artery.

Predictions of Panx3 Structure and docking with BCLiP

Candidate peptide sequences were identified based on literature review. Initial peptide and Panx3 dimer structures were generated using AlphaFold2 on the ColabFold¹⁵⁵ webserver. The highest-scored structures were used for docking studies. The structure of Panx3 dimer was generated by generating a structure of Panx3 heptamer, then removing all but two monomers. This was done to simulate the smallest protomer of Panx3, avoiding biasing the simulation with a higher-order oligomer. Docking between peptides and protein dimer was simulated with LightDock¹⁵⁶ using 400 swarms of 200 glowworms. Each docking run was comprised of 100 steps, Protein and peptide were treated as flexible structures through the course of the docking run and positional restraints were applied to bias peptide docking towards the intraluminal side of Panx3. Specifically, docking only considered peptide orientations in close proximity of GLU 177, GLN 158, GLU 183, ASP 354, ALA 372, THR 363, GLY 373, or HIS 538. Docking results were scored using the pyDock algorithm,¹⁵⁷ which generates a score by considering binding energetics due to electrostatic interactions and desolvation effects. Ramachandran plots were generated using the MolProbity program.¹⁵⁸

Generation and administration of BCL6 mimetic peptide

A region of BCL6 (residues 328-344 of BCL6; LVSPQSPQKSDCQPNSP) was selected due to its important role in regulating targeted degradation of BCL6.¹³⁹ This region of BCL6 was found to have a high degree of sequence conservation across mammalian species (as determined by multiple sequence alignment on NCBI blastp for Homo sapiens, Mus musculus, Rattus norvegicus and Macaca mulatta, see Figure 16A). Peptides mimicking this region of BCL6 (LVSPQSPQKSDCQPNSP; BCLiP) or a scrambled peptide (SPSDPPVLNSQCQSQPK) were synthesized with a N-terminal stearyl group to facilitate membrane permeability. For in vivo studies, BCLiP or the scrambled peptide were administered to C57Bl/6n mice via intraperitoneal (I.P.) injection at 2.5mg/kg and 12.5 mg/kg in sterile saline daily for a period of five days. All tissues were collected 6-8 hours following the last dose of BCLiP or scramble peptide. Protein and RNA were isolated from flash frozen lung tissue to be used for quantification. Third-

order mesenteric resistance arteries were collected, fixed in 4%PFA and prepared en face for proximity ligation assays (PLA).

Proximity ligation assay

Third-order mesenteric arteries were prepared en face as described above. Following fixation, arteries were permeabilized in 0.2% NP40 in PBS at room temperature for 30 minutes with gentle shaking. Proximity ligation staining was achieved by following the Duolink In Situ PLA fluorescent protocol (Millipore Sigma). Briefly, samples were blocked in Duolink blocking for 1 hour at room temperature. Next, samples were incubated with primary antibodies diluted 1:25 in Duolink antibody buffer at 4°C overnight. Primary antibodies were used against Panx3 (Invitrogen; 433270), BCL6 (Invitrogen #14-9887-82), endothelial nitric oxide synthase (BD; 610297), and caveolin-1 (Abcam, ab32577). Despite staining on whole tissue, small reaction volumes (25µL) were achieved by placing Sylgard squares holding arteries prepared en face within a 24-well plate and balancing the drop on the center of the Sylgard. Damp filter paper was placed over the wells of the plate and the lid to generate a humidified chamber. Reactions occurred under static conditions to avoid breaking surface tension and reduce the risk of sample drying. Anti-rabbit MINUS and anti-mouse PLUS probes (Millipore Sigma; DUO92005-30RXN; DUO92001-30RXN) in antibody diluent and incubated with samples for one hour at 37°C as per the manufacturer's instructions. Ligation reactions were then allowed to proceed for 30 minutes at 37°C, followed by amplification reactions which occurred for 100 minutes at 37°C. Samples were then mounted with Prolong Gold Antifade Mountant (Invitrogen, P36930). Images were collected LSM 880 with Airyscan and post processing was completed using Fiji. Briefly, the PLA puncta channel was first isolated and converted to greyscale. From this, a binary image was generated with a threshold of 0.55-0.65 in preparation to analyze particles (0.003-Infinity). The number of PLA puncta was normalized to the number of endothelial nuclei in view. Data from cells with nuclei that are not entirely visualized in the image were excluded from analysis. A minimum of four fields of view were analyzed and averaged per mouse.

Bcl6 DNA binding assessments

For in silico assessments: Potential for repression by Bcl6 was first assessed by identifying instances of transcription factor binding motifs in the promoter region sequences for genes in a similar manner to previously published methods.¹⁵⁹ Using the mm39 reference genome, the cis sequences 1kb upstream of the indicated genes were retrieved. The mouse Bcl-6 binding motif PSWM was retrieved from JASPAR (ID: MA0463.1). The Find Instances of Motif Occurrence (FIMO) algorithm¹⁶⁰ was then applied to these sequences to find a motif occurrence of the Bcl6 binding motif, using a threshold of 0.0005. The number of intervals above this threshold were then plotted for each gene. For assessments of publicly available Bcl6 ChIP-Seq datasets: A comprehensive set of Bcl6 ChIP-Seq reads were assembled and retrieved from the gene expression omnibus and aligned to the mm39 reference genome. Signal was then plotted, in aggregate, for 1kb upstream of genes of interest. The GSM accession numbers used for this analysis are: GSM1857225,¹⁶¹ GSM1857226,¹⁶¹ GSM3347610,¹⁶² GSM3347618,¹⁶² GSM3347625,¹⁶² GSM3347623,¹⁶² GSM3347624,¹⁶² GSM3347613,¹⁶² GSM3347612,¹⁶² GSM3347611,¹⁶² GSM419049,¹⁴¹ GSM419050,¹⁴¹ GSM611114,¹⁴¹ GSM611115,¹⁴¹ GSM851557.¹⁴¹

Flow Cytometry

Five-color flow cytometry was used to determine the number of leukocytes in the kidney, spleen and bone marrow. Counting beads (Caltag, Carlsbad, CA) were used as described previously⁶ to determine the total number of CD45⁺ cells per gram of kidney or spleen tissue. All samples were treated with anti-mouse CD16/CD32 (2.4G2) to block the nonspecific FcR binding, 7-AAD or LIVE/DEAD Fixable Green Dead Cell Stain (Invitrogen, Carlsbad, CA) to exclude dead cells and anti-CD45 to gate on the live leukocyte populations. To evaluate the pro- and anti-inflammatory cytokine production in splenic T cells from EC Panx3^{Δ/Δ} mice and littermate controls. Single cell suspensions of spleen cells were stimulated with PMA (Phorbol 12-Myristate 13-Acetate) and ionomycin, in the presence of monensin for five hours and analyzed by flow cytometry for intracellular cytokine expression. Follicular B cells and germinal center B cells were

identified as GL7⁺, CXCR5⁺, B220⁺ and GL7^{hi}, Fas⁺, B220⁺ splenic cells, respectively. Renal tissue was assessed for infiltration by macrophages and neutrophils, which were identified as F4/80^{low}/CD11b⁺ cells and PMN, GR-1⁺/CD11b⁺, respectively. CD4⁺CD25⁺FoxP3⁺ Tregs were stained, fixed, and permeabilized using the eBioscience (San Diego, CA) FoxP3 buffer set according to the manufacturer's protocol. ILC2s were assessed as CD90⁺, ST2⁺ cells in the spleen or as CD45⁺, CD90⁺ ST2⁺ cells in the kidney. Data were acquired on a FACScan cytometer (BD Biosciences) with a 5-color upgrade (Cytex Development, Inc.) and analyzed with FlowJo software .

Chapter 3: Endothelial Panx3-Bcl6 Interactions Protect Against Oxidative Stress

3.1: Abstract

Complex regulatory mechanisms control the abundance and localization of transcription factors due to the broad impact their transcriptional activity can have on cell, tissue and organism physiology. The activity of transcriptional repressor B cell lymphoma 6 (Bcl6), which has been well studied for its roles in immune cell specification and lymphocytogenesis, is largely regulated by its targeted degradation. However, outside of angiogenesis, a role for Bcl6 in the vasculature has yet to be explored. Here, we report the abundance of endothelial Bcl6 is regulated by its ability to interact with Golgi-localized Pannexin 3 (Panx3), and Bcl6 transcriptional activity in endothelium protects against vascular oxidative stress. Hypertensive humans and mice exhibit reduced vascular expression of Panx3. Immunohistological analyses suggest Panx3 is expressed uniquely in endothelial cells in the vascular wall where it localizes to the membrane of the Golgi Apparatus. An inducible, endothelial-cell specific Panx3 knockout mouse (*EC Panx3^{Δ/Δ}*) was generated and presented with spontaneous hypertension, akin to resistance arteries from hypertensive mice and human. Assessments of potential Panx3 channelopathy were unremarkable (ATP efflux, Ca²⁺ flux, Golgi luminal pH), bringing to question whether the *EC Panx3^{Δ/Δ}* phenotype may arise from channel-independent functions. Indeed, crosslinking endogenous Panx3 from arteries identified a dimeric protomer with multiple oligomeric assemblies. Panx3 was shown to interact with transcriptional repressor Bcl6 at Golgi Apparatus in resistance artery endothelium via proximity ligation assays. The *EC Panx3^{Δ/Δ}* mice exhibited significantly decreased Bcl6 protein, but not Bcl6 mRNA, hinting that interactions with Panx3 may stabilize BCL6 at ubiquitination sites. *EC Panx3^{Δ/Δ}* mice exhibit increased NFκB transcriptional activity and specific upregulation of Nox4, an H₂O₂ generating NADPH oxidase. Publicly available CHIP-Seq data supports that Bcl6 transcriptional repressive activity is regulated by its ability to interact with Panx3. To confirm Panx3-Bcl6 interaction, we designed a novel mimetic peptide to block Panx3-Bcl6 interactions (BCLiP). When BCLiP was administered into control mice, it recapitulated an increase in NFκB, Nox4 and blood pressure.

Our data elucidates for the first time a channel-independent function of Panx3 wherein its interactions with a perinuclear pool of Bcl6 can dictate transcriptional repression and protect against oxidative stress.

3.2: Introduction

Reactive oxidative species (ROS) are produced as a consequence of oxygen metabolism and include highly reactive free radicals, such as superoxide (O_2^-), as well as more stable, non-radical peroxide species, such as hydrogen peroxide (H_2O_2). While ROS participate in many physiological signaling mechanisms, their overproduction can overwhelm antioxidant capacity, causing deleterious effects on the cardiovascular system. For instance, mitochondrial-derived ROS are necessary for flow-mediated dilation of human arteries,^{163, 164} though insufficient scavenging of mitochondrial O_2^- can reduce nitric oxide (NO) bioavailability, leading to hypertension and atherosclerosis.¹⁶⁵⁻¹⁶⁷ Thus, the expression of ROS generating enzymes and endogenous antioxidant systems must be tightly regulated. Transcriptional control of oxidative stress related genes is paramount to achieving homeostatic redox balance.

B Cell Lymphoma 6 (Bcl6) is a transcription factor that has been shown to differentially regulate expression of oxidant stressors as well as redox proteins. As part of its well-documented role in the humoral response, Bcl6 transcriptional activity promotes B Cell survival during genotoxic and oxidative challenge of germinal center formation.^{121, 168-170} In non-Hodgkin's lymphoma, overexpression of Bcl6 in lymphoma has been shown to promote resistance to chemotherapeutics such as etoposide by preventing apoptotic ROS generation.¹⁷¹ Similarly, a subset of diffuse large B Cell Lymphoma (DLBCL) cells will undergo a metabolic shift to oxidative phosphorylation and require Bcl6-dependent expression of thioredoxin to tolerate the oxidative challenge.¹⁷² Oxidative protection by Bcl6 is not limited to its ability to directly alter expression of oxidants and reductants. Bcl6 exhibits mutual antagonism with pro-oxidant, proinflammatory transcription factor NF κ B, repressing many of the transcriptional targets that NF κ B activates.^{141, 142} Bcl6 engages in a diverse repertoire of protein-protein interactions to fulfill these roles. In the cytosol, MAPK can phosphorylate Bcl6 PEST motifs, resulting in rapid recruitment of Bcl6 to SCF ubiquitin ligase through interactions with FBXO11 resulting in proteasomal degradation.^{124, 139} However, functional roles have not been identified for all Bcl6 interactions. For example, an unbiased screen for binding partners of Bcl6 identified an interaction with pannexin 3 (Panx3),¹⁰⁸ though the product of this interaction is not known.

Panx3 belongs to the family of pannexin channels of which there are three isoforms: Panx1, Panx2 and Panx3. Panx1 has well-documented roles at the plasma membrane contributing to purinergic, adrenergic and calcium signaling in the vasculature.^{63, 72, 148-151, 173-176} While low levels of Panx3 expression has been noted in RNA-Seq datasets from endothelium throughout the systemic microvasculature,¹⁷⁷ its functional role has yet to be described. Published reports on the localization and functional implications of Panx3 demonstrate a high degree of plasticity across cell types and expression systems. When localized to the endoplasmic reticulum, Panx3 has been suggested to contribute to calcium store release.⁹¹ However, Panx3 has also been reported to localize to the plasma membrane where it has been implicated in dye uptake^{58, 60, 72, 178} and ATP release.^{68, 90, 91}

In this study, we demonstrate a channel-independent function of pannexins in general (Panx3), wherein its interactions with a Golgi-localized pool of Bcl6 can dictate transcriptional repression of oxidative stress related genes, and could provide novel insight into development of hypertension.

3.3: Results

Because pannexins have been implicated in hypertension,^{148, 149, 151, 173, 175} we examined mRNA transcripts from hypertensive humans and mice. In treatment resistant hypertensive humans (mean systolic pressure 158.5 ± 13.35 mmHg; Figure 1A), Panx3 mRNA (Figure 1B) was significantly reduced compared to controls (mean systolic pressure 118.8 ± 14.19 mmHg), which corresponded with expression patterns observed via immunofluorescence (Figure 1C). Panx1 mRNA trended upwards with variation, and Panx2 transcripts were unchanged (Figure 1B). A significant decrease in Panx3 was also observed in spontaneously hypertensive mice (Figure 2).

Because Panx3 has not previously been reported in resistance arteries, we examined its localization. Global Panx3^{-/-} mice were used to demonstrate Panx3 antibody specificity (Figure 3A-B). Transverse sections of thoracodorsal arteries indicated Panx3 was only in endothelium and not smooth muscle (Figure 3C). Next, mesenteric arteries were labeled with gold beads conjugated to Panx3 (Figure 3D). Qualitative assessment of the distribution of gold beads across four subcellular membranous domains (apical, intracellular, nuclear, and basal membranes) suggested Panx3 preferentially localizes to intracellular membranes (Figure 3D). Subcellular distribution was further assessed by immunohistochemical staining of Panx3 with markers of interendothelial junctions (CD31), endoplasmic reticulum (calnexin), and the Golgi Apparatus (GM130) in mesenteric arteries prepared en face (Figure 4A). Panx3 was restricted to the Golgi Apparatus, which was validated with Manders' colocalization analysis (Figure 4B). This polarized perinuclear Panx3 distribution pattern was distinct from that of Panx1, which traffics to the plasma membrane and colocalizes with Claudin 5 at interendothelial junctions (Figure 4C). Because Golgi is polarized in arterial endothelium due to flow, but not in low-flow veins, we corroborated Panx3 localization to Golgi by examining mesenteric arteries and veins. Distribution of Panx3 in both vessel types identified a polarization pattern similar to Golgi (Figure 4D). Last, glycosylation states of Panx1 and Panx3 help to traffic the channels to the cell surface.⁶⁰

Using PNGase F to remove glycosylation on the channels, we could not identify glycosylation of endogenous Panx3 in mesenteric arteries, unlike Panx1 (Figure 4E). Thus, Panx3 is endogenously expressed in endothelium at the Golgi Apparatus.

Assessments of Panx3 expression in endothelial cells grown in culture suggest that its subcellular distribution may be regulated by exposure to shear stress. Immunostaining of human aortic endothelial cells grown under static conditions demonstrates that Panx3 localizes to the endoplasmic reticulum with an anisotropic distribution pattern (Figure 5A). However, exposure to shear stress polarizes Panx3 within the cell (Figure 5B-C), suggesting that shear sensing traffics Panx3 from the endoplasmic reticulum to the Golgi Apparatus.

Genetic deletion of endothelial Panx3 results in spontaneous hypertension.

We posited the hypertension associated with attenuated Panx3 observed in Figures 1-2 may be recapitulated if we removed Panx3 from the endothelium. Thus, EC Panx3^{Δ/Δ} mice were generated by crossing mice carrying loxP sites flanking exon 2 of the murine Panx3 gene¹⁷⁹ with mice carrying the tamoxifen-inducible driver of Cre recombinase under the vascular endothelial cadherin promoter (Cdh5-CreER^{T2+}; Figure 6A). Following tamoxifen administration, Panx3 gDNA is excised (Figure 6B), and Panx3 mRNA and protein is significantly reduced (Figure 6C-F), with no corresponding change in Panx1 (Figure 6G). The EC Panx3^{Δ/Δ} mice do not recapitulate phenotypes reported in global Panx3^{-/-} mice; there is no change in body length⁹², body fat¹⁸⁰, gonadal fat¹⁸⁰, or blood lipids¹⁸¹ (Figure 7A-G). However, similar to the observation in humans and genetically inbred hypertensive mice in Figures 1-2, EC Panx3^{Δ/Δ} mice present with spontaneous hypertension with significantly increased mean arterial and systolic pressure (Figure 8A-B). There was no significant change in diastolic pressure, heart rate or cardiac output (Figure 8C-E). To determine if salt and water retention functions of the kidney were part of the etiology of the spontaneous hypertension, we examined plasma sodium, potassium and renin, and found no significant differences

(Figure 8F-H). Ejection fraction, creatinine, creatine kinase, and blood urea nitrogen levels in the blood were unchanged (Figure 7H-K). Assessments of renal immune infiltration was similarly unaffected by genetic deletion of endothelial Panx3 (Figure 9A-B). However, acetylcholine (ACh) cumulative dose-response curves from third-order mesenteric arteries demonstrated inhibition of dilatory capacity (Figure 8I). The dilation impairment was not due to loss of smooth muscle function, as the arteries constricted to KCl (Figure 8J), or changes in eNOS protein expression or inhibitory eNOS phosphorylation at Thr495 (Figure 8K); however, dilation to NS309 was significantly impaired (Figure 8L). Based on this data, we find mice with genetic deletion of Panx3 in endothelium develop spontaneous hypertension that is likely due to endothelial dysfunction impairing peripheral resistance, possibly through endothelial SK/IK inhibition.

Panx3 exerts channel-independent functions through interactions with Bcl6.

Because genetic deletion of endothelial Panx3 causes severe vascular impairments at the tissue and systemic level, we wanted to determine the functional role Panx3 in endothelium and first tested properties associated with Panx1. Mesenteric arteries exhibited no change in intracellular or stimulated release of ATP (Figure 10A-B) suggesting Panx3 may not contribute to endothelial purinergic signaling. Panx3 has previously been reported to facilitate IP₃-induced calcium store release.^{68, 91} However, assessments of calcium signaling in mesenteric arteries revealed no impairments between genotypes at baseline or following stimulation with muscarinic agonist carbachol (Figure 10C). Interestingly, examination of TRPV4-mediated extracellular calcium sparklets, accomplished through exposure to cyclopiazonic acid (CPA; 20μM) which inhibits sarcoplasmic/endoplasmic reticulum calcium ATPase (SERCA), demonstrated loss of endothelial Panx3 increases the number of TRPV4 events and increased TRPV4 channel open probability (Figure 11A-B).

Next, because Panx3 is localized to Golgi, we hypothesized it may regulate luminal pH. Subcellular distribution of glycosyltransferases was used as an indirect measurement of Golgi homeostasis as

neutralization of the Golgi luminal pH causes redistribution of Golgi-resident protein into the endosomal system (Figure 10D).¹⁸²⁻¹⁸⁴ However, the colocalization of B4GALT1 and MGAT1 with Golgi marker eNOS are unchanged by Panx3 expression in intact endothelium (Figure 10E-F; Figure 12A), indicating no impairments in Golgi homeostasis or luminal pH regulation. The sum of this data precipitated the question of whether Panx3 monomers assemble into a channel endogenously. To test this, the oligomeric state of endogenous Panx3 was assessed in mesenteric vascular lysates following exposure to chemical crosslinker bis-sulfosuccinimidyl-suberate (BS³). Crosslinking of vascular lysates was insufficient to identify an oligomeric species of Panx3, unlike Panx1, instead revealing a Panx3 doublet at ~80 kDa, which suggests the presence of a stable dimeric Panx3 protomer (Figure 10G). Without evidence for Panx3 channel function or confirmation of the oligomeric species, we next interrogated the possibility that Panx3 may exert its cellular function through protein-protein interactions. In an unbiased protein-protein interaction screen, Panx3 was reported to bind transcriptional repressor Bcl6.¹⁰⁸ Immunostaining indicates both proteins can be detected in the Golgi Apparatus of intact endothelium (Figure 10H). Proximity ligation assays on mesenteric endothelium corroborated Panx3 and Bcl6 interaction, with eNOS and Cav1 used as a positive control (Figure 10I; Figure 12B).

Panx3 interactions with Bcl6 protect against H₂O₂-induced oxidative stress via repression of Nox4.

In efforts to investigate how Panx3/Bcl6 interactions would affect Bcl6 transcriptional activity, Bcl6 expression was first assessed in EC Panx3^{ΔΔ} tissue. *Bcl6* mRNA is unaffected by loss of Panx3, though Bcl6 protein is significantly decreased, suggesting Bcl6 may be destabilized in the absence of Panx3 (Figure 13A-B). Notably, this reduction in vascular Bcl6 abundance was not associated with alterations in the development of B220⁺GL7⁺FasL⁺ splenic germinal centers via flow cytometry (Figure 7L). To understand how loss of vascular Bcl6 might alter oxidative-related genes, we levered publicly available genomic datasets, we first predicted Bcl6 transcriptional activity via in silico sequence assessments of the Bcl6 DNA binding motif (Figure 13C). The Bcl6 DNA binding motif was detected in the promoter region of Bcl6-sensitive genes in endothelium (*Ccna2*, *Ccnb1*, *Hes1*, and *Dll4*),¹²² as well as *Nfkb1a*, *Nfkb2*, and *Nox4*, but

not *Nox1* or *Cybb* (Figure 13C-D). This was further corroborated through evaluation of all publicly available murine Bcl6 ChIP-Seq datasets,^{141, 161, 162} which revealed numerous instances of Bcl6 binding of autoregulated NFκB family members *Nfkb1a* and *Nfkb2* (Figure 13E-F). Intriguingly, demonstration of Bcl6 repression predicts upregulation of transcript abundance in vascular tissues of EC *Panx3^{Δ/Δ}* mice for multiple genes, suggesting loss of Bcl6 transcriptional activity in the absence of endothelial Panx3. *Nfkb1a* and *Nfkb2* are significantly upregulated (Figure 13J-K), suggesting a Bcl6-dependent increase in NFκB activity following loss of endothelial Panx3. Because NFκB activity is associated with increased expression of vascular NADPH Oxidase enzymes,^{13, 185-188} we next interrogated their expression following deletion of endothelial Panx3. *Nox4* transcripts are uniquely upregulated following loss of endothelial Panx3 (Figure 13L-N), which can be explained by differential regulation of *Nox* expression by Bcl6 (Figure 13G-I). In the absence of endothelial Panx3, Bcl6 is destabilized resulting in de-repression of NFκB family members and *Nox4*.

To examine the vascular oxidative state, the abundance of *Nox4* was assessed via western blot. Following loss of Panx3, *Nox4*, but not cofactor *p22^{phox}*, was upregulated (Figure 14A). Because *Nox4* is understood to be a constitutively active oxidase^{189, 190} largely generating H₂O₂,⁴⁰ we next assessed oxidative damage in the circulation and vascular wall. EC *Panx3^{Δ/Δ}* mice exhibited increased 3-nitrotyrosine (3NT) protein adducts (Figure 14B) and increased H₂O₂ levels in deproteinized blood plasma (Figure 14C). Small arteries from EC *Panx3^{Δ/Δ}* mice exhibit increased levels of hyperoxidized peroxiredoxin, a specific measure of chronic H₂O₂ generation¹⁹¹ (Figure 14D). In large arteries, hyperoxidized peroxiredoxin and 3NT protein adducts are significantly increased, while 4-hydroxynonenal, marker of lipid peroxidation, exhibited a similar trend (Figure 15). No changes were observed in eNOS mRNA or coupling status (Figure 16A-B). Similarly, other redox related genes and H₂O₂-generating enzymes *Xdh*, *Ero1l*, *Prx4* and *Cyb5r3* were not altered by Panx3 expression (Figure 16C-F). Finally, ACh dose response curves were repeated on mesenteric arteries in the presence of H₂O₂-scavenger catalase (1000U/mL Pegylated-Catalase). Catalase

treatment abolished the significant difference in dilation between Panx3^{fl/fl} and EC Panx3^{Δ/Δ} arteries (Figure 14E). These data suggest Panx3-Bcl6 interactions stabilize Bcl6, which represses endothelial Nox4 expression under normal physiological conditions. In the absence of Panx3, Nox4 de-repression results in increased abundance and resultant chronic H₂O₂ generation in the vascular wall, impairing endothelial-mediated dilation of small arteries.

Blocking Panx3-Bcl6 interactions phenocopies genetic deletion of endothelial Panx3.

To further demonstrate the role for Panx3-Bcl6 interactions in maintaining oxidative balance, a mimetic peptide was designed to disrupt the Panx3-Bcl6 complex. BCLiP, which mimics L328-P344 of Bcl6, was selected from a pool of 10 candidate mimetic sequences for its potential to competitively inhibit the Panx3-Bcl6 interaction (Figure 17A-B, Table 1). To assess the ability of BCLiP to disrupt the Panx3-Bcl6 interaction, PANX3 and BCL6 were expressed in HEK293T cells and exposed to BCLiP. Following immunoprecipitation of Panx3-Flag, Bcl6 pull down was reduced by BCLiP treatment (Figure 17C). Next, stearylated BCLiP peptide or scramble control was administered to C57Bl/6n mice (12.5mg/kg via IP for five days) to assess its ability to disrupt the Panx3-Bcl6 interaction in vivo. Similar to the observation in EC Panx3^{Δ/Δ} mice, Bcl6 transcripts were unaffected by BCLiP exposure (Figure 17D), but Bcl6 protein abundance was significantly reduced by BCLiP treatment (Figure 17E), supporting the hypothesis that BCLiP promotes Bcl6 degradation, likely due to inhibition of Panx3-Bcl6 interactions. NFκB activity was increased following BCLiP exposure (Figure 17F-G), further mimicking the EC Panx3^{Δ/Δ} phenotype. Specific upregulation of Nox4, but not Nox1 or Cybb, was also induced following BCLiP administration (Figure 17H-J). Finally, BCLiP administration induced a sustained increase in mean arterial, systolic and diastolic blood pressure (Figure 17K-M), recapitulating hypertension observed following genetic deletion of endothelial Panx3.

Figure 1: Hypertensive humans exhibit significantly reduced expression of Panx3.

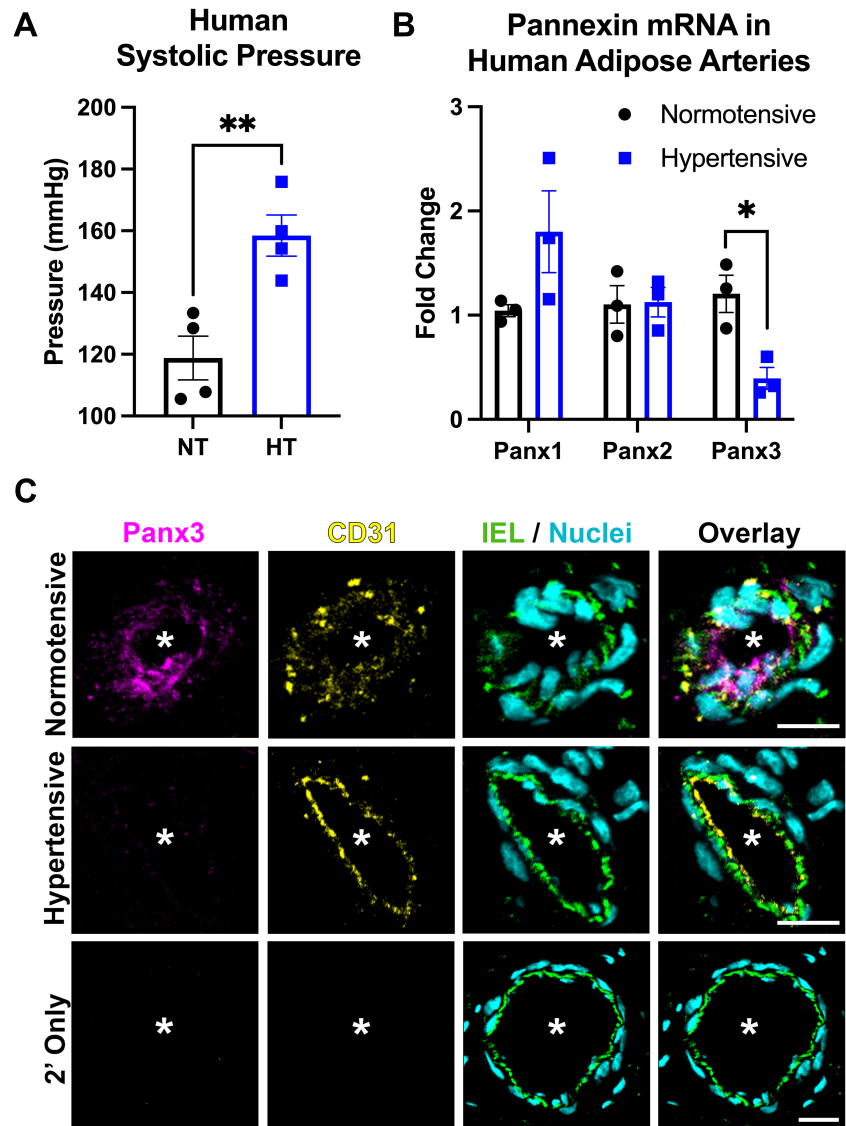


Figure 1: Hypertensive humans exhibit significantly reduced expression of Panx3. (A) Systolic blood pressure measurements in normotensive (black) and hypertensive (blue) human participants. (B) Transcript abundance of Pannexin isoforms in human adipose arteries. (C) Paraffin sections of normotensive and hypertensive human adipose arteries stained for Panx3 (magenta), CD31 to denote endothelial cells (yellow). Nuclei are depicted in cyan and IEL is shown in green. Scale bar is 50µm.

Figure 2: Murine vascular Panx3 is attenuated by hypertension.

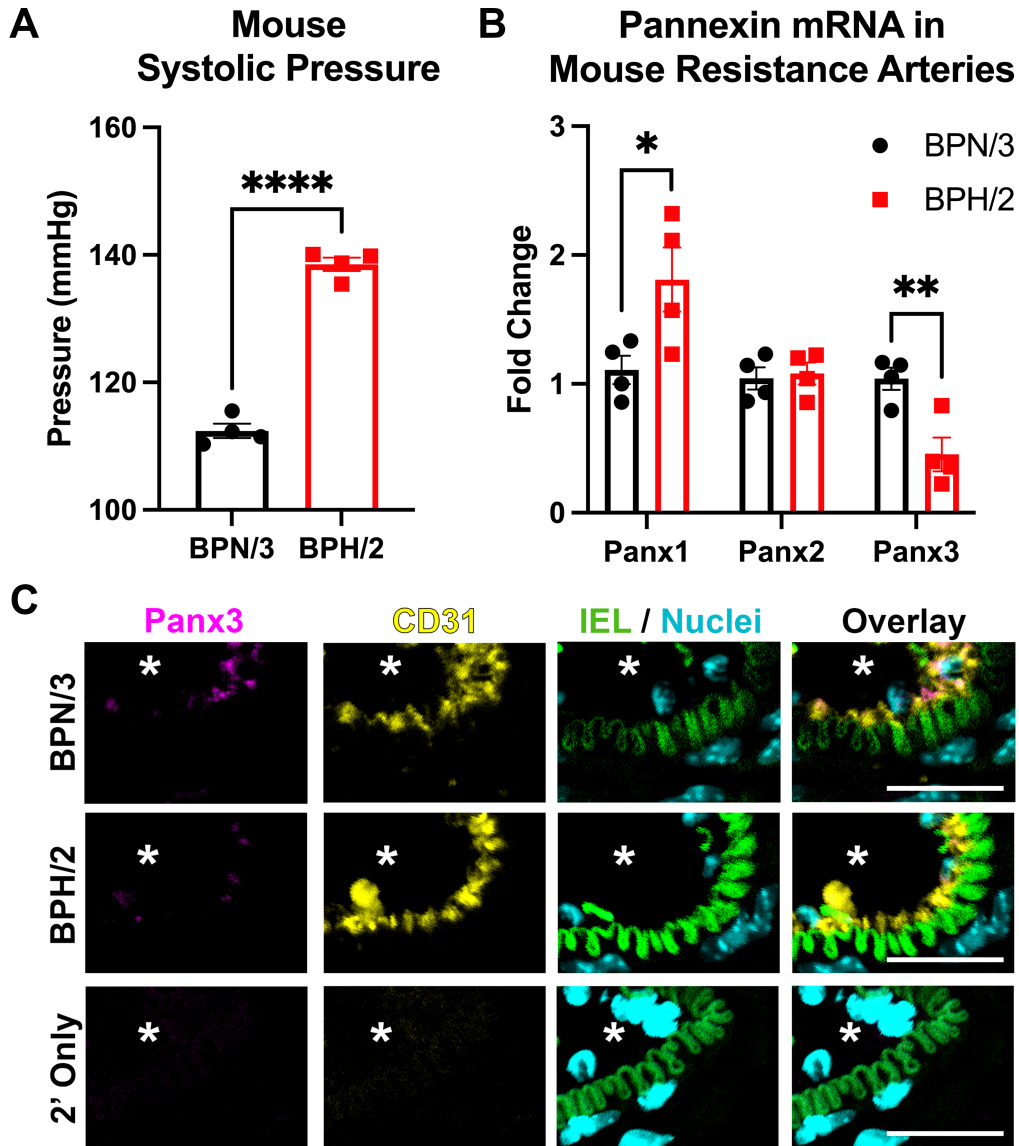


Figure 2: Murine vascular Panx3 is attenuated by hypertension. (A) Systolic pressure of genetically inbred BPH/2 mice (red) and their similarly inbred normotensive counterparts (BPN/3, black). (B) Pannexin isoform expression in the thoracodorsal arteries of BPN/3 and BPH/2 mice. (C) Immunostaining of Panx3 (magenta) and CD31 (yellow) with IEL in green and nuclei depicted in cyan. Scale bar is 50 μ m.

Figure 3: Endogenous Panx3 expression in vascular endothelium.

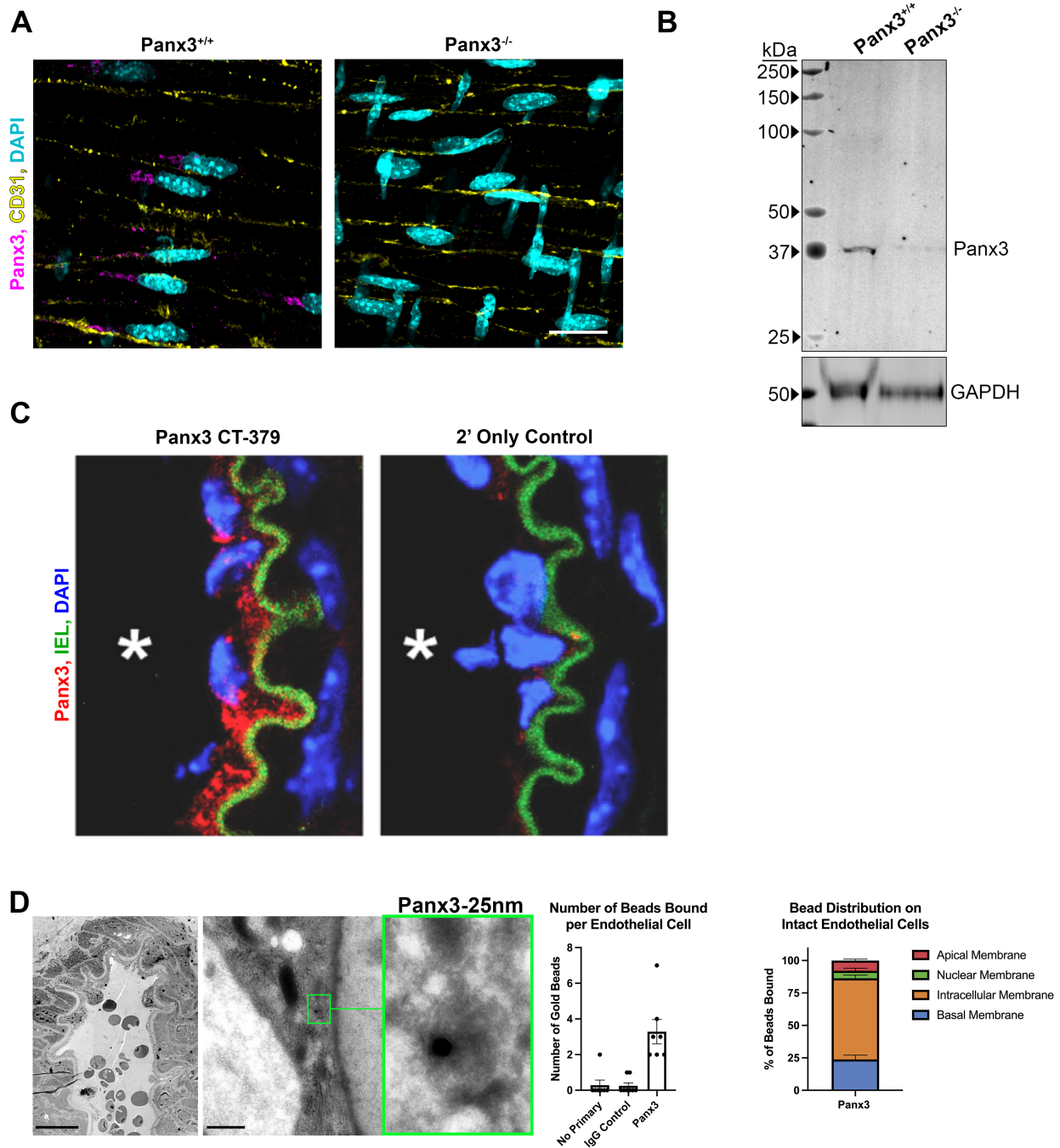


Figure 3: Endogenous Panx3 expression in vascular endothelium. (A) Panx3 (magenta) expression in third-order mesenteric artery prepared en face from control and Panx3 global knockout mice (Panx3^{-/-}). Interendothelial junctions are visualized by staining for CD31/PECAM-1 (yellow) and nuclei are represented in cyan. Scale bar is 20 μ m. (B) Western blot of Panx3 protein from control and Panx3^{-/-}

generated from lung tissue using the same Panx3 antibody (Thermo Fisher Scientific, #433270) depicted in (A). Full blot shown for transparency. (C) Murine thoracodorsal artery cross sections reveal Panx3 (red) visualized in endothelium via an alternative Panx3 antibody (Panx3 CT-379^{58, 60, 144}). Secondary only control shown at right. Autofluorescence from internal elastic laminae (IEL) is shown in green. Nuclei are represented in blue. Asterisks denote vessel lumen. (D) Immunogold labeling of Panx3 in third-order mesenteric resistance arteries demonstrates a preference to localize to intracellular membranes. Scale bar in lower magnification view is 10 μ m and 5nm in the inset. Abundance and distribution of gold beads conjugated to Panx3 antibody quantified at right.

Figure 4: Endothelial Panx3 localizes to the Golgi Apparatus of intact endothelium, unlike Panx1.

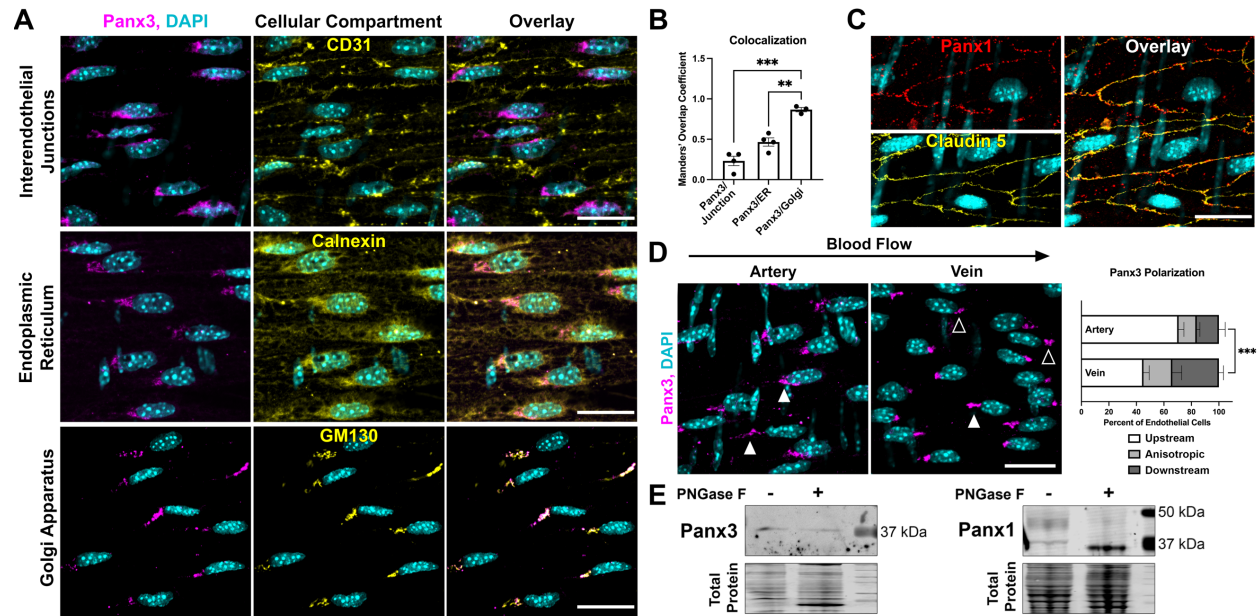


Figure 4: Endothelial Panx3 localizes to the Golgi Apparatus of intact endothelium, unlike Panx1. (A) Immunostaining of murine third-order mesenteric arteries prepared en face. Cellular compartment markers (yellow; Top: CD31/PECAM-1, interendothelial junctions; Middle: Calnexin, endoplasmic reticulum; Bottom: GM-130, Golgi Apparatus), Panx3 (magenta), nuclei (cyan). (B) Colocalization between Panx3 and each cellular compartment was quantified via unpaired t-tests of Manders' Overlap Coefficients (** is $p < 0.01$, *** is $p < 0.001$). Each dot represents one mouse (3 fields of view). (C) Panx1 (red) colocalizes with interendothelial junction marker Claudin 5 (yellow) in resistance endothelium prepared en face. Nuclei are shown in cyan. (D) Polarization of endothelial Panx3 is dependent on vessel type. Panx3 is polarized upstream (white arrowheads) of the nucleus in arteries, but polarization is lost in veins. Black arrowheads indicate downstream polarization. Blood flow arrow indicates direction of flow. Quantification at right. *** indicates $p < 0.001$ via two-way ANOVA ($p = 0.0003$). Artery N = 7 mice, Vein N = 3 mice. (E) Western blotting for Panx3 (mesenteric vascular lysate) and Panx1 (lung lysate) following deglycosylation by PNGase F. Scale bars are 20 μm throughout.

Figure 5: Subcellular distribution of endothelial Panx3 is regulated by shear stress.

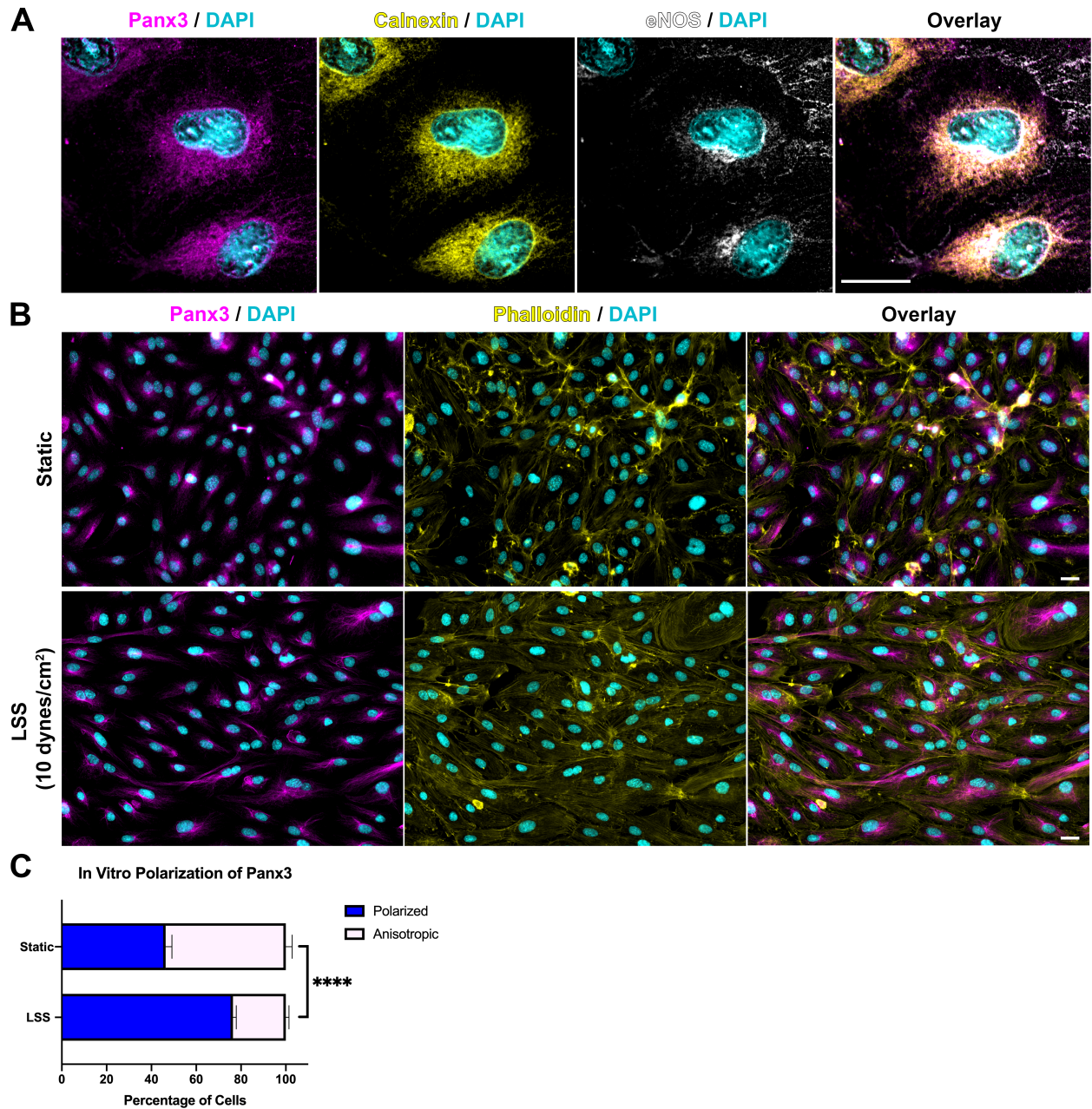


Figure 5: Subcellular distribution of endothelial Panx3 is regulated by shear stress. (A) Immunostaining of human aortic endothelial cells grown under static conditions. Panx3 is depicted in magenta. Endoplasmic reticulum is depicted in yellow, via Calnexin, and the Golgi Apparatus is shown in white via eNOS. (B) Comparison of Panx3 (magenta) and filamentous actin (phalloidin, yellow) in human aortic endothelial

cells grown under static conditions (top) or exposed to 10 dynes/cm² of laminar shear stress (LSS). (C)

Quantification of Panx3 polarization. Scale bars are 20μm.

Figure 6: Generation of an inducible, endothelial cell-specific *Panx3* knockout mouse (*EC Panx3^{Δ/Δ}*).

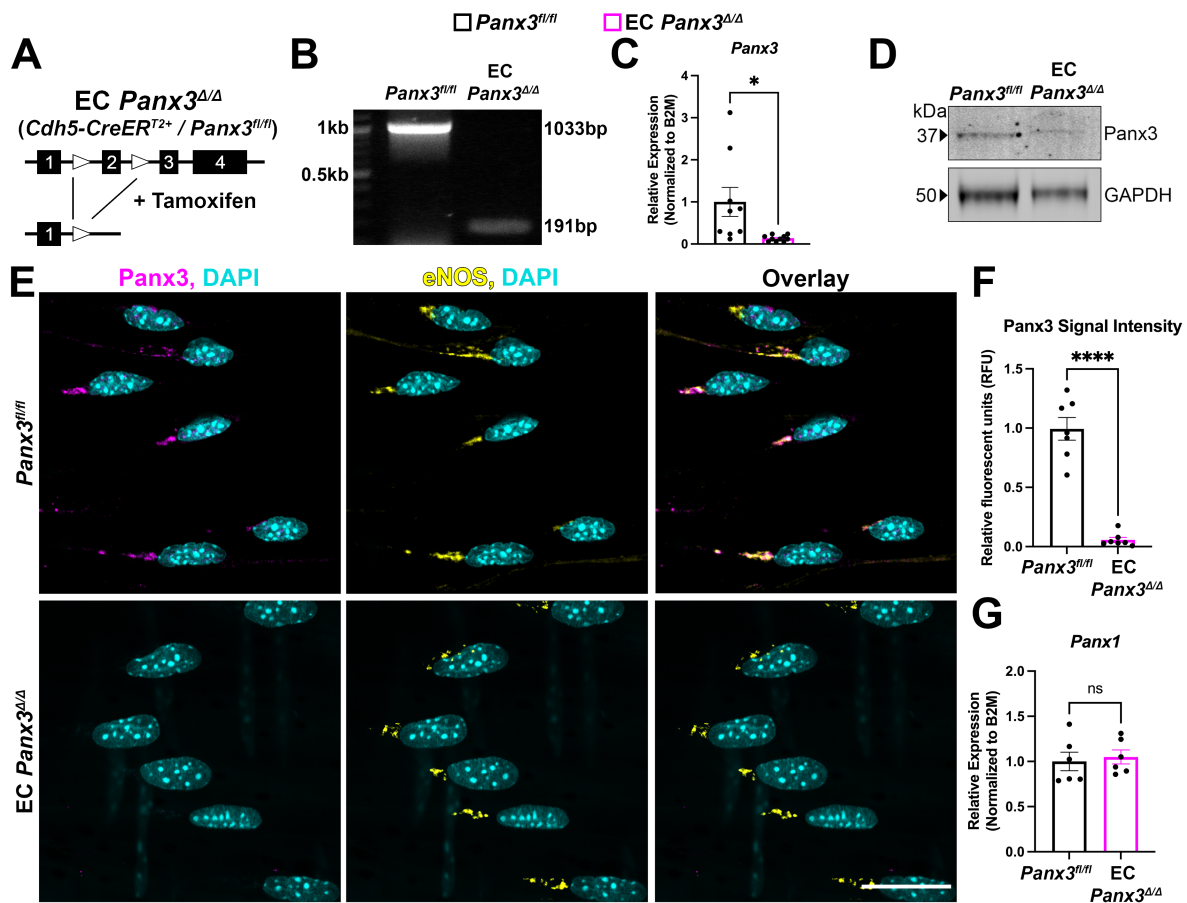


Figure 6: Generation of an inducible, endothelial cell-specific *Panx3* knockout mouse (*EC Panx3^{Δ/Δ}*). (A) Genetic targeting strategy for the generation of *EC Panx3^{Δ/Δ}* mice using the inducible *Cdh5-CreER^{T2}* system. (B) gDNA excision of the second exon of *Panx3*. (C) *Panx3* mRNA abundance is reduced ~85% in endothelial-rich lung tissue. * is $p < 0.05$ via unpaired t-test with Welch's correction. (D, E) Loss of *Panx3* protein in *EC Panx3^{Δ/Δ}* mice is shown by western blot from mesenteric vascular tissue and immunohistochemistry of the endothelium of third-order mesenteric arteries viewed en face. (F) Fluorescence intensity quantification. **** is $p < 0.0001$ via unpaired t-test with Welch's correction. (G) *Panx1* mRNA abundance is unchanged by loss of *Panx3* in endothelial-rich lung tissue. Throughout the figure, each dot represents one mouse.

Figure 7: EC $Panx3^{\Delta/\Delta}$ mice exhibit unremarkable gross anatomy, blood lipids, heart and kidney functions, and splenic B cell development.

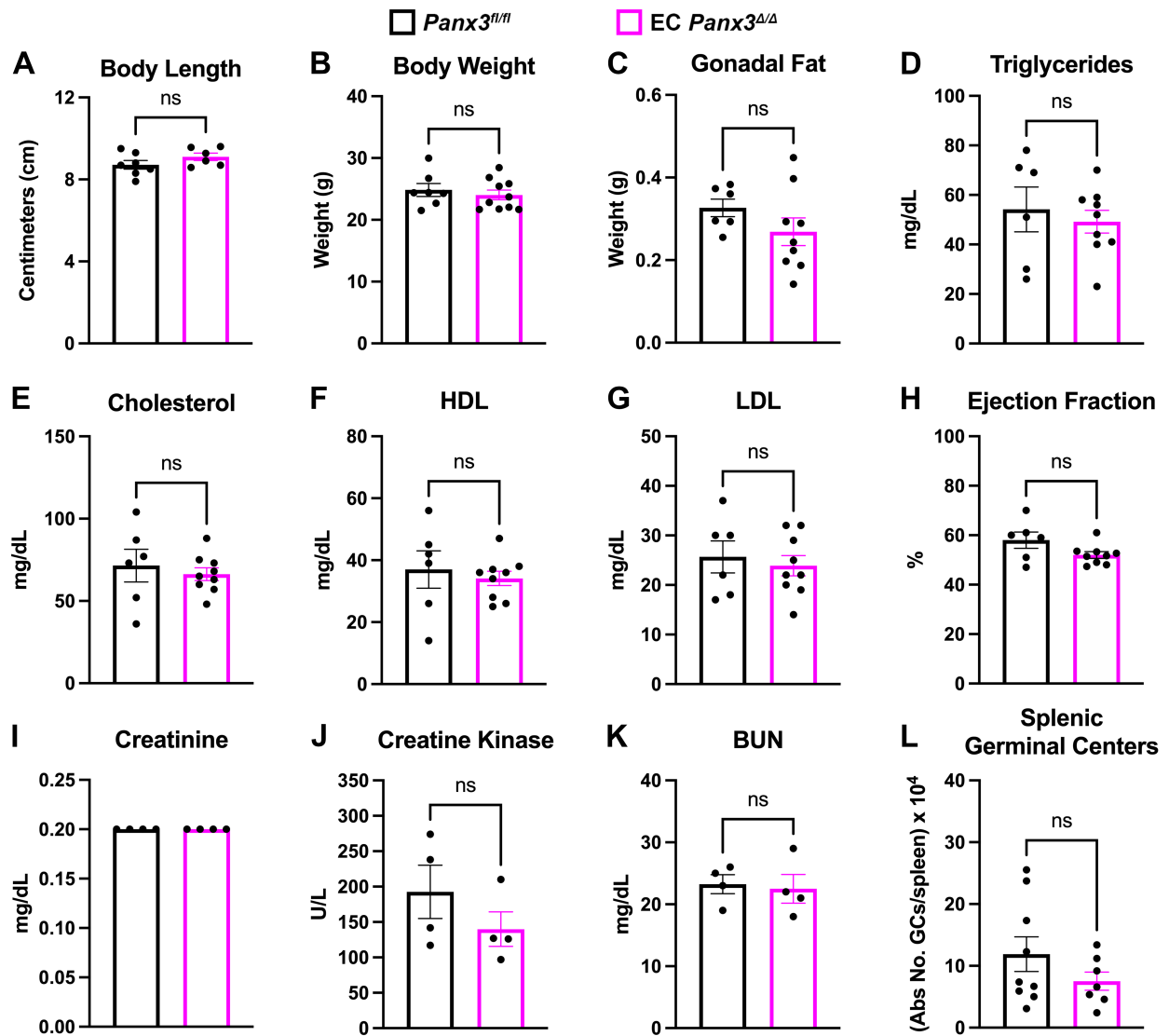


Figure 7: EC $Panx3^{\Delta/\Delta}$ mice exhibit unremarkable gross anatomy, blood lipids, heart and kidney functions, and splenic B cell development. (A, B, C) Body length (nose to anus), body weight, and gonadal fat pad weight are unchanged by loss of endothelial $Panx3$. (D-G) Blood lipids were unchanged by genotype. (H) Cardiac MRI revealed no significant differences in functional parameters including ejection fraction. (I-K) Blood testing for serum creatinine, creatine kinase, and Blood Urea Nitrogen (BUN) reveal no difference in kidney function between EC $Panx3^{\Delta/\Delta}$ mice and controls. (L) Flow cytometry reveals the abundance of $B220^{+}GL7^{+}FasL^{+}$ splenic germinal centers are unchanged by endothelial $Panx3$ expression.

Figure 8: Genetic deletion of endothelial Panx3 impairs peripheral resistance and induces spontaneous hypertension.

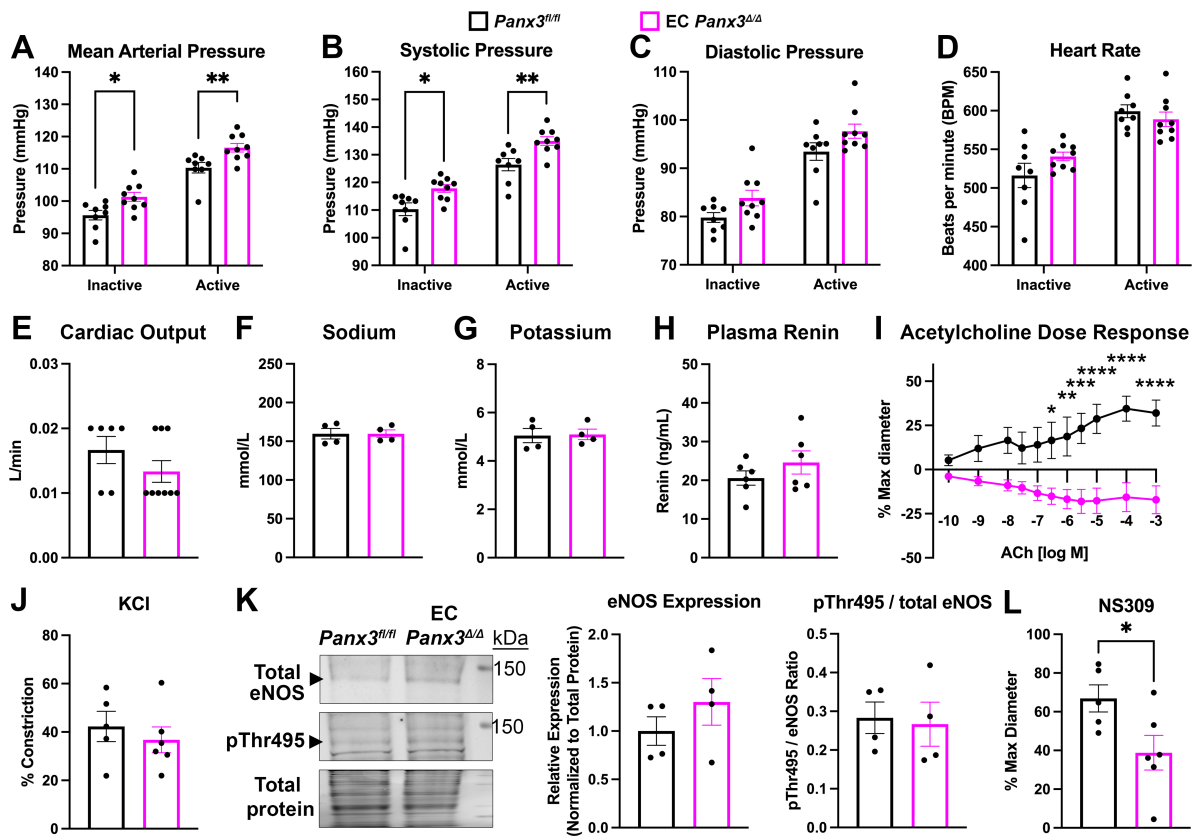


Figure 8: Genetic deletion of endothelial Panx3 impairs peripheral resistance and induces spontaneous hypertension. (A, B) EC Panx3^{Δ/Δ} mice exhibit significantly increased mean arterial and systolic blood pressure at each time period assessed as measure by implanted radiotelemetry. * is p<0.05; ** is p<0.01 via unpaired t-test. (C, D) Diastolic pressure and heart rate remain unchanged. (E) Cardiac output as measured by cardiac MRI. (F, G) Blood levels of sodium and potassium. (H) Renin concentrations in blood plasma collected during the active period. (I) Acetylcholine (ACh)-induced dilation of third-order mesenteric arteries from EC Panx3^{Δ/Δ} (magenta) mice is severely impaired as compared to Panx3^{fl/fl} littermates (black) via pressure myography. N = 5 mice/group with 1-3 arteries averaged per condition per mouse. * is p<0.05; ** is p<0.005; *** is p<0.0005 between genotypes via two-way ANOVA with Šídák's multiple comparison test. (J) Constriction to KCl. (K) Western blot analysis of eNOS expression and

phosphorylation at Thr495. (L) Dilation of third-order mesenteric arteries to 1 μ M NS309. * is $p < 0.05$ via unpaired t-test. Each dot represents one mouse.

Figure 9: Renal infiltration by macrophages and T_{reg} cells is unchanged by genetic deletion of endothelial *Panx3*.

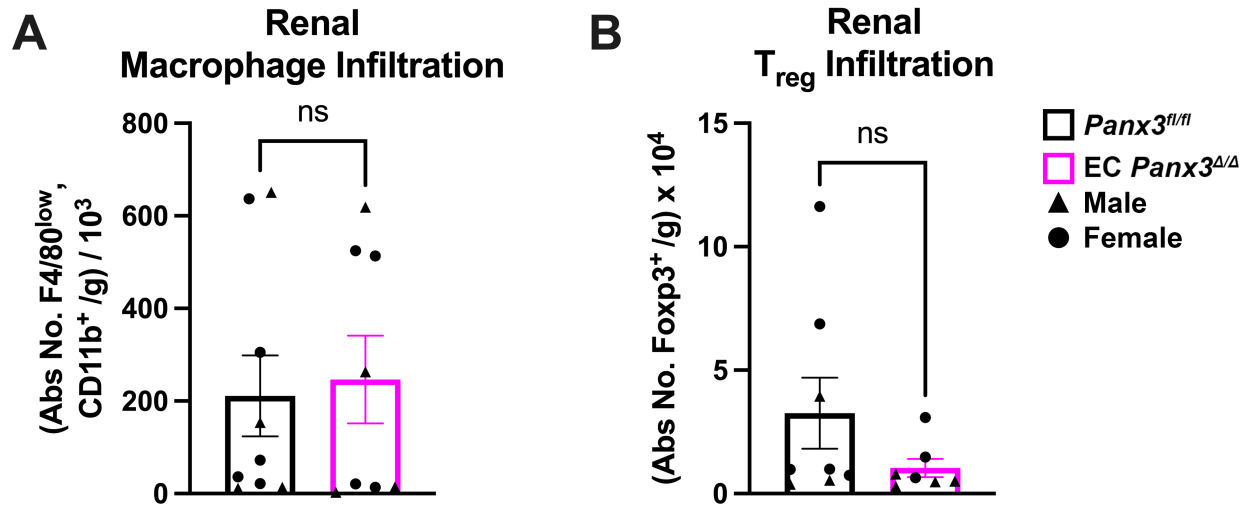


Figure 9: The abundance of CD4⁺, F4/80^{low}, CD11b⁺ macrophages and CD4⁺, CD25⁺, FoxP3⁺ Treg cells were assessed in kidney homogenates from EC *Panx3* mice by flow cytometry. Each dot represents one mouse, with sex indicated by symbol. 'ns' indicates $p > 0.05$ via unpaired t-test.

Figure 10: Channel-independent association of Panx3 and transcriptional repressor Bcl6 in intact endothelium.

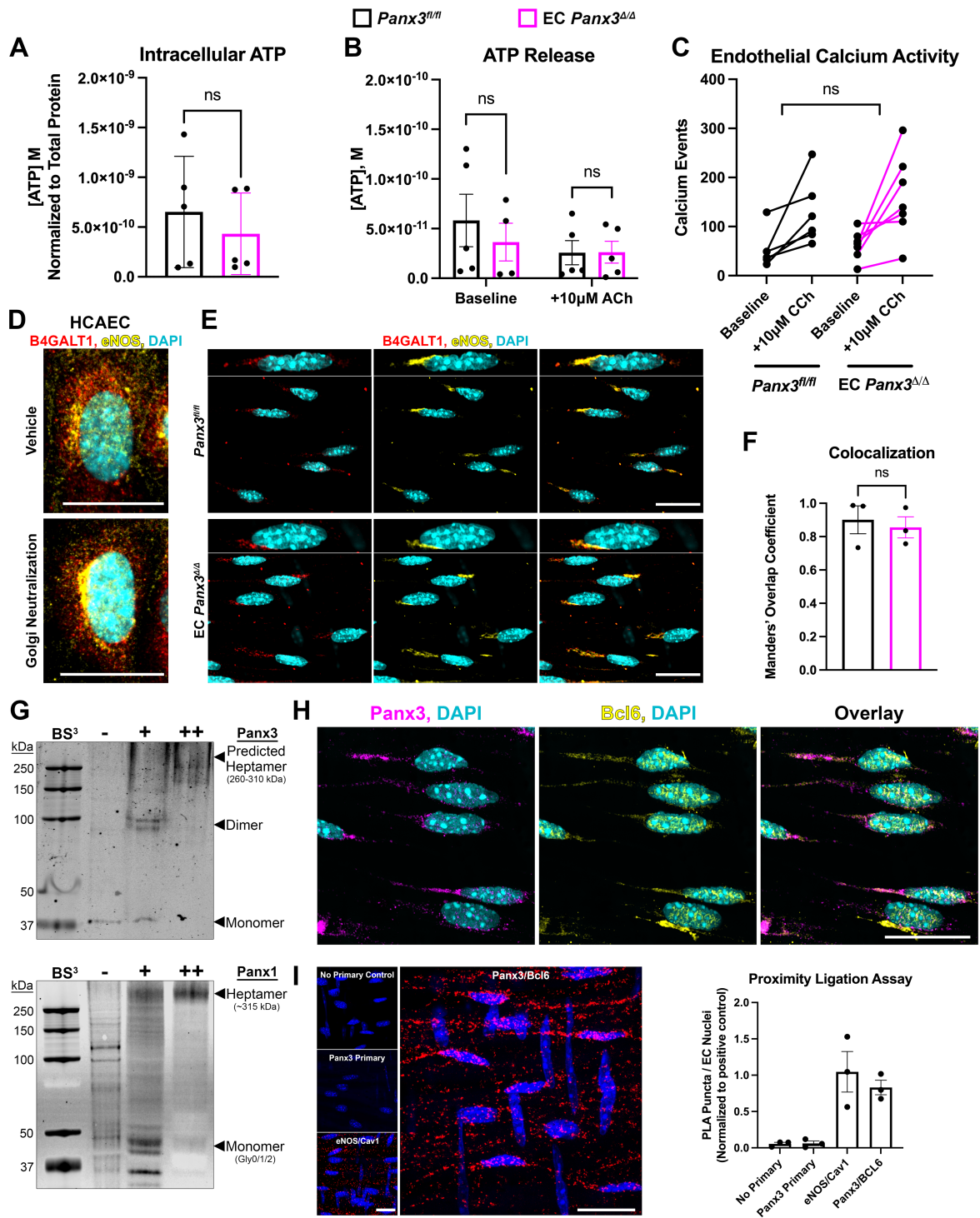


Figure 10: Channel-independent association of Panx3 and transcriptional repressor Bcl6 in intact endothelium. (A, B) Loss of endothelial Panx3 does not alter intracellular ATP or ATP released following

ACh stimulation (10 μ M, 5 min) of third-order mesenteric arteries. Each dot represents one mouse. (C) The number of transient calcium events per field of view under basal conditions or following 10 μ M carbachol (CCh) stimulation in third-order mesenteric arteries. Each dot represents one artery. N = 4 mice per group with 1-2 arteries per mouse. * indicates $p < 0.05$ via paired t-test. Unpaired t-tests were used to compare genotypes. (D) Golgi neutralization via treatment with 2.5mM NH₂Cl displaces B4GALT1 (red) from the Golgi (shown in yellow via eNOS) in human coronary artery endothelial cells. Nuclei are depicted in cyan. (E) Intact mesenteric endothelium exhibits no change in the subcellular distribution of B4GALT1 (red) following loss of EC Panx3. Golgi is depicted in yellow (eNOS), nuclei are shown in cyan. (F) Colocalization analysis of B4GALT1 and eNOS in resistance endothelium. (G) Top: Crosslinking of endogenous Panx3 from mesenteric vascular tissue with 0.5mM (+) or 2.5mM (++) BS3 results in a doublet at ~90 kDa but larger heptameric species are not observed. Bottom: Crosslinking of Panx1 from lung tissue reveals heptameric state. (H) Immunostaining for Panx3 (magenta) and Bcl6 (yellow) in intact resistance endothelium. Nuclei are depicted in cyan. (I) Proximity ligation assay suggests Panx3 and Bcl6 are within close proximity in intact resistance endothelium. Negative (No Primary, Panx3 Primary alone) and positive controls (eNOS/Cav1) shown at left. PLA puncta generation quantified at right. Each dot represents one mouse. Scale bars are 20 μ m.

Figure 11: EC $Panx3^{\Delta/\Delta}$ mice exhibit increased endothelial TRPV4 activity.

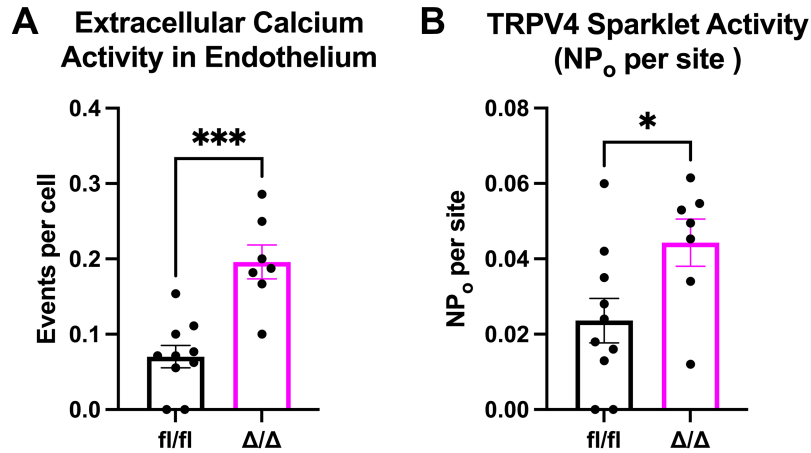


Figure 11: EC $Panx3^{\Delta/\Delta}$ mice exhibit increased endothelial TRPV4 activity. (A) The number of transient calcium events per field of view in the presence of SERCA inhibitor, CPA (20 μ M; included to deplete intracellular calcium stores) in third-order mesenteric arteries from $Panx3^{fl/fl}$ (fl/fl, black) and EC $Panx3^{\Delta/\Delta}$ (Δ/Δ , magenta) mice. (B) Endothelial TRPV4 sparklet activity (NP_0) per site in en face preparations of third-order mesenteric arteries. ‘N’ is the number of channels per site and ‘ P_0 ’ is the open probability of the channel. Each dot represents one artery. N = 4 mice per group with 1-2 arteries per mouse. *** indicates $p < 0.0005$, * indicates $p < 0.05$ via unpaired t-tests were used to compare genotypes.

Figure 12: Genetic deletion of endothelial *Panx3* does not alter Golgi pH but does ablate interaction of *Panx3/Bcl6* in intact endothelium.

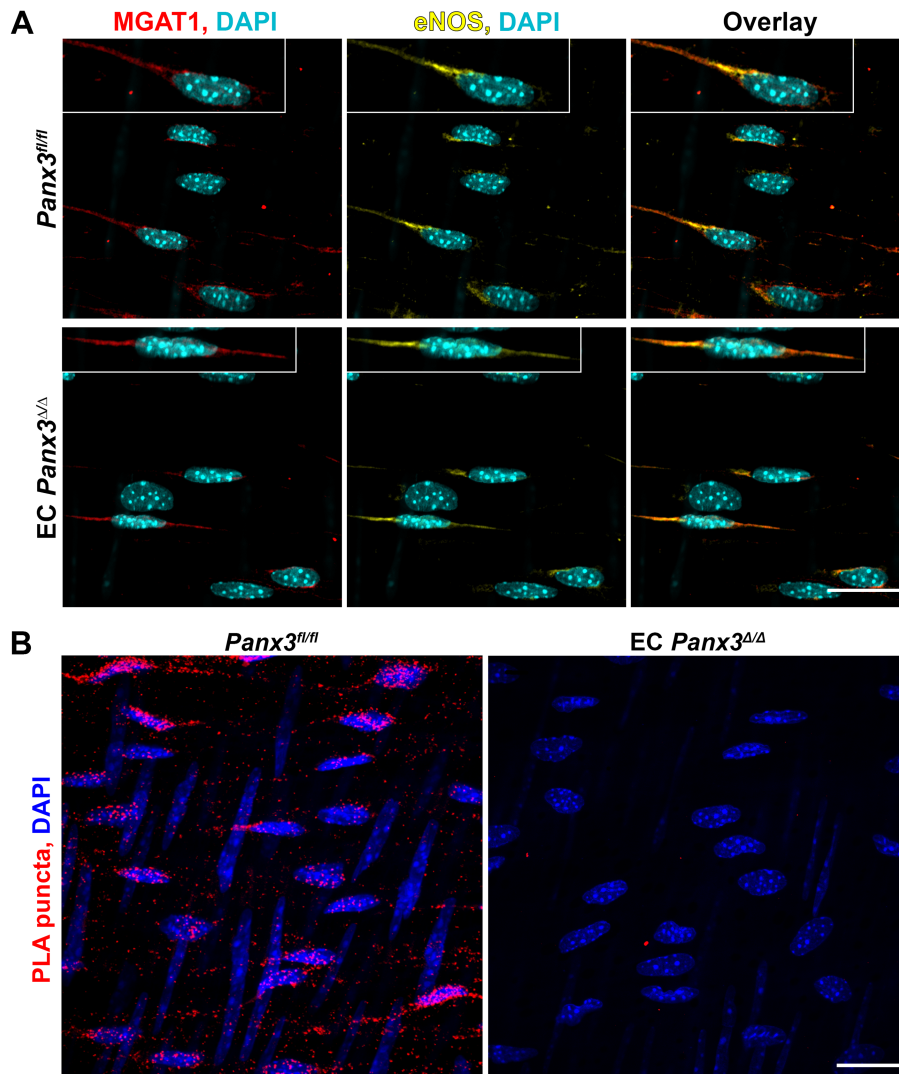


Figure 12: Genetic deletion of endothelial *Panx3* does not alter golgi luminal pH regulation but does ablate interaction of *Panx3/Bcl6* in intact endothelium. (A) Visualization of MGAT1 (red) in mesenteric resistance endothelium with Golgi apparatus depicted in yellow (eNOS), and nuclei are shown in cyan. (B) Proximity ligation assay for *Panx3* and *Bcl6* in *Panx3^{fl/fl}* and EC *Panx3^{Δ/Δ}* resistance endothelium. Scale bars are 20 μ m.

Figure 13: Genetic deletion of endothelial *Panx3* is associated with decreased *Bcl6* protein, increased $\text{NF}\kappa\text{B}$ activity and the specific upregulation of *Nox4*, which can be predicted by evidence of *Bcl6* transcriptional activity.

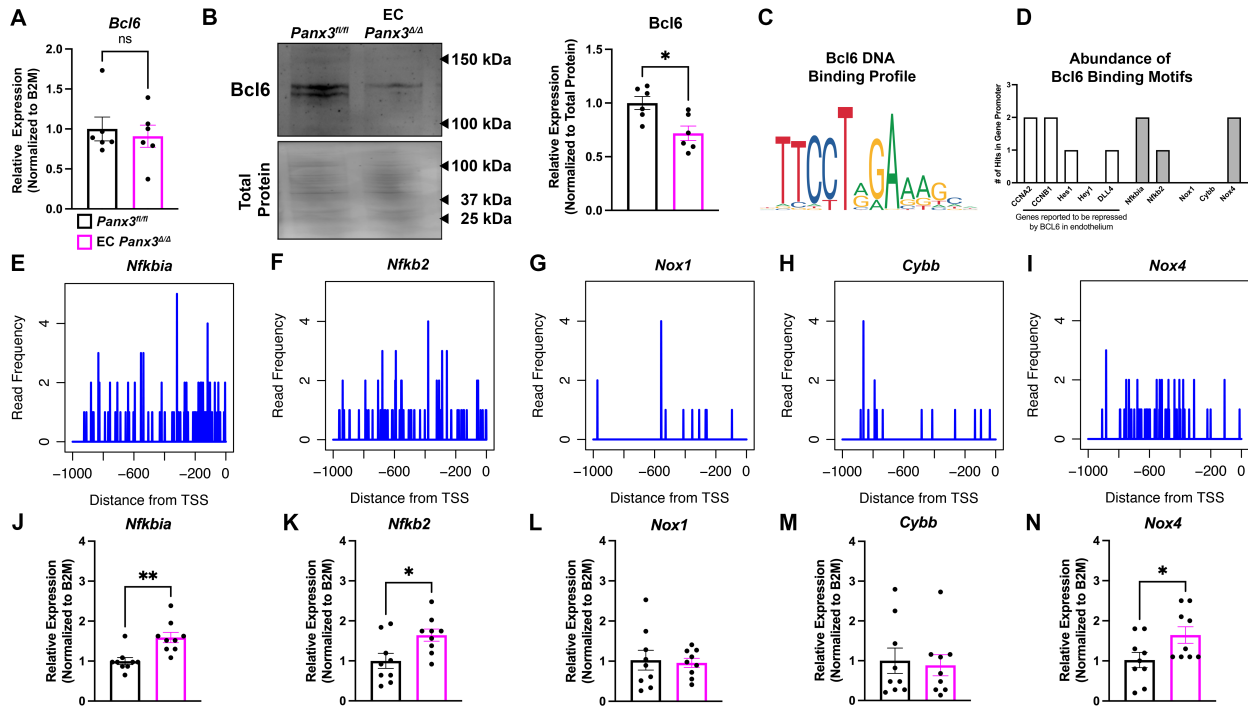


Figure 13: Genetic deletion of endothelial *Panx3* is associated with decreased *Bcl6* protein, increased $\text{NF}\kappa\text{B}$ activity and the specific upregulation of *Nox4*, which can be predicted by evidence of *Bcl6* transcriptional activity. (A) *Bcl6* mRNA is unchanged following deletion of EC *Panx3*. (B) Western blotting for *Bcl6* in endothelial-rich lung tissue. (C, D) The JASPAR sequence logo for murine *Bcl6* (MA0463.1) was used for in silico assessments of the 1000bp sequences preceding the transcriptional start side (TSS) of genes of interest. (E-I) *Bcl6* ChIP-Seq^{141, 161, 162} binding profiles in the promoter region of genes of interest. (J-N) Transcript abundance for the same genes of interest assessed in lung tissue from *Panx3*^{fl/fl} and EC *Panx3*^{Δ/Δ} mice. Each data point represents one mouse. * indicates $p < 0.05$; ** indicates $p < 0.001$ via unpaired t-test.

Figure 14: Endothelial *Panx3* protects against H_2O_2 -induced oxidative stress and prevents endothelial-mediated vascular dysfunction in resistance arteries.

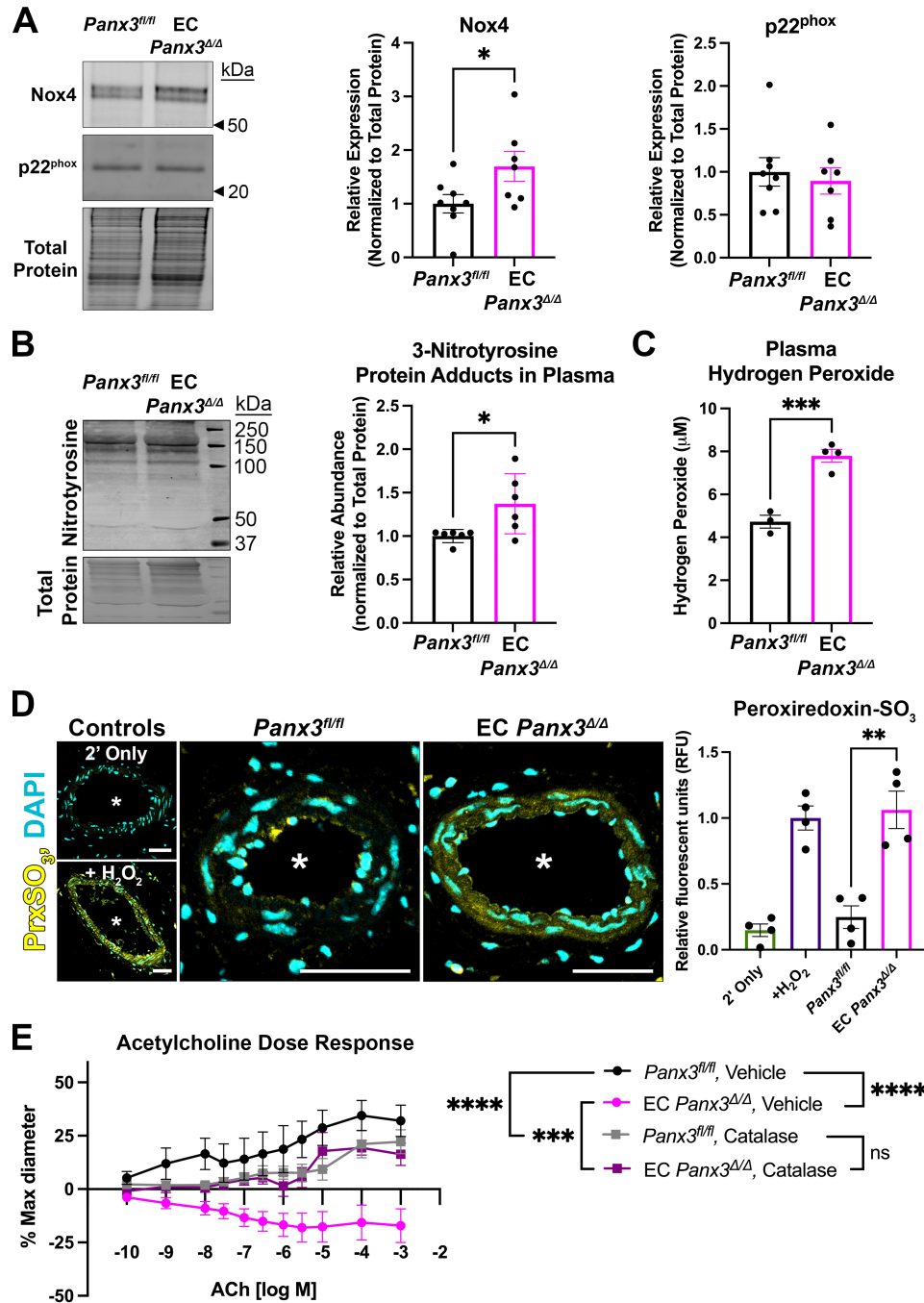


Figure 14: Endothelial *Panx3* protects against H_2O_2 -induced oxidative stress and prevents endothelial-mediated vascular dysfunction in resistance arteries. (A) Western blot and quantification of Nox4 and p22^{phox} in lung lysates. (B) Relative abundance of 3-Nitrotyrosine protein adducts assessed from plasma. * indicates statistical significance.

indicates $p < 0.05$ via unpaired t-test with Welch's correction. (C) Quantification of H_2O_2 in deproteinized plasma collected via AmplexRed fluorescence. *** indicates $p < 0.001$ via unpaired t-test. (D) Immunodetection and quantification of hyperoxidized peroxiredoxin (PrxSO₃, yellow) in transverse sections of third-order mesenteric arteries. Nuclei are shown in cyan. In images, * indicates vessel lumen. '+ H₂O₂' positive controls were exposed to 1mM H₂O₂ and 1mM NaNO₂ prior to antigen retrieval. Mean fluorescent signal was normalized to positive controls. Scale bars are 50μm. ** indicated $p < 0.005$ via unpaired t-test. (E) Acetylcholine (ACh)-induced dilation of third-order mesenteric arteries. Vehicle conditions replicated from Figure 8I. Pretreatment with PEG-catalase (1000U/mL) results in partial rescue of the dilatory response. Repeated measures one-way ANOVA with Geisser-Greenhouse correction and Šídák's multiple comparisons test was used to compare the dose response curves between each condition. *** indicates $p < 0.001$, **** indicates $p < 0.0001$.

Figure 15: Evidence of Oxidative Stress in the aortic vascular wall in EC $Panx3^{\Delta/\Delta}$ mice.

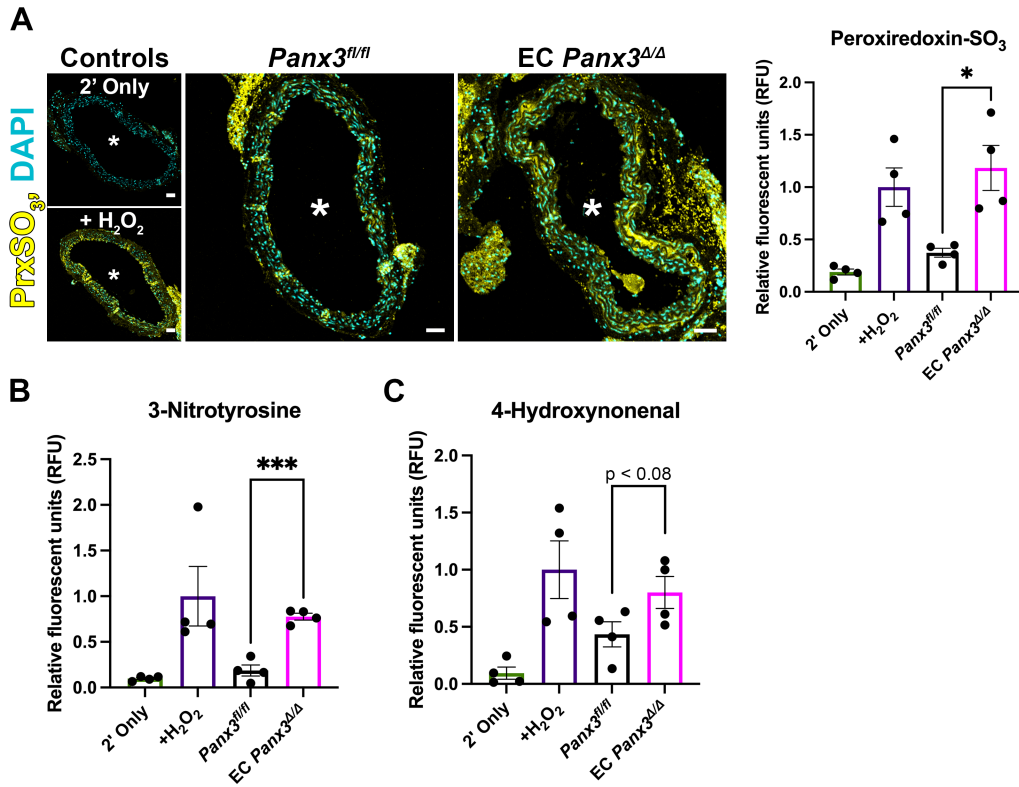


Figure 15: Evidence of Oxidative Stress in the aortic vascular wall in EC $Panx3^{\Delta/\Delta}$ mice. (A) Immunodetection and quantification of hyperoxidized peroxiredoxin (PrxSO₃, yellow) in transverse sections of descending thoracic aorta. * indicates $p < 0.05$ via unpaired t-test between genotypes. Scale bars are 50 μ m. (B) 3-Nitrotyrosine protein adducts are significantly elevated in the vascular wall of EC $Panx3^{\Delta/\Delta}$ mice as compared to controls. *** indicates $p < 0.005$ via unpaired t-test between genotypes. (C) Lipid peroxidation as observed via 4-hydroxynonenal staining exhibits a similar trend ($p = 0.0846$ via unpaired t-test). In all graphs, '+ H_2O_2 ' indicates that samples were briefly exposure to 1mM H_2O_2 and 1mM $NaNO_2$ prior to antigen retrieval to be used as positive controls. Mean fluorescent signal was normalized to positive controls. Each dot represents the average from 2-3 cross sections per mouse.

Figure 16: Assessment of other potential sources of oxidative stress following genetic deletion of endothelial *Panx3*.

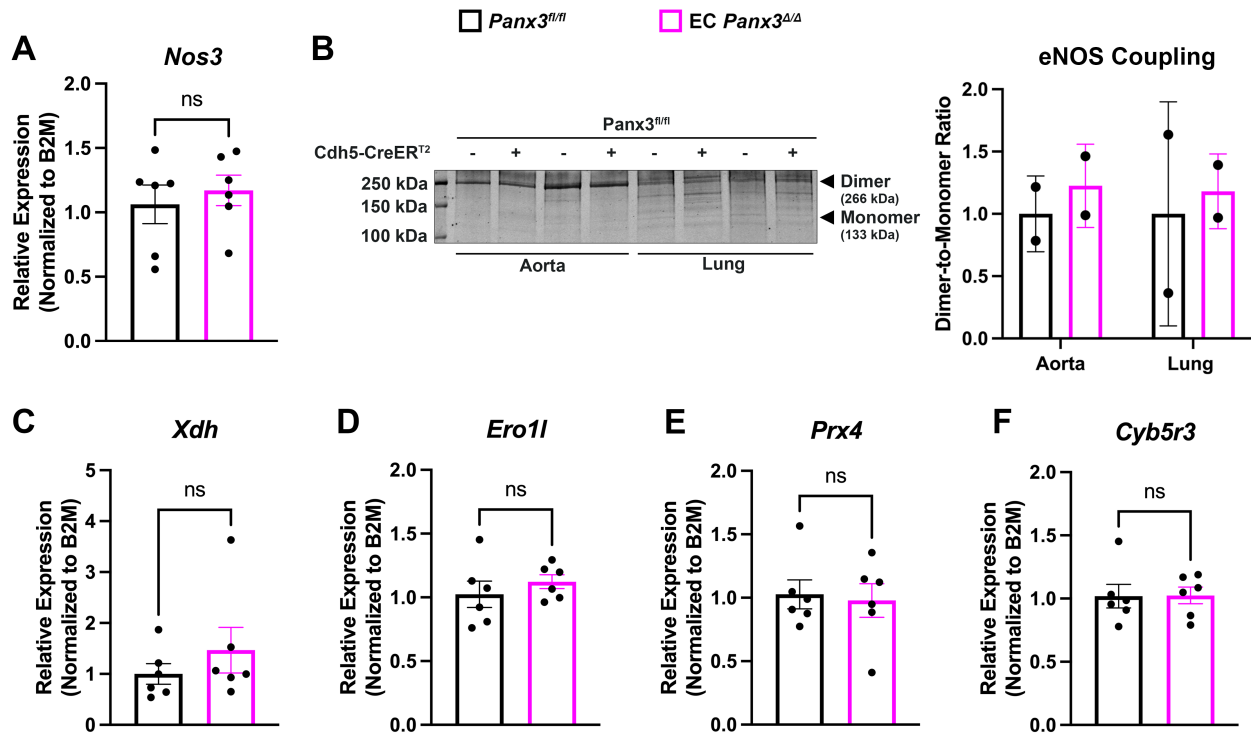


Figure 16: Assessment of other potential sources of oxidative stress following genetic deletion of endothelial *Panx3*. (A) Transcript levels of *Nos3* (eNOS) are unchanged in endothelial-rich lung tissue by endothelial *Panx3* expression. (B) Structural eNOS coupling is not altered by loss of *Panx3* in thoracic aorta and lung tissue. Dimer to monomer ratio is normalized to controls. (C-F) mRNA abundance for *Xdh* (xanthine oxidase), *Ero1l* (endoplasmic reticulum oxidoreductase 1 α), *Prx4* (peroxiredoxin 4), *Cyb5r3* (cytochrome B5 reductase 3) are consistent in lung tissue between *EC Panx3^{Δ/Δ}* mice (magenta) and controls (black).

Table 1: Rational Design of BCLiP peptide

| Candidate Sequences | Bcl6 Region | Features | E ¹ | Homology | | | Rationale for Exclusion |
|-------------------------------|---------------|---|----------------|---------------|----------------|----------------|----------------------------------|
| | | | | Protein | Query Coverage | Identity Match | |
| LVSPQSPQKSDCQP NSP (BCLiP) | L328- P344 | Phosphorylation of S333 and S343 target Bcl6 for degradation ¹³⁹ | 18.07 | | | | Not excluded |
| VNRSMTGSPRSSSES HSP | N450- P467 | Polar, disordered regions ¹⁹² | 15.67 | | | | Lower predicted binding affinity |
| SGLFYISFTDQLKCN LS | S54- S70 | Mutagenesis of S59 impairs Bcl6 ubiquitinylation and degradation ¹⁹³ | 23.65 | Svs2 | 41% | 100% | Not unique peptide sequence |
| KACNWKKYKFIVL NSLN | K371- Q388 | K376-K379 is required for interaction with NuRD complex and transcriptional activity ¹³¹ | 26.43 | Bcl6b | 100% | 100% | Not unique peptide sequence |
| RLSPRAYTAPPACQ PPM | R402- M418 | S404 is a predicted phosphorylation site ¹⁹⁴ | 17.98 | mCG14 6998 | 41% | 100% | Not unique peptide sequence |
| HSGEKPYKCETCGA RFVQVA | H596- A615 | Zinc finger domain, C604-C607 facilitates nuclear localization ¹⁹⁵ | 23.03 | Bcl6b | 100% | 95% | Not unique peptide sequence |
| IHTGEKPYHCEKCN LHFR | I651- R674 | Zinc finger domain, C660-C663 facilitates nuclear localization ¹⁹⁵ | 22.49 | Znf300 | 100% | 72% | Not unique peptide sequence |
| | | | | Bcl6b | 100% | 83% | |

| | | | | | | | |
|--------------------------|---------------|--|-------|--|--|--|---|
| ACILQASGSPPAKSP TDP | A353- P370 | S361 is a predicted phosphorylation site ¹⁹⁴ | 20.82 | | | | Predicted binding is inaccessible in physiological conditions |
| FTDQLKCNLSVINL DPEINP | F61- P80 | Fragment of BTB domain | 21.62 | | | | Predicted binding is inaccessible in physiological conditions |
| PLNRKGLVSPQSPQ KSDC | P322- C339 | Polar, disordered regions ¹⁹² | 18.32 | | | | Predicted binding is inaccessible in physiological conditions |

Table 1: Rational Design of BCLiP peptide. This table summarizes the selection of the BCLiP amino acid sequence (highlighted in green). Ten candidate Bcl6 mimetic sequences were initially identified based on literature review were modeled with the predicted Panx3 structure to assess potential interactions and identify regions in Panx3 involved with the interaction (Figure 16). Docking scores (‘E’) assess binding energetics due to electrostatic interactions and desolvation effects. Exclusion criteria for candidate peptides include non-unique peptide sequences, binding predictions involving regions that would be inaccessible under physiological conditions, and lower predicted binding affinity.

Figure 17: Inhibition of the Panx3/BCL6 interaction via BCLiP peptide phenocopies genetic deletion of endothelial Panx3.

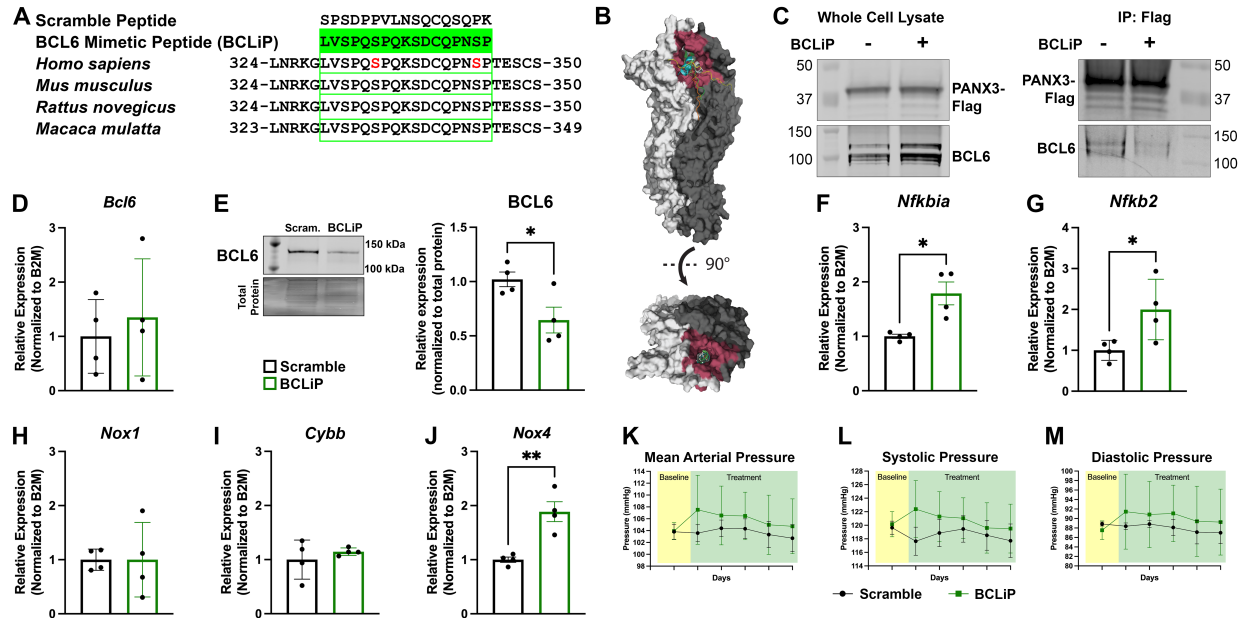


Figure 17: Inhibition of the Panx3/Bcl6 interaction via BCLiP peptide phenocopies genetic deletion of endothelial Panx3. (A) The BCLiP amino acid sequence mimics a highly evolutionarily conserved region of BCL6 (L328-P344). S333 and S343 are highlighted in red to denote MAPK phosphorylation sites which drive Bcl6 degradation. (B) Side view (top) and top-down view (bottom) of dimeric Panx3 (monomers in shades of grey) interaction with BCLiP (colored). Panx3 residues involved with peptide interactions are depicted in maroon. (C) Immunoprecipitation of Bcl6 using Panx3-Flag as bait from HEK cells transfected with Panx3-Flag and Bcl6. (D, E) mRNA of *Bcl6* is unchanged following five days of BCLiP or scramble peptide administration (12.5mg/kg via I.P.), while Bcl6 protein is significantly reduced. (F, G) mRNA expression of autoregulated NFκB family members *Nfkb1a* and *Nfkb2* is increased following BCLiP administration. *Nfkb1a* was compared via unpaired t-test with Welch's correction. (H-J) BCLiP treatment significantly increased *Nox4* expression but not *Nox1* or *Cybb*. (K-M) Radiotelemetry reveals elevation of mean arterial (K), systolic (L) and diastolic (M) blood pressure throughout the period of BCLiP administration. * is $p < 0.05$; ** is $p < 0.01$ via unpaired t-test.

Figure 18: Schematic of endothelial Panx3/Bcl6 interactions.

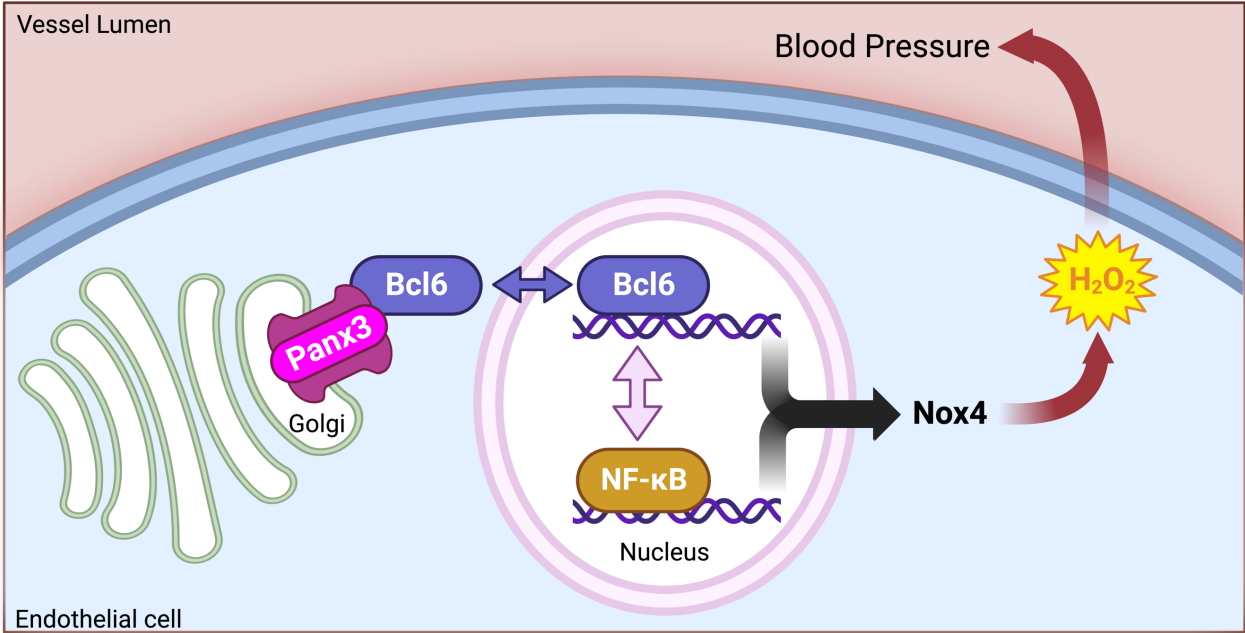


Figure 18: Schematic of endothelial Panx3/Bcl6 interactions.

3.4: Discussion

Using both genetic and pharmacological systems, we present the first demonstration of the Panx3-Bcl6 interaction as an important regulator of vascular oxidative stress and systemic blood pressure. In our current model (Figure 18), endothelial Panx3 distributes to the Golgi membrane where it can interact with the extranuclear pool of Bcl6. In the absence of Panx3 or following peptide inhibition of the Panx3-Bcl6 interaction, the abundance of Bcl6 is significantly reduced, NF κ B activity is increased, and Nox4 is selectively upregulated, driving chronic H₂O₂ generation and elevating blood pressure. In this system, imbalance in endogenous ROS generation drives oxidative stress and cardiovascular disease.

Oxidative stress is a critical determinate of cardiovascular health. O₂⁻ has well-established roles driving hypertension,^{196, 197} atherosclerosis,^{198, 199} and ischemia/reperfusion injury.^{200, 201} Obesity-related imbalances of peroxynitrite (ONOO⁻) in endothelium have been shown to impair endothelial cell function and drive hypertension.¹⁰ Circulating levels of O₂⁻ and H₂O₂ are increased in hypertensive patients, though the abundance of both ROS were effectively reduced when antihypertensive therapies successfully attenuate blood pressure.²⁰² However, redox signaling is an important tenet of normal cardiovascular physiology. H₂O₂ in particular has been recognized as a major redox signaling molecule involved in many beneficial cell processes.^{14, 52, 203-208} Perhaps it is not surprising that administration of general antioxidants have been ineffective at reducing oxidative stress-related cardiovascular diseases.^{36, 37} It is possible that healthy physiological systems require a balance, not an ablation, of oxidant generation and antioxidant defenses to avoid injurious effect. Indeed, ROS are mediators of a variety of cellular process in the vasculature including but not limited to nitric oxide (NO)-mediated dilation, and O₂⁻ production downstream of renin-angiotensin-aldosterone signaling. Here we uncover a novel mechanism of redox dysregulation which develops following disruption of the Panx3/Bcl6 interaction, involving persistent overproduction of H₂O₂. Initial studies in human patients hint that maintenance of the Panx3-Bcl6 interaction may hold clinical relevance as a potential therapeutic target for resistant hypertension (Figure 1). Developing clinical

strategies to target specific ROS imbalance may prove to be more effective than general antioxidants administration for cardiovascular diseases.

Our evidence implicates oxidative dysfunction of resistance arteries and blood pressure is due to H_2O_2 , likely by Nox4. However, although the majority of reactive species produced by Nox4 appear to be H_2O_2 , it does not completely preclude effects due to superoxide (O_2^-).⁴⁰ We observe a significant increase in 3-nitrotyrosine in the circulation (Figure 14B) and aortic wall (Figure 15B) following loss of endothelial Panx3. 3NT protein adducts are canonically generated following tyrosine nitration by $ONOO^-$. H_2O_2 is insufficient to directly drive production of $ONOO^-$, but nitric oxide (NO) reacts rapidly with O_2^- to generate $ONOO^-$, which may suggest dysregulation of O_2^- following genetic deletion of endothelial Panx3. However, it is unclear if this occurs downstream of disrupting the Panx3-Bcl6 interaction because tyrosine nitration can alternatively be generated when H_2O_2 and nitrite (NO_2^-) react with heme-containing proteins,²⁰⁹ such as endothelial α -globin.^{210, 211}

In the vasculature, H_2O_2 has been shown to induce contradictory vasoactive effects based on dose, duration, and vascular tone. Ex vivo systems across multiple species and vascular beds demonstrate exposure to low levels ($<10^{-4}M H_2O_2$) strengthens basal tone and induces a mild constriction, likely mediated by thromboxane A_2 /prostaglandin H_2 .^{52, 204, 206, 208} Higher concentrations ($>10^{-4}M H_2O_2$) induce a potent dilatory response following a brief constriction,^{52, 204, 205, 208} with many works suggesting a role for H_2O_2 as an endothelium-derived hyperpolarization factor (EDHF).²¹²⁻²¹⁷ Constitutive endothelial-specific overexpression of Nox4 has been reported to lower blood pressure.⁵³ While Nox4 expression was not quantified, vascular H_2O_2 was increased 7-fold in this system via xylenol orange assay, suggesting a dramatic increase in Nox4 abundance in their system.⁵³ In contrast, interruption of the Panx3-Bcl6 interaction, either from our genetic model or following BCLiP administration, results in mild, but significant increase in expression and abundance of H_2O_2 -producing Nox4 (Figures 13N, 14A, and 17J). This was associated with catalase-sensitive impairments in ACh-induced dilation (Figure 8I and 14E) and

systemic hypertension (Figure 8A-B) following genetic deletion of endothelial Panx3. Thus, interruption of the Panx3-Bcl6 interaction induces a mild elevation of intracellular H₂O₂, as the catalase-sensitive dose response to ACh was significantly impaired. Hydrogen peroxide exposure drives phosphorylation of TRPV4 at Ser284, by protein kinase A²¹⁸ as well as Src family of kinases,^{219, 220} ultimately enhancing conductance through TRPV4, which is in line with our observations from intact EC Panx3^{Δ/Δ} endothelium (Figures 11, 13N, and 14A-D). Interestingly, arteries from EC Panx3^{Δ/Δ} mice also exhibit reduced dilation to NS309 (Figure 8L), suggesting that H₂O₂ imbalances impair conductance through small- and intermediate-conductance Ca²⁺-activated K⁺ channels (SK, IK). This finding is not in alignment with reports that exposure to H₂O₂ promotes conductance through SK/IK channels, though the discrepancy may be due to high doses of H₂O₂ (>10⁻⁴M) used in each study.^{221, 222}

Indeed, much of the literature on the effects of H₂O₂ involve bath applied exposure to exogenous H₂O₂, often provided at supraphysiological levels.²⁰³ Recent advances in chemogenetic H₂O₂ probes have been used to demonstrate endogenous imbalance of H₂O₂ can drive distinct localized cellular effects in endothelial cells as compared to application of exogenous H₂O₂, even when intracellular H₂O₂ abundance is perturbed to the same degree.²⁰⁷ For instance, when the H₂O₂ generating probe was targeted to caveolae at the plasma membrane, H₂O₂ generation caused a rapid increase in inhibitory eNOS phosphorylation at Thr495 which was not observed following bath exposure to the same concentration of exogenous H₂O₂.²⁰⁷ The work presented here establishes EC *Panx3*^{Δ/Δ} mice and BCLiP administration as models of redox imbalance which could be used for future studies uncovering role of mild H₂O₂ elevation generated from cellular dysfunction rather than exogenous addition.

Hypertension in EC *Panx3*^{Δ/Δ} mice is independent of renal immune infiltration. Both hypertensive patients and murine models of hypertension are commonly associated with increased tubulointerstitial immune infiltration.²²³⁻²²⁵ Proinflammatory leukocytes can act locally to damage renal tissue through overproduction

of ROS,^{226,227} exacerbating hypertension through activation of the renin-angiotensin-aldosterone system^{228,}
²²⁹ and promotion of sodium retention to increase blood volume.²³⁰ On the other hand, there is a negative
association between renal accumulation of anti-inflammatory white blood cells and high blood pressure.
Aldosterone-induced hypertension is associated with a reduction in T_{reg} cells in the kidney, and adoptive
transfer of FoxP3⁺ T_{reg} cells, but not other CD4⁺ T cells, protects against the development of hypertension.²³¹
However, kidneys from EC *Panx3*^{Δ/Δ} mice and littermate controls exhibit similar degrees of renal invasion
by proinflammatory macrophages and anti-inflammatory T_{reg} cells (Figure 9), indicating that these cell
types are unlikely to contribute to their H₂O₂-induced spontaneous hypertension. Hypertension induced
following deletion of endothelial Panx3 is not likely to be driven by the pathological positive feedback loop
of renal invasion by proinflammatory macrophages, or by anti-inflammatory T_{reg} cells. BCLiP, the novel
Bcl6 mimetic peptide, was generated as an orthogonal means to inhibit the Panx3-Bcl6 interaction from
our genetic model. BCLiP exposure reduced the ability of PANX3 to immunoprecipitate with BCL6 from
human cells (Figure 17C). After five days of IP administration to wildtype mice, BCLiP exposure
successfully recapitulates every mechanistic step of our model, including: (1) reduction in Bcl6 protein, but
not mRNA (Figure 13A-B, 17D-E), (2) increased NFκB activity (Figure 13J-K, 17F-G), (3) specific
upregulation of Nox4 (Figure 13L-N, 17H-J) and (4) elevation of blood pressure (Figure 8A-B, 17K-M).
Further refinement of the dosing schedule and route of administration could likely escalate the effect of
BCLiP on blood pressure. While the use of the BCLiP peptide enabled us to corroborate our findings from
our genetic model, we recognize its various limitations. First, we cannot draw conclusions about the
participation of the L328-P344 region of Bcl6 in the endogenous Panx3-Bcl6 interactions from our current
findings. Moreover, given that BCLiP mimics a region of Bcl6 involved in interaction with MAPK, BCLiP
could potentially compete with Bcl6 for MAPK binding. However, inhibition of Bcl6 binding MAPK would
protect Bcl6 from targeted degradation. Our evidence contradicts this prediction, as BCLiP exposure is
associated with reduced Bcl6 protein abundance (Figure 17E). In addition, BCLiP indiscriminately
interrupts Panx3-Bcl6 interactions, thus we cannot preclude the possibility of BCLiP additionally inducing

oxidative stress in other cell types, such as lymphocytes from which the Panx3-Bcl6 interaction was first reported.¹⁰⁸ Endogenous Nox4 expression is largely restricted to the vasculature and the kidney,⁷² which would limit these confounding effects. Despite these limitations, BCLiP administration phenocopies genetic inhibition of the Panx3-Bcl6 interaction.

Bcl6 stabilization is crucial to redox balance though this has not been studied in endothelium. During germinal center B cell development, Bcl6 is required to drive B cell proliferation and survival despite genotoxic and oxidative damage.^{121, 168-170} Whole mouse genetic knockout of Bcl6 results in premature cardiovascular death due to myocarditis and pulmonary vasculitis by mechanisms that still are not understood.¹²¹ Studies of Bcl6 in endothelium have been limited to its role in angiogenesis, where Bcl6 has been reported to inhibit vascular sprouting and branching,¹²² possibly through Bcl6-associated zinc finger protein (BAZF)-mediation of VEGF signaling and downregulation of notch signaling.¹²⁸ The current study presents the first evidence of a homeostatic role for repression by Bcl6 in endothelium to prevent vascular oxidative stress, as well as a novel regulatory mechanism of Bcl6 activity via interactions with Panx3. The transcriptional activity of Bcl6 is canonically regulated through its targeted degradation, which is accomplished by multiple MAPK phosphorylation sites (including S333 and S343) within PEST motifs driving recruitment to a SCF ubiquitin ligase complex containing FBXO11.^{139, 232} Minor alterations in the balance of Bcl6 expression and degradation have been reported to significantly alter the transcriptome.¹²⁴ In endothelium, the expression of Panx3 promotes Bcl6 stability (Figure 13A-B), suggesting that the Panx3-Bcl6 perinuclear interaction inhibits Bcl6 degradation. Here, Bcl6 protein is significantly reduced, and NFκB activity (Figure 13J-K) and expression of Nox4 (Figure 13N, 14A) are significantly increased. Mutual antagonism between Bcl6 and NFκB has been described in other cell types,¹⁴⁰⁻¹⁴² but these data are the first description of this negative feedback regulation of vascular NFκB. Bcl6 has previously been suggested to regulate vascular Nox4 expression: spontaneously hypertensive rats (SHR) exhibit increased Nox4 expression and reduced Bcl6 expression as compared to Wistar-Kyoto rats (WKY).²³³ Furthermore

lentiviral expression of Bcl6 was able to rescue Nox4 expression and reduce systemic blood pressure in SHR,²³³ further supporting our assertions that stabilization of Panx3-Bcl6 has potential as antihypertensive therapy. Overall, our data suggests Bcl6 promotes homeostatic redox signaling; in the vasculature, interactions with Panx3 maintain Bcl6 expression.

This study also elucidates novel roles and characteristics of endogenous Panx3, for which there is little described in the literature. Vascular Panx3 appears to exert its effect solely through this protein-protein interaction. Although it is unconventional for a channel-based protein to have channel-independent functions, there are examples from other large-pore channels, including connexins and innexins where this has been documented.²³⁴⁻²³⁸ Unlike Panx1, many characteristics of Panx3 appear to vary based on cell type and expression system. Many of the previous works reporting functional roles (dye transfer,^{58, 78, 91, 178} ATP release,^{68, 78, 91} calcium store release^{68, 91}) for Panx3 rely on exogenous overexpression systems, which can dramatically alter Panx3 subcellular distribution^{58-60, 75} and potentially even Panx3 oligomeric state. The endothelial-specific Panx3 knockout mouse model enabled us to study the function of endogenous Panx3 despite its low expression level. For example, we found Panx3 does not contribute to endothelial purinergic signaling (Figure 10A-B) or IP₃-mediated calcium store release (Figure 10C) in intact endothelium. In the vasculature, Panx3 is not sensitive to deglycosylation by PNGase F (Figure 4E), and Panx3 is retained in the membrane of the Golgi apparatus (Figure 4A, 3A, and 3D), suggesting that Panx3 exhibits minimal, if any, glycosylation in this tissue. Unexpectedly, we noted that the subcellular distribution of Panx3 varied between our in vivo and in vitro systems. We consistently observed Panx3 localizing to the Golgi Apparatus in intact endothelium (Figures 3A, 3D, and 4A-B). However, in cultured endothelial cells, endogenous Panx3 is distributed to the endoplasmic reticulum under static culture conditions (Figure 5A), though it readily traffics to the polarized perinuclear region following exposure to shear stress (Figure 5B-C). It is unclear if reports of Panx3 localizing to the endoplasmic reticulum and contributing to calcium store release (as reported in: osteoprogenitor C2C12 cells,⁹¹ primary calvarial cells,⁹¹ primary dental mesenchymal cells,⁶⁹ primary chondrocytes⁶⁸ or immortalized ATDC5 cells⁶⁸) would be similarly confounded when cells

are exposed to physiological stimuli. This illustrates the importance of defining Panx3 subcellular distribution in intact tissue prior to making functional conclusions.

The Panx3 structural conformation is another parameter for which the field has little direct evidence. In order to generate our predicted Panx3 structure, we levered AlphaFold2 computational structural predictions and the Panx3 amino acid sequence. Panx1 has been well-documented as a heptameric large-pore ion channel.^{70, 239} However, the precise structure of Panx3 has yet to be described. Our crosslinking studies were unable to support heptameric Panx3 assemblies as has been observed for Panx1. As a comparison, chemical crosslinking of Panx2 was previously used to demonstrate octameric oligomerization,⁶⁷ which sets precedence that pannexin isoforms may exhibit variation in oligomeric state. Exposure to low concentrations of BS₃ produced a band roughly the molecular weight of two 40kDa Panx3 monomers (Figure 10G), suggesting a dimeric Panx3 promoter may be a stable structural unit within a greater Panx3 oligomer. Exposure higher concentrations of BS₃, in which we can readily resolve the Panx1 heptamer (Figure 10G), produced faint bands at approximately 160 and 240kDa, suggesting serial incorporation of dimeric Panx3 promoters into a tetramer (160kDa) and hexamer (240kDa). It is unclear from the current data if tetrameric or hexameric Panx3 oligomers are stable, functional channels and further work would need to be completed to assess the Panx3 oligomerization. Furthermore, it is unclear if Panx3 would exhibit the same oligomerization patterns in different tissues or expression systems. Together, these data suggest Panx3 to be a highly plastic channel protein. In endothelium, there is no direct evidence for channel functionality; instead we posit that Golgi-localized Panx3 exerts oxidative effects on the cardiovascular system through protein-protein interactions with Bcl6.

Chapter 4: A potential role for basophils in blood pressure regulation

4.1: Abstract

Due to their position at the interface of the circulation, endothelial cells are poised to interact with immune cells in the blood through physical interactions, such as leukocyte extravasation, as well as through secreted cytokines and signaling molecules. In the previous chapter, endothelial Panx3 was shown to protect against vascular oxidative stress through interactions that stabilize transcriptional repressor Bcl6. These studies make use of the same inducible, endothelial cell-specific Panx3 knockout mouse to assess the potential for endothelial Panx3/Bcl6 interactions to contribute crosstalk between the endothelium and inflammatory cells. Genetic deletion of endothelial Panx3 is associated with increased myeloid expression of IL4 and increased expression of the IL4R in vascular tissue, suggesting immune-endothelial signaling through IL4. Because IL4 is commonly associated with Th2 cells, we tested the ability of splenic T cells to produce various cytokine including IL4, however results indicate endothelial Panx3 expression has no effect on IL4 production by T cells. However, analysis of whole blood demonstrated a significant increase in the circulating basophil population, a primary source of IL4, while other white blood cell types were unchanged. To understand if basophilia observed in EC *Panx3^{Δ/Δ}* mice was associated with their hypertensive phenotype, we tested the effects of basophil expansion on their blood pressure. Surprisingly, we found that systemic blood pressure was reduced by ~2mHg in EC *Panx3^{Δ/Δ}* mice but not controls, suggesting a relationship between circulating basophil populations and systemic blood pressure regulation. To confirm the role for basophilic IL4 to mediate these effects, we next induced IL4 secretion from basophils with acute IPSE exposure. This rescued Bcl6 protein abundance and likely transcriptional activity in EC *Panx3^{Δ/Δ}* as Nox4 expression was restrained to levels nearly below controls. IL4R expression was also rescued. To test if basophilic IL4 could be general mechanism of blood pressure regulation, we next asked whether basophil depletion via functional antibody administration would alter hemodynamics in wildtype mice. Basophil depletion was indeed associated with increased mean arterial pressure. Altogether,

these studies suggest a potential role for a basophil-endothelial signaling axis for the regulation of blood pressure.

4.2: Introduction

The immune system is composed of a wide variety of specialized cell types which work in concert to protect against foreign bodies and restore tissue integrity after insult or injury. Basophils are circulating granulocytes that have well described roles in allergy and asthma. Basophils are the least abundant white blood cell in the circulation, comprising less than 1% of white blood cells. The basophilic lifespan is relatively short, estimated to be 1-2 days.²⁴⁰ Their paucity and short lifespan added considerable challenges to study basophils, and in many early studies, they were improperly characterized as circulating mast cells.

While their low abundance in the circulation may suggest basophils play peripheral or redundant physiological roles, basophil-like cells have been conserved throughout evolution. Basophil-like granulocytes, which respond to basic dyes from which the basophil was named,²⁴¹ have been identified in the circulation of agnathan jawless fish, like hagfish and lampreys, and Chondrichthyes cartilaginous fish, like sharks.²⁴² Perhaps more surprising, ascidian sea squirts, urochordates which are thought to have evolved nearly 500 million years ago, exhibit circulating granular hemocytes with functional heparin and histamine granules.²⁴³ Their evolutionary conservation implies selective pressures favoring the maintenance and survival of basophils due to their beneficial physiological effects.

While basophils and mast cells share many features due to their functional similarities, recent work has highlighted their important physiological distinctions. Mast cells reside in mucosal and epithelial tissues such as the peritoneum, while basophils stay in the peripheral blood unless activated.²⁴⁴⁻²⁴⁷ In another distinction, mast cells are relatively long lived as they can survive for more than ten months and maintain the ability to replicate in their resident tissues, unlike post-mitotic basophils.²⁴⁸ Mast cells and basophils are both granulocytes, though mast cells typically contain more numerous, smaller granules while basophils contain fewer, larger granules.²⁴⁹ Despite their morphological distinctions, basophilic and mast granules contain much of the same contents including heparin, histamine, serotonin, chondroitin sulfate and many cytokines (IL2, IL3, IL4, IL5, IL6, IL9, IL13, IL15).^{244, 247, 250-252}

In the context of allergic response, basophils and mast cells play similar but distinct roles. Allergen detection activates IL4 and IL13 secretion from Th2 cells. These cytokines act on B cells to stimulate production and secretion of allergen-specific IgE antibodies. IgE binds the FcεRI receptor expressed on basophils and mast cells. Mast cell activation comprises the bulk of the allergic response as their degranulation has two functional effects; mast cell release of histamine, proteases, leukotrienes and prostaglandins triggers the acute allergic response, while their release of VEGF and other proteases drives tissue remodeling, angiogenesis and lymphangiogenesis. At the same time, activation of the basophil FcεRI receptor leads to basophilic secretion of IL4 and IL13 which positively feeds back on Th2 cells, B cells and mast cells to amplify the allergic response. Mast cells facilitate much of the acute response while basophils promote cellular coordination and amplification of the inflammatory signals.

Both cell types arise from common and interwoven progenitors. Briefly, multipotent progenitor cells (MPP) in the bone marrow can give rise to common myeloid progenitors (CMP) or to mast cell progenitors directly (MCP). CMP can give rise to granulocyte monocyte progenitors (GMP). GMP can differentiate into MCP or basophil/mast cell progenitors (preBMCP). Both MCP and preBMCP cells can migrate from myeloid tissue to the spleen to give rise to basophil/mast cell progenitors (BMCP). However, if preBMCP are retained in the marrow, they can generate MCP or basophil progenitors (BaP). As the name suggests, circulating basophils are derived only from BaP.²⁵³ As one can assume from this convoluted differentiation scheme, mast cells are much more abundant than their circulating counterpart. It does pose the question, if basophils and mast cells are functionally redundant, why is the differentiation of basophils so tightly controlled while mast cells differentiation is so permissive? Why limit the abundance of basophils?

Perhaps basophil specification is subject to more stringent regulation due to their exceptional capacity to facilitate interactions and coordinate the operations of disparate cellular populations. A mounting body of

evidence would support this argument. Basophil-secretion of IL4 plays a unique role initiating a positive feedback loop of Th2 activation following immune stimulus,²⁵⁴ indicating a potential for basophil-derived cytokine release in homeostatic regulation of other cell types. Lung-resident basophils have been shown to support normal pulmonary development through the secretion of IL6, IL13 and Csf1 which is required for maturation of functional alveolar macrophages.²⁵⁵ Moreover, following myocardial infarction, basophil-derived IL4/IL13 is required to switch from an initial inflammatory phase to the proliferative phase by impairing recruitment of classically-activated M1 macrophages and promoting recruitment of alternatively-activated M2 macrophages. Here, IPSE administration, which induces IL4 secretion from basophils but no other cell types,^{256, 257} was shown to improve ejection fraction, end diastolic volume and longitudinal volume in a basophil-dependent manner just four weeks after infarction.²⁵⁸ Similarly, in the cecal-puncture model of sepsis, basophils are the first leukocyte recruited to the site of injury and basophil-derived TNF directs the immune response. When basophilic TNF secretion was blocked, compensatory TNF secretion by macrophages and neutrophils was insufficient to rescue bacterial clearance and mortality.²⁵⁹ This implies that cytokine secretion by basophils may be more effective at coordinating a response from multiple cell types than the same factors secreted by other cell types in the same vicinity, though the reason for this distinction is not known. In addition to its roles coordinating the behavior of immune populations, basophils have also been reported to facilitate interactions with non-immune cell types including nervous and vascular tissue. In atopic dermatitis, basophils induce mast cell-independent IgE-mediated acute itch episodes through leukotriene secretion and direct interactions with sensory nerve fibers. Basophils even exhibit unique strategies to facilitate direct interactions with other cell types. During the process of transmigration and tissue extravasation, basophils can effectively alter their migratory kinetics, pausing to enable prolonged, direct interactions with endothelium in spite of circulatory forces. These extended interactions facilitate efficient delivery of basophil-derived IL4 directly onto the endothelial surface, resulting in altered expression of adhesion molecules.²⁶⁰ Altogether, these studies indicate basophils exhibit a unique mastery of intercellular communication with important effects in normal and pathological conditions.

In this study, we demonstrate a potential basophil-endothelial signaling axis which contributes to systemic blood pressure regulation. Our data indicate the circulating basophil population appears to respond to undetermined cues from the vascular endothelium and we propose that basophil derived IL4 acts upon endothelium to protect against vascular oxidative stress

4.3: Results

Because genetic deletion of endothelial Panx3 results in significantly reduced Bcl6 protein (Figure 13A-B) and inhibits repression by Bcl6 (Figure 13E-I), we considered that loss of endothelial Panx3 could potentially impair Bcl6 activity in other cell types. Because Bcl6 expression is necessary for differentiation of germinal center B cells,^{117, 169} we first assessed the abundance of splenic Follicular B cells and germinal center B cells. $GL7^+$, $CXCR5^+$, $B220^+$ Follicular B cells and $GL7^{hi}$, Fas^+ , $B220^+$ germinal center B cells were unchanged in EC *Panx3^{Δ/Δ}* mice (Figure 19A-B), indicating that B cell Bcl6 expression and activity is unaffected by genetic deletion of Panx3 from endothelium. Similarly, endothelial expression of Panx3 had no effect on stimulated production of proinflammatory ($IFN\gamma$, $TNF\alpha$, $IL17$) or anti-inflammatory ($IL4$, $IL10$) cytokines from splenic T cells (Figure 20). However, we observed increased $IL4$ in bone marrow lysates from EC *Panx3^{Δ/Δ}* mice via ELISA (Figure 21A), indicating that endothelial Panx3 may alter cytokine production from myeloid cells, but not splenic cells. Furthermore, expression of the $IL4$ type II receptor was increased in endothelial-rich lung tissue from EC *Panx3^{Δ/Δ}* mice (Figure 21B), corroborating that loss of endothelial Panx3 may promote signaling from myeloid cells to the vasculature through $IL4$. Next, we assayed $IL4$ receptor expression in human aortic endothelial cells (HAoEC) which endogenously express Panx3. RNA interference (RNAi)-mediated knockdown of Panx3 results in increased *Il4r* expression (Figure 21C), recapitulating observation from EC *Panx3^{Δ/Δ}* mice that loss of endothelial Panx3 primes endothelium to respond to $IL4$ signaling. Despite its effect on vascular Bcl6 activity, endothelial Panx3 does not impact splenic B cell differentiation. However, inhibition of endothelial Panx3, in vitro or in vivo, appears to prime the system for signaling from bone marrow to the vasculature through $IL4$, but the product of this signaling is not yet known.

In order to characterize systemic immune environment in EC *Panx3^{Δ/Δ}* mice, white blood cell populations were assessed by complete blood count. Circulating populations of lymphocytes, neutrophils and monocytes were unchanged, though loss of endothelial Panx3 resulted in a significantly increased basophil

population (Figure 22). Because IL33 has been shown to induce basophil mobilization from the bone marrow,²⁶¹ we measured IL33 from the circulation. Plasma levels of alarmin IL33 were unchanged (Figure 23).

We next posited whether our initial observation of increased vascular oxidative stress following deletion of endothelial Panx3 could contribute alter circulating basophil populations. Intravenous administration of the H₂O₂-scavenger catalase (PEG-catalase, 40U/kg) trended toward a reduction in circulating basophils (Figure 24), indicating that vascular ROS may alter basophils in the blood. This observation led us to hypothesize ROS-induced hypertension could alter circulating basophil population, and that basophil-derived IL4 could act through endothelial IL4 type II receptors to promote Bcl6 expression in a negative feedback loop. To test this, we assessed blood pressure in freely moving, conscious EC *Panx3^{ΔΔ}* mice following in vivo basophil expansion via IL3C treatment¹⁴⁷ (Figure 25A). Loss of endothelial Panx3 was associated with a 2mmHg decrease in blood pressure during IL3C treatment, which was not observed in littermate controls (Figure 25B).

Next, we sought to determine if IL4 mediates the effect of basophils on blood pressure. To assess the potential for basophil-derived IL4 to alter systemic blood pressure regulation, we administered IL4-inducing principle from *S. mansoni* eggs (IPSE, 25μg), to trigger basophil-specific release of IL4 in vivo.^{256, 257} Mice fitted with implanted radiotelemeters underwent daily I.V. injections of IPSE (25μg) or vehicle for a period of five days prior to euthanasia and tissue harvesting.²⁵⁸ Following IPSE treatment, there was no significant difference in *Bcl6* mRNA expression, though the trend may suggest that IPSE treatment promoted *Bcl6* mRNA expression (Figure 26B). This resulted in a rescue of the Bcl6 protein abundance in EC *Panx3^{ΔΔ}* mice (Figure 26C). *Nox4* mRNA expression was also rescued, with a trend suggesting that under IPSE treatment, lung endothelium lacking Panx3 may exhibit reduced Nox4 expression compared to littermate controls (Figure 26D). Similarly, IPSE treatment ablated the genotype difference in *Il4ra*

expression (Figure 26E). Baseline blood pressure was recorded for 48 hours prior to IPSE administration and compared with continuous blood pressure recordings during IPSE administration. IPSE treatment was insufficient to normalize the blood pressure of EC *Panx3^{ΔΔ}* mice (Figure 26F). Basophilic release of IL4 rescued endothelial expression of *Bcl6* and *Nox4* in mice following genetic deletion of endothelial *Panx3*. Over the short five-day treatment schedule, the reduction in *Nox4* expression was insufficient to reduce systemic blood pressure in EC *Panx3^{ΔΔ}* mice. However, it is unclear if an optimized dose or schedule of IPSE administration would modulate systemic blood pressure.

Next, we investigated whether basophils may have a homeostatic role in systemic blood pressure regulation, independent of endothelial *Panx3* expression. We used IP injections with a functional antibody against MAR-1 (FcεRIα, 5μg), which has been shown to induce basophil depletion *in vivo*.¹⁴⁶ Each C57Bl/6n mouse treated with the basophil depletion antibody exhibited increased mean arterial blood pressure (Figure 27B), suggesting the presence of circulating basophils negatively regulates homeostatic blood pressure regulation.

Figure 19: Splenic B Lymphocytes are unchanged by endothelial Panx3 expression.

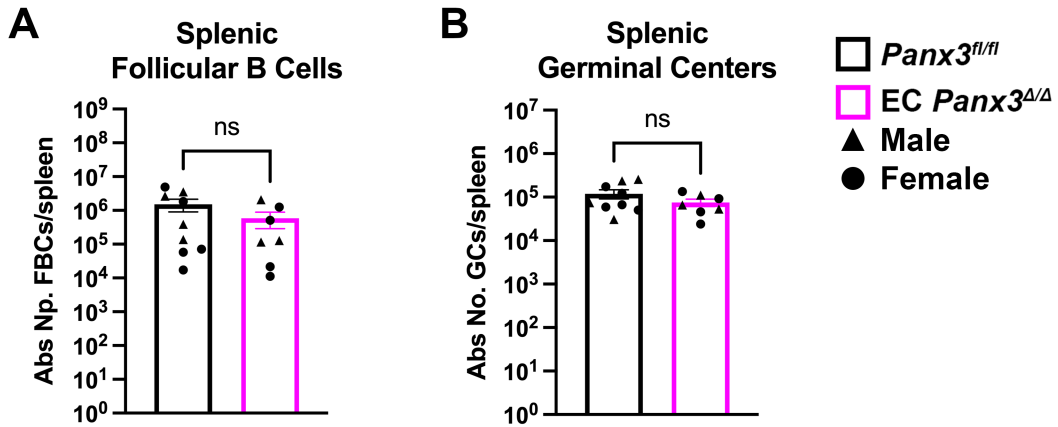


Figure 19: Splenic B Lymphocytes are unchanged by endothelial Panx3 expression. (A) $GL7^+$, $CXCR5^+$, $B220^+$ Follicular B Cells and $GL7^{hi}$, Fas^+ , $B220^+$ germinal centers (B) were quantified by flow cytometry. Each dot represents one mouse. Symbol indicates sex. Unpaired t-tests were used to compare groups.

Figure 20: Endothelial *Panx3* expression has no effect on cytokine production by splenic T cells.

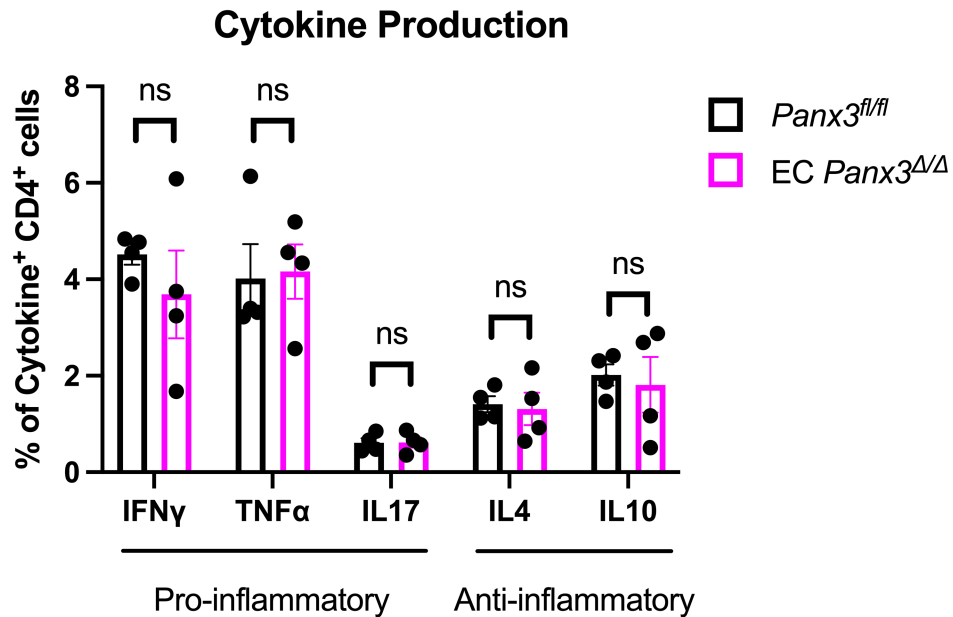


Figure 20: Endothelial *Panx3* expression has no effect on cytokine production by splenic T cells. Splenic cells were exposed to ionomycin and Phorbol 12-Myristate 13-Acetate (PMA) in the presence of monesin for five hours prior to analysis of the intracellular cytokines produced in T cells by flow cytometry. Genetic deletion of endothelial *Panx3* has no effect on T cell accumulation of IFN γ , TNF α , IL17, IL4, or IL10. Each dot represents one mouse. Unpaired t-tests were used to compare cytokine production across genotypes.

Figure 21: Loss of endothelial *Panx3* results in increased myeloid IL4 and increased IL4 receptor expression.

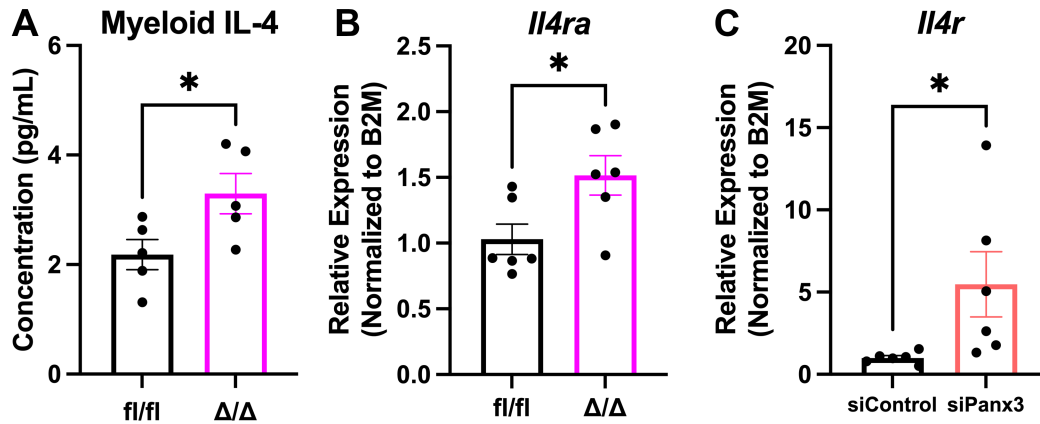


Figure 21: Loss of endothelial *Panx3* results in increased myeloid IL4 and increased IL4 receptor expression. (A) Abundance of IL4 assessed from bone marrow lysates of EC *Panx3*^{Δ/Δ} mice by ELISA. (B) Expression of *Il4ra*, the murine IL4 type II receptor, in endothelial-rich lung tissue from EC *Panx3*^{Δ/Δ} mice. (C) Quantification of the human IL4 type II receptor, *Il4r*, in HAoEC following inhibition of *Panx3* expression via RNAi (5nM, 72 hours). In A and B, each dot represents one mouse and * indicates $p < 0.05$ via two-tailed unpaired t-test. In C, each dot represents one technical replicate over the span of two biological replicates, with * indicating $p < 0.05$ via one-tailed unpaired t-test with Welch's correction.

Figure 22: Circulating basophils are uniquely increased following *Panx3* deletion from endothelium.

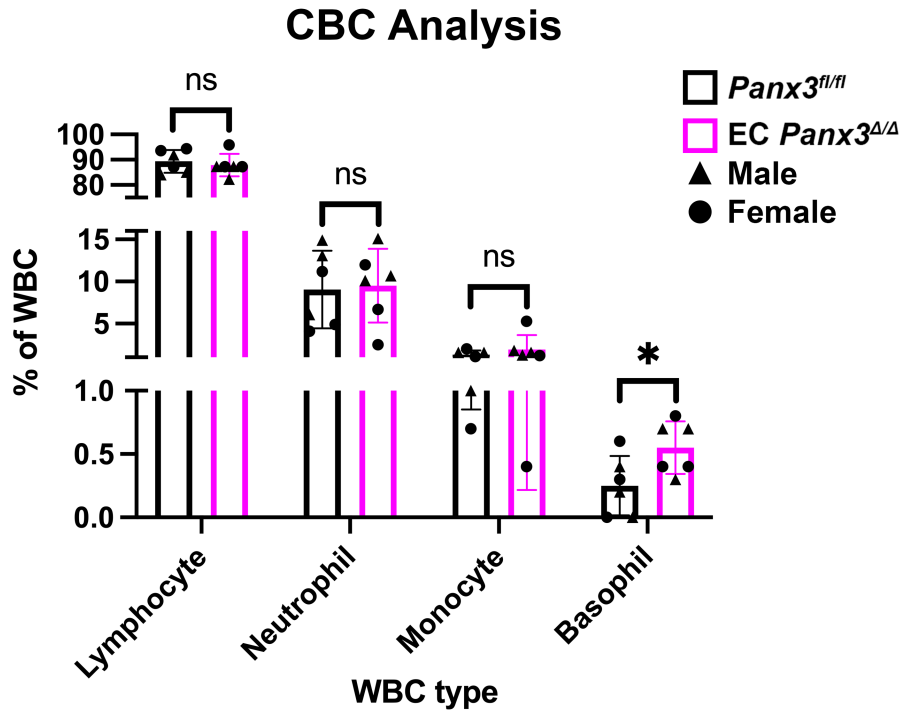


Figure 22: Circulating basophils are uniquely increased following *Panx3* deletion from endothelium. Terminal cardiac puncture was used to collect circulating blood for analysis by complete blood count (CBC). Each dot represents one mouse with sex indicated by symbol. * indicates $p < 0.05$ via unpaired t-test.

Figure 23: Circulating levels of IL33 are unaffected by endothelial Panx3 expression.

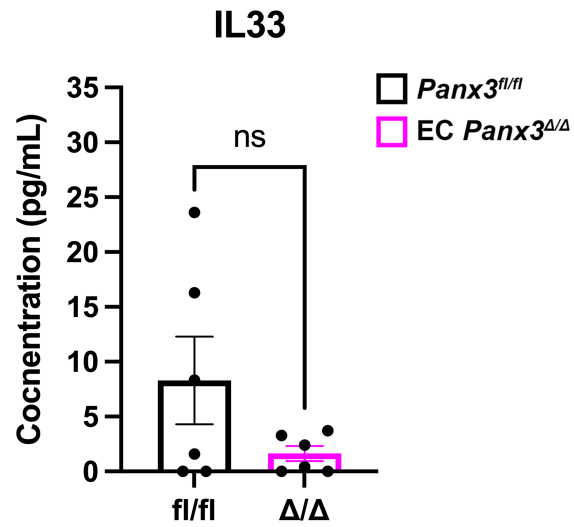


Figure 23: Circulating levels of IL33 are unaffected by endothelial Panx3 expression. Blood plasma from EC *Panx3*^{Δ/Δ} mice was assessed for IL33 content by ELISA. Each dot represents one mouse. Unpaired t-test used to compare genotypes.

Figure 24: Scavenging hydrogen peroxide in vivo may attenuate the circulating basophil population.

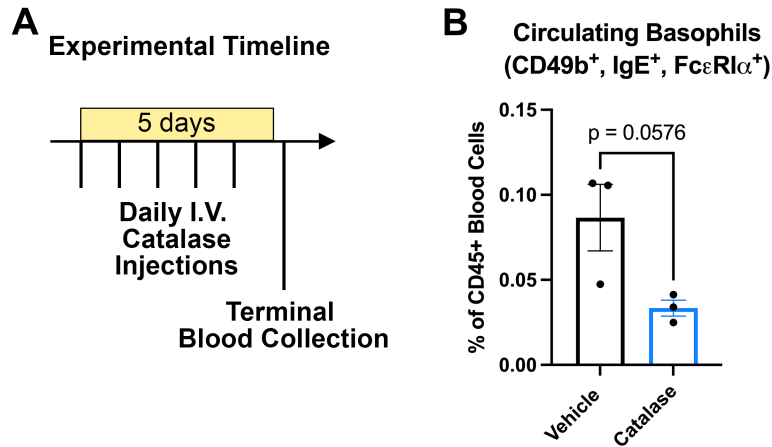


Figure 24: Scavenging hydrogen peroxide in vivo may attenuate the circulating basophil population. (A) C57Bl/6n mice underwent five days of daily IV injections with 40U/kg of pegylated catalase prior to terminal blood collection via cardiac puncture. (B) Flow cytometry was used to assess the circulating basophil population (CD45⁺, CD49b⁺, IgE⁺, FcεRIα⁺) and represented as percentage of total CD45⁺ cells. Unpaired t-test was used to compare circulating basophil counts between treatment groups.

Figure 25: In vivo basophil expansion relieves blood pressure elevation following loss of endothelial Panx3.

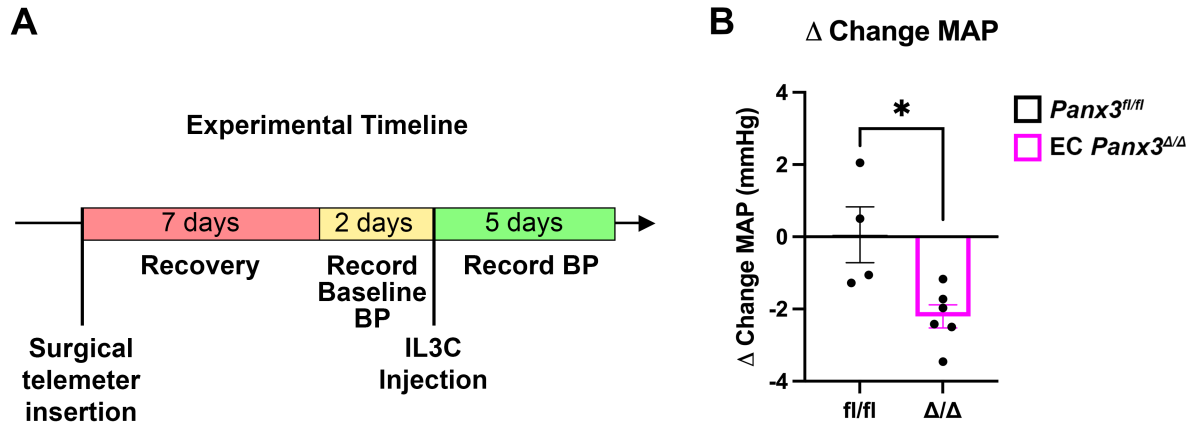


Figure 25: In vivo basophil expansion relieves blood pressure elevation following loss of endothelial Panx3.

(A) EC *Panx3^{Δ/Δ}* mice were allowed seven days to recover from surgical implantation of the radiotelemeter units before recording baseline blood pressure for 48 hours. To induce basophil expansion, mice were then retroorbitally injected with IL3C, a solution containing recombinant IL3 (10 μ g) and anti-IL3 antibody (5 μ g) in sterile saline. After a single IL3C injection, mice resumed blood pressure recordings for five days.

(B) The change in mean arterial blood pressure following IL3C administration was compared between EC Panx3 mice and littermate controls. * indicates $p < 0.05$ via unpaired t-test. Each dot represents one mouse.

Figure 26: Stimulation of basophilic IL4 release with IPSE in EC *Panx3^{Δ/Δ}* mice.

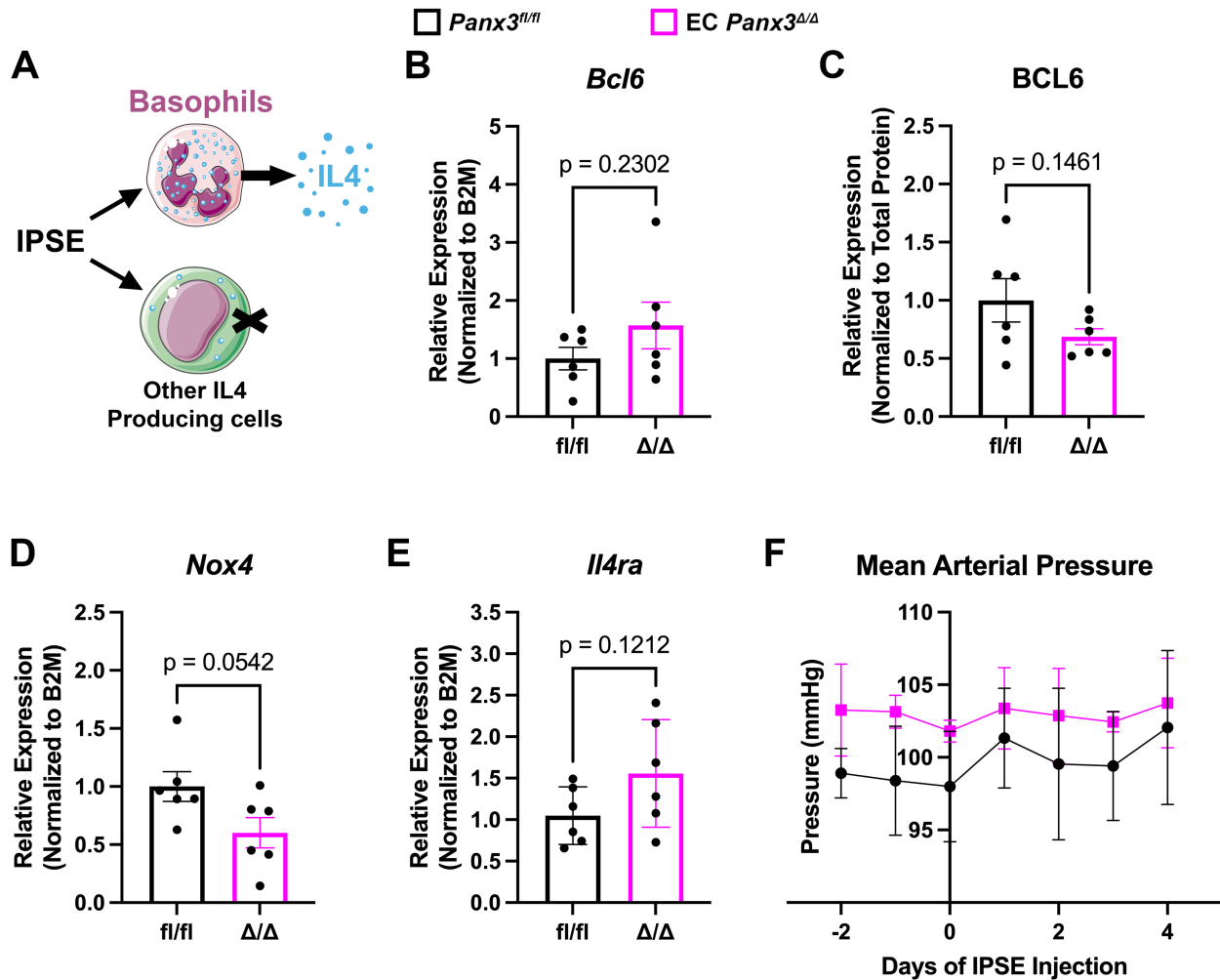


Figure 26: Stimulation of basophilic IL4 release with IPSE in EC *Panx3^{Δ/Δ}* mice. (A) IPSE promotes IL4 secretion from basophils without affecting other sources of IL4 including mast cells, eosinophils and Th2 cells.^{256,257} (B, C) Under IPSE treatment, there is no genotype difference for *Bcl6* mRNA or protein in lung tissue. (D) *Nox4* mRNA expression in lung tissue. (E) Transcript abundance for IL4 type II receptor in lung tissue. (F) Mean arterial pressure, averaged over 24 hours, is shown over time. N = 3 mice per group. In A-E, each dot represents one mouse with unpaired t-tests used to compare groups. Welch's correction was used in C.

Figure 27: Basophil depletion significantly elevates systemic blood pressure.

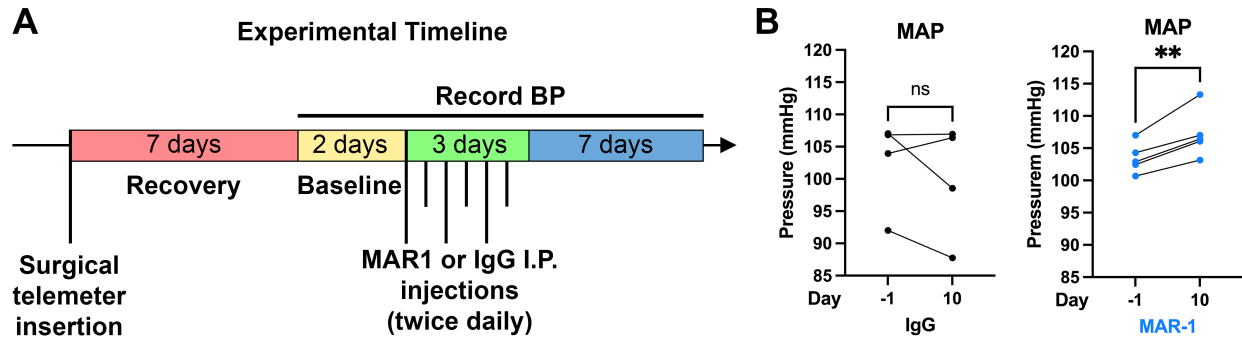


Figure 27: Basophil depletion significantly elevates systemic blood pressure. (A) C57Bl/6n mice were allowed seven days to recover from surgical implantation of the radiotelemetry units before recording baseline blood pressure. Twice daily IP injections of MAR-1 antibody or the IgG control was used to deplete circulating basophils.¹⁴⁶ (B) Mean arterial pressure from baseline recordings (-1) and following basophil depletion (10). IgG mice (left) show no alterations in blood pressure while mice treated with MAR-1 exhibit moderate blood pressure increase. ** indicates $p < 0.01$ via paired t-test.

4.4: Discussion

Our data propose that the peripheral basophil population responds to cues from endothelium and likely exert homeostatic regulation on blood pressure through IL4 signaling to endothelium in a bidirectional signaling mechanism. EC *Panx3^{ΔΔ}* mice are primed for cytokine signaling through IL4 (Figure 20). While most white blood cell populations are unaffected, EC *Panx3^{ΔΔ}* mice exhibit significantly increased circulating basophils (Figure 22), granulocytes known to be a primary source of IL4.²⁶² Manipulation of the circulating basophil population in vivo was negatively associated with systemic blood pressure, in EC *Panx3^{ΔΔ}* as well as wildtype mice, further suggesting the basophil-endothelial signaling axis could be a general mechanism of blood pressure control independent of endothelial Panx3 expression.

There are several notable limitations of the current study. First, these data demonstrate an association between endothelial expression of Panx3 and IL4R, basophil abundance and blood pressure regulation, though together they fail to establish causal connections between these variables. It is tempting to suggest that the absence of endothelial Panx3 induces hypertension and triggers basophil mobilization through an undetermined mechanism. In this scenario, the expanded population of circulating basophils can feedback on the endothelium through IL4 signaling, potentially driving endothelial Bcl6 expression as has been shown in other cell types,²⁶³ which may result in normalization of blood pressure. However, further work is required to substantiate this hypothesis. In addition, while multiple techniques are used to in attempts to expand or deplete the circulating basophil population in vivo (Catalase, IL3C, MAR-1), confirmation of the intended effects were not included in the original study. Thus, future studies would benefit from quantification of the circulating basophil population with each treatment. Despite these limitations, the data presented in the current study justify further investigation of the endothelial-basophil signaling axis.

While peripheral basophil numbers are increased by parasitic infection or allergic inflammation,^{240, 246, 264-}
²⁶⁶ the stimulus driving basophil expansion in EC *Panx3^{ΔΔ}* mice has yet to be identified. We first considered

whether the alarmin IL33 could mediate this response. Basophils are a direct target of IL33, and have been reported to mobilize from the bone marrow²⁶¹ and degranulate, secreting IL4,²⁶⁷ in response to IL33 exposure. IL33 has been shown to promote proliferation of other cell types.²⁶⁸⁻²⁷⁰ Furthermore, hypertension can trigger vascular expression of the alarmin IL33.²⁷¹ Thus, we hypothesized basophilia in EC *Panx3^{Δ/Δ}* mice could have been driven by increased concentrations of plasma IL33 as a consequence of hypertension, however this was not observed (Figure 24). It is worth noting that these measurements were taken from mice nearly ten weeks after tamoxifen administration. In other models, neonatal exposure to IL33 has been shown to impart effects on immune cells long into adulthood.²⁷² As such, further investigation into the temporal dynamics of plasma IL33 abundance in relation to genetic deletion of endothelial Panx3, the consequent development of hypertension and basophilia would be needed to conclude whether IL33 mediates this effect.

We next posited whether the vascular oxidative stress observed in EC *Panx3^{Δ/Δ}* mice (Figure 13) could contribute to their overabundance of peripheral basophils. While it has yet to be shown to drive basophil mobilization directly, common myeloid progenitor cells, which eventually give rise to basophils,²⁵³ preferentially differentiate into another basophil progenitor intermediate when treated with H₂O₂ in culture.²⁷³ Our attempts to modulate vascular H₂O₂ by intravenous administration of catalase was promising but ultimately insufficient to significantly deplete basophils in wildtype mice (Figure 25). It remains to be seen if catalase administration would be more effective at reducing the overabundant basophils in EC *Panx3^{Δ/Δ}* mice. In addition to IL33 and ROS as candidates to induce basophil mobilization, it would be prudent to assess STAT5 expression in basophils isolated from EC *Panx3^{Δ/Δ}* mice in future studies. While not required for normal maturation, IL-3, GM-CSF and TSLP have each been shown to promote basophil specification and activation by activating the STAT5 pathway.²⁷⁴

There are many unanswered questions when considering the role of IL4 signaling in this proposal. While IL4 is commonly associated with Type II inflammatory responses,^{252, 274-277} its potential role in blood pressure regulation has only been superficially explored. Hypertensive patients exhibit significantly elevated levels of IL4.^{278, 279} Exogenously dosing IL4 is coupled with a reduction in blood pressure,^{280, 281} although the mechanism isn't defined. Cellular responses to IL4 are dependent on the type of IL4 receptor (IL4R) complex expressed. The type I IL4R complex is composed of IL4R α and the common γ chain (γ_c), and is expressed hematopoietic lineage cells,^{282, 283} as well as the heart, skeletal muscle and kidney.²⁸² The type II IL4R complex is IL4R α /IL13R α and expressed on nonhematopoietic cells, including endothelium.^{284, 285} Interestingly, in murine splenic B cells, which also express type II IL4R complexes,²⁸⁶ IL4 stimulation drives significant increases in protein expression of Bcl6.²⁶³ It is possible basophil expansion is a response to hypertension, and rescuing Bcl6 transcriptional activity could ameliorate this effect. Next, we attributed the increased IL4 in myeloid tissue to basophils/basophil progenitors, but other myeloid derived cells have been shown to secrete IL4, including eosinophils, Th2 cells and mast cells.^{252, 287, 288} In addition, our attempts to quantify IL4 in the circulation were inconclusive (data not shown), likely because the abundance of the cytokine was below the limits of detection for the assay. This is of little concern, because endothelium has been shown to respond to quantities of IL4 10-fold less than what is required to activate other cell types.²⁸⁹ However, this may further support a role for basophilic release of IL4. Basophils have been reported with the unique ability to instigate prolonged instances of direct contact with endothelium for the purpose of efficient IL4 signaling.²⁶⁰ Thus, it is possible for basophils to signal to endothelium through IL4 in the absence of IL4 accumulation in the circulation. In support of this, administration of IPSE into EC *Panx3^{Δ/Δ}* mice normalized Bcl6 protein abundance and restricted Nox4 and IL4R expression (Figure 26). IPSE has been reported to induce IL4 secretion from basophils but no other cell types,^{256, 257} basophil IL4 stores were not assessed in the current study. Additional studies enabling tracking of IL4 expression in vivo would strengthen this notion. One option could be the use of the 4get bicistronic IL4 reporter mouse strain,²⁷⁷ which paired with flow cytometry could be used to identify IL4⁺ cell types.

Chapter 5: General Discussion and Future Directions

Altogether, the data in these studies demonstrate previously unrecognized roles for Panx3 and Bcl6 to modulate blood pressure as well as interactions between endothelium and circulating basophils. In endothelium, Panx3 and Bcl6 interact physically which shields Bcl6 from degradation and alters the endothelial transcriptomic landscape. In the absence of endothelial Panx3, Bcl6 is degraded, allowing NF κ B to predominate. This results in elevated Nox4 expression and overproduction of H₂O₂, which impairs endothelial-mediated dilation of resistance arteries and culminates in systemic hypertension. Through an undisclosed mechanism, this is associated with a significantly increased population of circulating basophils. While a role for basophils in the regulation of blood pressure has yet to be described, we accumulate evidence to suggest that basophil-derived IL4 acts on the endothelial IL4R, perhaps to drive Bcl6 expression in a negative feedback mechanism of homeostatic blood pressure regulation. This study represents the first exploration of the functional contributions of Panx3 in the vasculature. Our findings that Panx3 contributes to blood pressure regulation and vascular-immune interactions are in line with what we know about vascular Panx1.

Pannexin channels expression has been shown to be regulated in a cell-type- and vascular bed-specific manner. Panx1 is expressed in endothelium throughout the vasculature and in SMC of renal, coronary and resistance arteries.²⁹⁰ In the vasculature, Panx2 expression is restricted to the pulmonary vessels where it is expressed in endothelium, smooth muscle and alveoli.²⁹⁰ We show Panx3 is expressed in the endothelium of resistance arteries, where it is localized to the Golgi Apparatus, though Panx3 expression has also been noted throughout the vessel wall in small coronary arteries, arterioles of the cortical kidney and pulmonary arteries.²⁹⁰

Panx1 and Panx3 have both been shown to contribute to blood pressure, albeit through distinct mechanisms. Panx1 channels on smooth muscle cells open in response to α 1-adrenergic receptor activation, where

Panx1-dependent release of ATP promotes constriction through the activation of P2Y receptors.^{145, 151} Endothelial Panx1 largely contributes to vascular-immune interactions, though it has been shown to exhibit vasoactive effects on cerebral myogenic tone development²⁹¹ and on pulmonary vessels, where signaling between Panx1 and TRPV4 can lower pulmonary pressure.²⁹² In each case, ATP release following Panx1 channel activation mediates these vasoactive effects. Meanwhile, our data demonstrate a role for endothelial Panx3 to contribute to blood pressure regulation in a channel-independent manner via interactions which stabilize Bcl6 and restrict Nox4 expression.

Immune interactions with endothelial Panx1 and Panx3 serve distinct purposes. ATP release by endothelial Panx1 channels can recruit immune cells and regulate leukocyte emigration. Under acute inflammation, exposure to TNF α promotes ATP release by Panx1 through Src-dependent phosphorylation of Tyr198.⁶³ However, under chronic TNF α exposure, NF κ B activation drives Panx1 expression which is associated with increased endothelial calcium activity and secretion of proinflammatory cytokine IL1 β .¹⁷⁶ To this end, inhibition of Panx1 channel activity through genetic deletion and pharmacological inhibition have been associated with improved outcomes following stroke and ischemia reperfusion injury. However, our findings indicate genetic deletion of endothelial Panx3 may have initiated communication between endothelium and basophils, possibly mediated through Nox4-dependent H₂O₂ and IL4. Our data suggests this signaling mechanism is likely to negatively feedback against oxidative stress-induced hypertension and normalize blood pressure.

It is becoming increasingly clear that there are many exciting avenues for future research. In particular, my findings have pointed towards a number of intriguing questions related to the role of Panx3/Bcl6 interactions in developmental angiogenesis, the potential application of our BCLiP peptide as a therapeutic Bcl6 inhibitor, the regulation of Panx3 subcellular distribution by shear stress, and the impact of physiological levels of hydrogen peroxide on conductance through SK/IK in endothelial-mediated dilation.

These areas of inquiry offer significant potential for advancing our understanding of the mechanisms underlying vascular development and function. In the following sections, I propose several experimental approaches aimed at addressing these important questions.

5.1: Elucidate the influence of endothelial Panx3/Bcl6 interactions on angiogenesis

Angiogenesis gives rise to new blood vessels formed through the proliferation and tissue invasion of endothelial cells from preexisting vessels. This process involves coordination of endothelial proliferation, specification, migration, and interendothelial signaling. During vascular sprouting, VEGF and Notch signaling specify endothelial cells as polarized, invasive ‘tip’ cells or proliferative ‘stalk’ cells.²⁹³ Arterial and venous specification occurs later during vascular remodeling, in a complex process which integrates morphogen signaling with precisely timed cell cycle arrest.²⁹⁴ A 2017 study by the Brostjan lab assessed endothelial Bcl6 in the context of tumor-related angiogenesis, demonstrating that endothelial Bcl6 activity was associated with increased proliferation and inhibition of endothelial sprouting.¹²² While previous chapters demonstrate that Panx3/Bcl6 interactions can dictate Bcl6 transcriptional activity in adult endothelium (Figure 13J-N, 17F-J), it is unclear if Panx3 would regulate Bcl6 activity during angiogenesis. In addition, Bcl6 has been shown to drive cell specification in other cell types²⁹⁵⁻²⁹⁷ and has been suggested to promote endothelial stalk cell phenotypes,¹²² yet the effect of Bcl6 activity on arteriovenous specification has yet to be described.

Future studies could assess the effect of endogenous Panx3/Bcl6 interactions on multiple aspects of retinal angiogenesis by administering BCLiP peptide to wildtype pups or inducing perinatal genetic deletion of endothelial Panx3 through modification of the tamoxifen dosing schedule. The perinatal mouse retina is a well-characterized model of angiogenesis where, after some manipulation, the outward progression of angiogenesis from the optic nerve to the retinal edge can be assessed in a flat preparation suitable for microscopy.^{294, 298} Measurement of Bcl6 expression and abundance would demonstrate if loss of endothelial

Panx3/Bcl6 interactions in the developing retina would result in reduced Bcl6 transcriptional activity, as occurs in adult endothelium (Figure 13J-N, 17F-J). Next, plexus expansion would be quantified as a percent of covered area to deduce how Panx3/Bcl6 interactions would affect progression of the angiogenic front. Pharmacological inhibition of Bcl6 with small molecule inhibitor 79-6 on P5 and P6 resulted in increased vascularized area with a greater number of branch points and more sprouting cells at the angiogenic edge of P7 retinas.¹²² In contrast, preliminary studies generated with P6 retinas from EC *Panx3^{Δ/Δ}* mice following tamoxifen administration on P1-P3 suggest the potential for impaired angiogenesis (Figure 28). This discrepancy may indicate a Bcl6-independent role for Panx3 in angiogenesis, though further experimentation would be required. While Bcl6 ChIP-Seq would directly measure how endothelial Panx3/Bcl6 interactions affect DNA binding of the transcriptional repressor, one could also use transcript abundance of a set of genes known to be regulated by Bcl6 (*Ccna2*, *Ccnb1*, *Hes1*, *Hey1*, *Nfkbia*, *Nfkb2*)^{141, 161, 162, 299} as an indirect method of Bcl6 activity. If Bcl6 activity is unaffected following perinatal deletion of endothelial Panx3, it would further suggest a Bcl6-independent role for Panx3 in angiogenesis. However, if Bcl6 activity is reduced following loss of endothelial Panx3, then it instead would suggest that the effect of Panx3/Bcl6 interaction on retinal angiogenesis is temporally regulated.

To this end, through Bcl6 repressive actions, endothelial Panx3/Bcl6 interactions could sway arteriovenous specification by modulating cell cycle arrest,²⁹⁴ or directly regulating arterial or venous genes such as *Efrnb2* and *Emcn*, respectively. A pilot study using overexpression of Panx3 in HAoECs to promote Panx3/Bcl6 interactions showed reduced expression of Bcl6-regulated targets *Ccna2* and *Ccnb1*, suggesting stabilization of Bcl6 and increased transcriptional repressive activity (Figure 29A-C). In this condition, venous marker *Emcn* was dramatically upregulated while expression of *Efrnb2* was reduced (Figure 29D-E), suggesting that Bcl6 activity would promote venous specification of endothelium. Immunohistological staining and quantification of Endomucin and Ephrin B2 in P6-P8 retinas from EC *Panx3^{Δ/Δ}* mice could be used to determine if Panx3/Bcl6 interactions promote venous specification in vivo.

5.2: Evaluate the use of our novel BCLiP peptide as a therapeutic Bcl6 inhibitor

Bcl6 has a broad range of physiological functions including (1) regulating immune cell differentiation and proliferation,^{117, 295-297, 300} (2) repressing proinflammatory NFκB activity,^{140, 141} (3) facilitating pathological immune responses in autoimmune encephalitis³⁰¹ and systemic lupus erythematosus.³⁰² Dysregulation of Bcl6 expression and activity has also been implicated in an expanding scope of soft tissue and solid tumors (e.g. DLBCL,³⁰³⁻³⁰⁵ B-acute lymphoblastic leukemia,^{306, 307} chronic myeloid leukemia,^{308, 309} breast cancer,^{310, 311} non-small cell lung cancer,^{312, 313} glioma³¹⁴). In all of these diseases, Bcl6 protein is upregulated,³⁰²⁻³¹⁴ and this increased Bcl6 protein is an important target of pharmacological repression.^{303,}

315

In B cell development, Bcl6 is a master regulator of germinal center development. Upon immune activation, germinal centers develop in secondary lymphoid organs, generating massive clonal expansion of B cells and affinity maturation of the antibodies they produce. During this process, Bcl6 transcriptional activity represses DNA damage response and inhibits transcription of cell cycle genes, for the ultimate goal of promoting B Cell proliferation and survival.¹¹⁵ While this process is required to mount an appropriate immune response to foreign antigens, overriding the cellular checkpoints that regulate proliferation and cell death are fundamental mechanisms of oncogenesis. In fact, mutations and chromosomal rearrangements of Bcl6 are the most common genetic abnormalities associated with DLBCL,¹¹³ the most common form of Non-Hodgkin's Lymphoma. Minor alternations in the precise balance of Bcl6 expression and degradation can significantly alter the transcriptome. In fact, a study out of the Pagano lab in 2012 found that the intracellular half-life of Bcl6 was extended in DBLCL in culture following the mutagenesis of FBXO11, which forms a SCF ubiquitin ligase complex that targets Bcl6 for degradation.¹²⁴ Interestingly, researchers also observed that the gene encoding FBXO11 was commonly mutated or deleted in human primary DBLCLs,¹²⁴ further supporting that dysregulation of Bcl6 degradation can have deleterious effects on the tissue and the system.

In addition to its role in B cells, Bcl6 is also expressed in macrophages as well as in several subtypes of T cells. In macrophages, Bcl6 inhibits expression of the cytokine IL-6,³⁰¹ which promotes macrophage crosstalk with T cells and pathological Th17 differentiation while inhibiting differentiation of immunosuppressive Treg cells.³¹⁶ Furthermore, CD4⁺ T follicular helper cells (Tfh), which are characterized in part by their expression of Bcl6, have been implicated in autoimmunity.^{302, 317, 318} Inhibition of Bcl6 has been shown to rescue experimental models of autoimmunity, effectively reducing the generation of autoantibodies and preventing immune complex deposition in the kidney.³⁰² Altogether, this suggests that Bcl6 upregulation is associated with immune overactivation and demonstrates that Bcl6 is a promising therapeutic target in autoimmune diseases.

The BCLiP peptide is a 17- amino acid sequence which mimics L328-P344 of Bcl6, a highly evolutionarily conserved region containing degradation-targeting phosphorylation sites Ser333 and Ser343 (Figure 17A). We added a N-terminal stearyl group to facilitate cell entry. Bcl6 is uniquely suited as a promising target for the therapeutic strategy of inducing protein degradation, as its activity in vivo is largely regulated by its targeted degradation.^{139, 232} Previous chapters demonstrate exposure to BCLiP promotes degradation of endogenous vascular Bcl6 (Figure 17D-E) following interruption of Panx3/Bcl6 interactions (Figure 17C). In order to evaluate the potential application of the BCLiP peptide as a therapeutic to promote degradation of the protein in pathologies driven by Bcl6 transcriptional activity (e.g. DLBCL,³⁰³⁻³⁰⁵ B-acute lymphoblastic leukemia,^{306, 307} chronic myeloid leukemia,^{308, 309} breast cancer,^{310, 311} non-small cell lung cancer,^{312, 313} glioma³¹⁴, and autoimmune disorders³⁰²), I propose a large scale study to first assess how BCLiP exposure affects proliferation of several immortalized cancer lines (including the LL-100 panel of Lymphoblast and Leukemia cell lines,³¹⁹ as well as the 30-4500K breast cancer panel,³²⁰ the TCP-1018 Glioma tumor cell panel,³²¹ the TCP-1016 Lung cancer panel). While the use of tumor cell lines has considerable limitations, including genomic instability and lack of interaction with non-tumor components

(vasculature, immune cells), these experiments will demonstrate which pathology merits further study of BCLiP administration in animal models.

5.3: Uncover the mechanism by which the subcellular distribution of Panx3 is regulated by shear stress

The subcellular distribution of Panx3 is highly variable, with reports localizing the channel to intracellular membranes and/or plasma membrane across a variety of cell types and expression systems.^{58-60, 62, 68, 69, 71, 73-77, 79, 97} Previous work demonstrates that Panx3 delivery to the cell surface of BICR-M1R_k cells involves Sar1- and Arf1-dependent trafficking mechanisms,⁷⁵ though mechanisms behind its variable localization have yet to be described. Even when considering a single cell type such as the endothelium, there can be inconsistencies in the localization of Panx3. In static cultures of primary endothelial cells, Panx3 colocalizes with Calnexin (Figure 5A), suggesting its localization to the ER. However, Panx3 traffics to the Golgi Apparatus in the endothelium of mesenteric arteries (Figure 4A, B). In vitro studies indicate that the distribution of endothelial Panx3 can be regulated by shear stress; Panx3 polarizes in a manner reminiscent of the Golgi Apparatus³²² following exposure to laminar flow (Figure 5B-C). These data strongly support a role for shear stress to dictate localization of the channel, as has been observed in other systems. For instance, proximal tubule cells (PTC) in the kidney must tightly regulate electrolyte uptake in response to variations in the glomerular filtration rate. In response to physiologically-relevant levels of shear stress, PTC have been shown to differentially distribute salt balance machinery. Following exposure to shear stress, NHE3 transporter and the Na⁺/K⁺ ATPase pump will move in an actin-dependent manner from intracellular membranes to apical and basolateral membranes, respectively. Nonetheless, the mechanism driving this phenomena has yet to be determined. This section contains a discussion of the endothelial relationship to shear stress in addition to brief discussion on the mechanisms involved with Golgi polarization and anterograde/retrograde transport of proteins.

Endothelial cells are specialized to respond to not only the rate, but also the pattern of circulatory flow. Large conduit arteries must contend with the volume of blood rapidly ejected from each ventricular

contraction of the heart. Thus, the endothelium of conduit arteries is exposed to pulsatile flow patterns at a relatively high speed (pulsatile flow ~ 10 dynes/cm²). Arterioles and capillaries experience the highest degree of shear stress, at ~ 50 and 40 dynes/cm², respectively. This decreases dramatically at the venules (~ 15 dynes/cm²), with the lowest values of shear stress occurring in the vena cava (~ 1 dynes/cm²).^{323, 324} In arteries, the endothelial microtubule organizing center (MTOC) is localized upstream of the nucleus.³²⁵ Large veins exhibit MTOC localization downstream of the nucleus.³²⁵ Similar polarization patterns have been reported in localization of the Golgi Apparatus, which is localized upstream of bovine endothelial cells grown under laminar shear stress in culture.³²² Polarization of the golgi upstream of nuclei has also been observed in live zebrafish embryos using a fluorescent reporter for in endothelial cells. The Golgi was localized upstream of endothelial nuclei in the dorsal aorta and branching arteries.³²⁶ In contrast, in the posterior cardinal vein, where shear stress is much lower, endothelial cells do not exhibit golgi polarization.³²⁶

Golgi polarization occurs not only in shear-responsive tissues like endothelium, but also in most migrating cells, where it re-orientes towards the leading-edge protrusion. Both events are thought to be driven by the same mechanism. However, Golgi polarization is thought to support forward migration of the leading edge with directed delivery of newly translated proteins, though the need for upstream-direct protein trafficking does not seem as apparent. At its onset, polarization cues activate a polarity complex made up of Par6-Par3-PKC^{327, 328} which recruits dynein motor proteins to the upstream side/leading edge. Once anchored at the pole, the dynein motor activity instead pulls on microtubule filaments, drawing the MTOC at their minus end towards its new orientation.³²⁹ Golgi reorientation occurs after MTOC, though fragmentation of the organelle, though GRASP65 phosphorylation or other means, is required for this process. Despite receiving a great deal of research attention (as reviewed in^{330, 331}), the mechanisms regulating the final steps of Golgi positioning are not well understood. Golgi resident protein Golgin160 recruits dynein, which generates force required to move the Golgi fragments. However, many other components have been shown to regulate the process, including focal-adhesion associated paxillin which is required to inhibit activity of the

cytoplasmic microtubule deacetylase HDAC6.^{332, 333} Microtubule acetylation is associated with stabilizing newly nucleated microtubule filaments,³³⁴ suggesting that Golgi repositioning requires polymerization of new filaments. However, due to their inherent differences in size and complexity, the redistribution of an entire organelle is likely differentially regulated than that of a single protein.

Newly translated membrane will travel through the ER and Golgi Apparatus before reaching their final destination. Coat protein complex II (COPII) move cargo from ER exit sites toward the MTOC/Golgi via association with dynein motor proteins. This was classically thought to occur via vesicle mediated transport although recent work has challenged that dogma, instead proposing a complex network of interconnected membrane tubules to facilitate anterograde transport.³³⁵ Transmembrane proteins often contain ER export signals which can facilitate interactions with cargo adapters. Dihydrophobic³³⁶ and dibasic motifs³³⁷ in the C-tail and diacidic motifs proximal to transmembrane regions³³⁶ have all been reported to promote transport from the ER. In yeast, COPII vesicles are sufficient to delivery cargo to the Golgi directly³³⁸ though in mammalian systems, COPII delivers cargo to ER-Golgi intermediate compartments (ERGIC), and COPI proteins facilitate the transfer of vesicles from the ERGIC to the Golgi. COPI vesicles also facilitate retrograde trafficking from the Golgi back to the ER.^{339, 340}

The COPI and COPII complexes are composed of layers of interacting proteins which facilitate cargo selection, vesicle generation and transport. In COPII coats, the inner layer is initiated by Sar1 GTPase which when bound to GTP, becomes embedded in the membrane and recruits with Sec23/Sec24. The outer coat of COPII vesicles is formed by heterodimers of Sec13 and Sec31.^{338, 341} Notably, the content of these transport vesicles is determined through direct and indirect interaction with Sec24. Mammalian systems express four isoforms of Sec24^{342, 343} which are thought to facilitate the transport of a diverse repertoire of vesicular cargo.^{341, 344, 345} In comparison, the composition of COPI coat is less well understood. Following its activation, the small GTPase Arf1 associates with the membrane and recruits the F-subcomplex (β -COP, δ -COP, γ -COP and ζ -COP) and B-subcomplex (α -COP, β' -COP, ϵ -COP) of COPI proteins. The B-

subcomplex is thought to regulate cargo discrimination of COPI vesicles.^{346,347} In COPII vesicles, isoforms of Sec24 differentially discriminate cargo contents while recent proteomic studies have shown that COPI vesicles made from different coatomer isoforms contain similar contents.³⁴⁴

Shear stress may alter how Panx3 associates with isoforms of COPII cargo adapter Sec24. Based on its expression patterns, I would hypothesize that under static conditions, Panx3 would be excluded from COPII structures mediating exit from the ER while under shear stress Panx3 would be permitted into COPII structures for passage to the Golgi Apparatus. To test this, I would perform proximity ligation assays and co-immunoprecipitation experiments to assess the proximity and interaction between Panx3 and each of the Sec24 isoforms (Sec24A, Sec24B, Sec24C, and Sec24D). In static HAoEC cultures, I would expect Panx3 to be restricted from interaction with the COPII structures as it is retained in the ER. However, in HAoEC cultured under laminar flow conditions, I would anticipate that Panx3 association with one or more Sec24 isoforms to be readily detected. If shear stress does not alter the ability of Panx3 to interact with Sec24, that would indicate ER retention of Panx3 under static conditions may instead result from retrograde transport of Panx3 that is abolished under flow conditions.

5.4: Effects of hydrogen peroxide exposure on SK/IK channels

One aspect of the current work which merits further investigation is the effect of hydrogen peroxide on calcium-activated small and intermediate potassium channels (SK/IK). Under normal physiological conditions and redox balance, SK/IK channels are opened downstream vasodilatory signaling such as muscarinic activation, inducing potassium efflux and membrane hyperpolarization, which is transduced to signal relaxation of smooth muscle fibers. Hydrogen peroxide exposure induces a well-documented biphasic effect on small arteries, where low concentrations can induce rapid constriction or augmentation of basal tone, while high concentrations provoke a dramatic dilation.^{52, 53, 205, 208, 213} However, the question of how hydrogen peroxide affects SK/IK channel conductance specifically remains to be seen.

Hydrogen peroxide activation of TRPV4 channels has been previously reported in the literature,²¹⁸⁻²²⁰ which is in line with our observations from intact mesenteric arteries (Figures 10, 12N, and 13A-D), and could contribute to dilation induced following exposition to high concentrations of hydrogen peroxide. However, incubation of small arteries with SK/IK inhibitors charybdotoxin and apamin, or with non-selective K⁺ channel blocker tetrabutylammonium chloride (TBA), effectively blocks hydrogen peroxide-induced dilation,⁵² suggesting hydrogen peroxide-induced dilation involves conductance through SK/IK channels. However, in the context of genetic deletion of endothelial Panx3, resistance arteries exhibit impaired dilation to SK/IK agonist NS309 (Figure 8L), despite normal calcium store release (Figure 9C) and enhanced TRPV4 sparklet activity (Figure 10). This suggests oxidative stress may inhibit current through SK/IK channels in a calcium-independent manner. While this may seem to challenge reports that conclude hydrogen peroxide promotes conductance through SK/IK channels, it is possible that hydrogen peroxide exhibits an as of yet undescribed dose-dependent biphasic effect on SK/IK activity. While it has not yet been linked to oxidant dosing, oxidation of large-conductance calcium activated channels (BK) can either increase or decrease current through the channel, depending on whether methionine or cysteine residues have been oxidized, respectively.^{348, 349} To that end, it is possible that SK/IK residues are differentially oxidized such that current is inhibited following exposure to mild hydrogen peroxide and augmented in severe oxidative stress.

A two-pronged approach will enable assessment of the effect of hydrogen peroxide on SK/IK activity with increasing specificity of our results. First, one should confirm that the hydrogen peroxide-induced dilation impairments are derived from endothelial dysfunction rather than smooth muscle defects. This could be accomplished by performing a dose response to an endothelial-independent dilation signal, such as nitric oxide-donor sodium nitroprusside (SNP) on mesenteric arteries from EC *Panx3*^{ΔΔ} mice and controls. If there is no difference in dilation to SNP, it can be concluded that the EC *Panx3*^{ΔΔ} mice exhibit endothelial-derived dilation impairments. If, however, EC *Panx3*^{ΔΔ} arteries are unable to dilate to SNP to the same

degree as controls, it would indicate that dilatory impairments (to SNP as well as ACh in Figure 8I, and NS309 in Figure 8L) may arise from smooth muscle relaxation machinery (soluble guanylyl cyclase, cGMP, or cGMP-dependent channels and kinases).

To continue examination of endothelial SK/IK activity, dose response to SK/IK agonist NS309 should be performed via pressure myography in mesenteric arteries under redox balance or oxidative stress. In addition to the use of EC *Panx3*^{Δ/Δ} mice, which exhibit mild hydrogen peroxide overproduction, it would be informative to include an additional model which enables precise tuning of hydrogen peroxide generation. To drive Nox4-independent H₂O₂ overproduction in endothelium, we will capitalize on recent innovations in hydrogen peroxide chemogenetic probes. Mice have been generated with a transgenic construct inserted into the ROSA26 locus which drives expression of D-amino acid oxidase (DAAO) fused with HyPer, an H₂O₂-specific, ratiometric fluorescent biosensor,^{350, 351} following Cre-mediated excision of upstream stop codons. The yeast-derived DAAO generates H₂O₂ at equimolar concentrations while catalyzing the oxidation of D-amino acid substrates into their α-keto acids, such as pyruvate generated from D-alanine.³⁵¹ Similar chemogenetic targeting was used to demonstrate that oxidative stress is sufficient to induce heart failure³⁵² and that oxidative impairments in heart function are reversible when the D-amino acid substrates are removed.³⁵³ Here, inducible endothelial-specific targeting will be achieved via interbreeding with *Cdh5*-ER^{T2+} mice. With these mice, we will be able to precisely tune the degree of endothelial hydrogen peroxide generation and assess SK/IK channel activity indirectly via dilation to NS309. The conclusions from these studies will clarify how H₂O₂ effects endothelial mediated dilation of resistance arteries and contribute to our understanding of ROS in blood pressure regulation.

Figure 28: Perinatal genetic deletion of endothelial *Panx3* may impair angiogenesis.

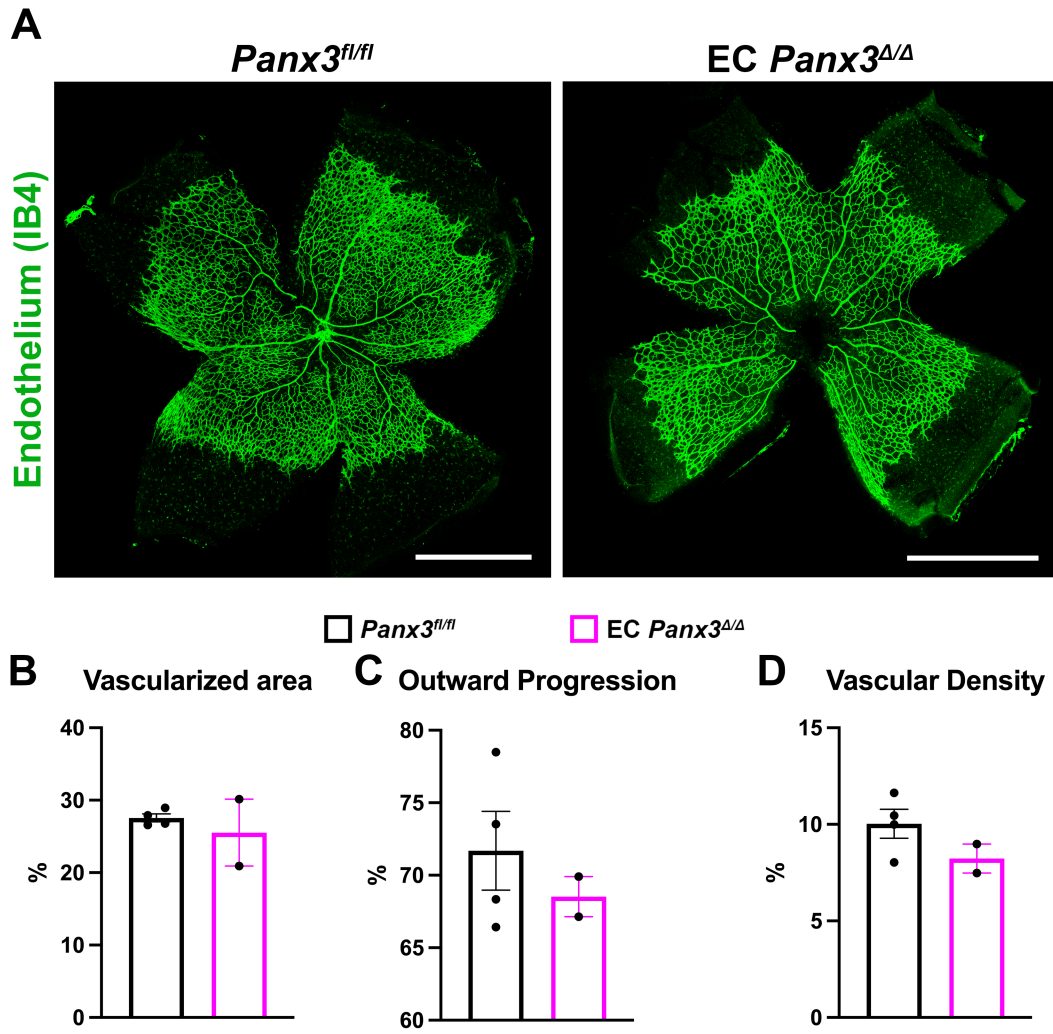


Figure 28: Perinatal genetic deletion of endothelial *Panx3* may impair angiogenesis. (A) P6 retinas from *EC Panx3^{Δ/Δ}* pups and littermate controls stained with IB4 to visualize endothelium in the developing vascular network. Scale bar is 1mm. (B) Vascularized area was calculated as a percentage of IB4+ area over total area of four ROIs. (C) Outward progression was averaged from 8 measurements of distance from optic nerve to angiogenic front normalized to the distance from optic nerve to retinal edge. (D) Vascular Density was calculated from skeletonized vessel area and normalized to total area. Each dot represents one mouse.

Figure 29: Endothelial *Panx3* expression may promote venous specification through modulation of repression by *Bcl6*

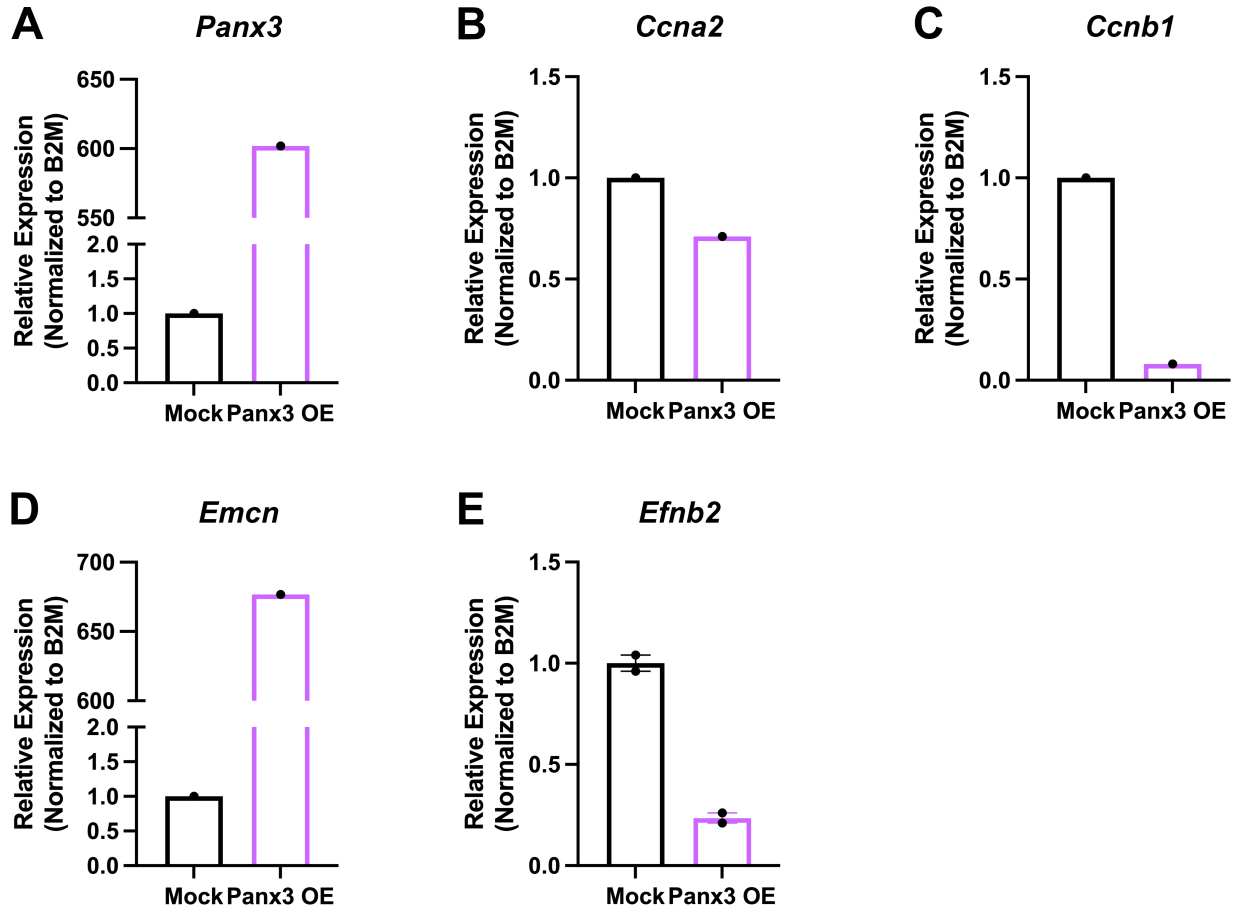


Figure 29: Endothelial *Panx3* expression may promote venous specification through modulation of repression by *Bcl6*. Transcript abundance of (A) *Panx3*, (B) Cyclin A2, (C) Cyclin B1, (D) Endomucin, and (E) Ephrin B2 in HAoEC following mock transfection (mock) or overexpression of h*Panx3* (*Panx3* OE).

Chapter 7: References

1. Zhou B, Perel P, Mensah GA and Ezzati M. Global epidemiology, health burden and effective interventions for elevated blood pressure and hypertension. *Nature Reviews Cardiology*. 2021;18:785-802.
2. Segal SS and Duling BR. Communication between feed arteries and microvessels in hamster striated muscle: segmental vascular responses are functionally coordinated. *Circulation research*. 1986;59:283-290.
3. Moore DH and Ruska H. The fine structure of capillaries and small arteries. *The Journal of Cell Biology*. 1957;3:457-462.
4. Griffith OW and Stuehr DJ. Nitric oxide synthases: properties and catalytic mechanism. *Annual review of physiology*. 1995;57:707-734.
5. Shesely EG, Maeda N, Kim H-S, Desai KM, Krege JH, Laubach VE, Sherman PA, Sessa WC and Smithies O. Elevated blood pressures in mice lacking endothelial nitric oxide synthase. *Proceedings of the National Academy of Sciences*. 1996;93:13176-13181.
6. Baylis C, Mitruka B and Deng A. Chronic blockade of nitric oxide synthesis in the rat produces systemic hypertension and glomerular damage. *The Journal of clinical investigation*. 1992;90:278-281.
7. Thum T, Fraccarollo D, Schultheiss M, Froese S, Galuppo P, Widder JD, Tsikas D, Ertl G and Bauersachs J. Endothelial nitric oxide synthase uncoupling impairs endothelial progenitor cell mobilization and function in diabetes. *Diabetes*. 2007;56:666-674.
8. Yang Y-M, Huang A, Kaley G and Sun D. eNOS uncoupling and endothelial dysfunction in aged vessels. *American Journal of Physiology-Heart and Circulatory Physiology*. 2009;297:H1829-H1836.
9. Daneva Z, Marziano C, Ottolini M, Chen Y-L, Baker TM, Kuppusamy M, Zhang A, Ta HQ, Reagan CE and Mihalek AD. Caveolar peroxynitrite formation impairs endothelial TRPV4 channels and elevates pulmonary arterial pressure in pulmonary hypertension. *Proceedings of the National Academy of Sciences*. 2021;118:e2023130118.
10. Ottolini M, Hong K, Cope EL, Daneva Z, DeLalio LJ, Sokolowski JD, Marziano C, Nguyen NY, Altschmied J, Haendeler J, Johnstone SR, Kalani MY, Park MS, Patel RP, Liedtke W, Isakson BE and Sonkusare SK. Local Peroxynitrite Impairs Endothelial Transient Receptor Potential Vanilloid 4 Channels and Elevates Blood Pressure in Obesity. *Circulation*. 2020;141:1318-1333.
11. Manea A, Manea SA, Florea IC, Luca CM and Raicu M. Positive regulation of NADPH oxidase 5 by proinflammatory-related mechanisms in human aortic smooth muscle cells. *Free Radical Biology and Medicine*. 2012;52:1497-1507.
12. Anrather J, Racchumi G and Iadecola C. NF- κ B regulates phagocytic NADPH oxidase by inducing the expression of gp91phox. *Journal of Biological Chemistry*. 2006;281:5657-5667.
13. Manea A, Tanase LI, Raicu M and Simionescu M. Transcriptional regulation of NADPH oxidase isoforms, Nox1 and Nox4, by nuclear factor-kappaB in human aortic smooth muscle cells. *Biochem Biophys Res Commun*. 2010;396:901-7.
14. Bretón-Romero R and Lamas S. Hydrogen peroxide signaling in vascular endothelial cells. *Redox Biol*. 2014;2:529-34.

15. Harrison DG, Gongora MC, Guzik TJ and Widder J. Oxidative stress and hypertension. *J Am Soc Hypertens*. 2007;1:30-44.
16. Forrester SJ, Preston KJ, Cooper HA, Boyer MJ, Escoto KM, Poltronetti AJ, Elliott KJ, Kuroda R, Miyao M, Sesaki H, Akiyama T, Kimura Y, Rizzo V, Scalia R and Eguchi S. Mitochondrial Fission Mediates Endothelial Inflammation. *Hypertension*. 2020;76:267-276.
17. Xie H, Ray PE and Short BL. NF-kappaB activation plays a role in superoxide-mediated cerebral endothelial dysfunction after hypoxia/reoxygenation. *Stroke*. 2005;36:1047-52.
18. Pierce GL, Lesniewski LA, Lawson BR, Beske SD and Seals DR. Nuclear factor- κ B activation contributes to vascular endothelial dysfunction via oxidative stress in overweight/obese middle-aged and older humans. *Circulation*. 2009;119:1284-92.
19. Touyz R, Chen X, He G, Quinn M and Schiffrin E. Expression of a gp91phox-containing leukocyte-type NADPH oxidase in human vascular smooth muscle cells: modulation by Ang II. *Circ Res*. 2002;90:1205-1213.
20. Queisser N and Schupp N. Aldosterone, oxidative stress, and NF- κ B activation in hypertension-related cardiovascular and renal diseases. *Free Radical Biology and Medicine*. 2012;53:314-327.
21. Pu Q, Neves MF, Virdis A, Touyz RM and Schiffrin EL. Endothelin antagonism on aldosterone-induced oxidative stress and vascular remodeling. *Hypertension*. 2003;42:49-55.
22. Dobrian AD, Schriver SD, Khraibi AA and Prewitt RL. Pioglitazone prevents hypertension and reduces oxidative stress in diet-induced obesity. *Hypertension*. 2004;43:48-56.
23. Dobrian AD, Davies MJ, Schriver SD, Lauterio TJ and Prewitt RL. Oxidative stress in a rat model of obesity-induced hypertension. *Hypertension*. 2001;37:554-560.
24. Zhu J, Huang T and Lombard JH. Effect of high-salt diet on vascular relaxation and oxidative stress in mesenteric resistance arteries. *Journal of vascular research*. 2007;44:382-390.
25. Bayorh MA, Ganafa AA, Socci RR, Silvestrov N and Abukhalaf IK. The role of oxidative stress in salt-induced hypertension. *American Journal of hypertension*. 2004;17:31-36.
26. Awe SO, Tsakadze NL, D'Souza SE and Adeagbo AS. Tert-butyl hydroperoxide-mediated vascular responses in DOCA-salt hypertensive rats. *Vascul Pharmacol*. 2003;40:51-7.
27. Amaral JH, Ferreira GC, Pinheiro LC, Montenegro MF and Tanus-Santos JE. Consistent antioxidant and antihypertensive effects of oral sodium nitrite in DOCA-salt hypertension. *Redox biology*. 2015;5:340-346.
28. Russo C, Olivieri O, Girelli D, Faccini G, Zenari ML, Lombardi S and Corrocher R. Antioxidant status and lipid peroxidation in patients with essential hypertension. *Journal of hypertension*. 1998;16:1267-1271.
29. Rodrigo R, Prat H, Passalacqua W, Araya J and Bächler JP. Decrease in oxidative stress through supplementation of vitamins C and E is associated with a reduction in blood pressure in patients with essential hypertension. *Clinical Science*. 2008;114:625-634.
30. Rodrigo R, Bächler JP, Araya J, Prat H and Passalacqua W. Relationship between (Na⁺ K)-ATPase activity, lipid peroxidation and fatty acid profile in erythrocytes of hypertensive and normotensive subjects. *Molecular and cellular biochemistry*. 2007;303:73-81.
31. Appel LJ, Moore TJ, Obarzanek E, Vollmer WM, Svetkey LP, Sacks FM, Bray GA, Vogt TM, Cutler JA, Windhauser MM, Lin PH and Karanja N. A clinical trial of the effects of dietary patterns on blood pressure. DASH Collaborative Research Group. *N Engl J Med*. 1997;336:1117-24.

32. Galley HF, Thornton J, Howdle PD, Walker BE and Webster NR. Combination oral antioxidant supplementation reduces blood pressure. *Clinical science*. 1997;92:361-365.
33. Hercberg S, Galan P, Preziosi P, Bertrais S, Mennen L, Malvy D, Rousset A-M, Favier A and Briançon S. The SU. VI. MAX Study: a randomized, placebo-controlled trial of the health effects of antioxidant vitamins and minerals. *Archives of internal medicine*. 2004;164:2335-2342.
34. Kim MK, Sasaki S, Sasazuki S, Okubo S, Hayashi M and Tsugane S. Lack of long-term effect of vitamin C supplementation on blood pressure. *Hypertension*. 2002;40:797-803.
35. Plantinga Y, Ghiadoni L, Magagna A, Giannarelli C, Franzoni F, Taddei S and Salvetti A. Supplementation with vitamins C and E improves arterial stiffness and endothelial function in essential hypertensive patients. *American journal of hypertension*. 2007;20:392-397.
36. Ward NC, Hodgson JM, Croft KD, Burke V, Beilin LJ and Puddey IB. The combination of vitamin C and grape-seed polyphenols increases blood pressure: a randomized, double-blind, placebo-controlled trial. *Journal of hypertension*. 2005;23:427-434.
37. Ward NC, Wu JH, Clarke MW, Puddey IB, Burke V, Croft KD and Hodgson JM. The effect of vitamin E on blood pressure in individuals with type 2 diabetes: a randomized, double-blind, placebo-controlled trial. *Journal of hypertension*. 2007;25:227-234.
38. Baradaran A, Nasri H and Rafieian-Kopaei M. Oxidative stress and hypertension: Possibility of hypertension therapy with antioxidants. *J Res Med Sci*. 2014;19:358-67.
39. Rodrigo R, González J and Paoletto F. The role of oxidative stress in the pathophysiology of hypertension. *Hypertension Research*. 2011;34:431-440.
40. Nisimoto Y, Diebold BA, Cosentino-Gomes D and Lambeth JD. Nox4: a hydrogen peroxide-generating oxygen sensor. *Biochemistry*. 2014;53:5111-5120.
41. McKinley BA and Butler BD. Comparison of skeletal muscle PO₂, PCO₂, and pH with gastric tonometric PCO₂ and pH in hemorrhagic shock. *Critical care medicine*. 1999;27:1869-1877.
42. Sharp FR and Bernaudin M. HIF1 and oxygen sensing in the brain. *Nature Reviews Neuroscience*. 2004;5:437-448.
43. Lu X, Murphy TC, Nanes MS and Hart CM. PPAR γ regulates hypoxia-induced Nox4 expression in human pulmonary artery smooth muscle cells through NF- κ B. *American Journal of Physiology-Lung Cellular and Molecular Physiology*. 2010;299:L559-L566.
44. Mittal M, Roth M, König P, Hofmann S, Dony E, Goyal P, Selbitz A-C, Schermuly RT, Ghofrani HA and Kwapiszewska G. Hypoxia-dependent regulation of nonphagocytic NADPH oxidase subunit NOX4 in the pulmonary vasculature. *Circulation research*. 2007;101:258-267.
45. Pendyala S, Gorshkova IA, Usatyuk PV, He D, Pennathur A, Lambeth JD, Thannickal VJ and Natarajan V. Role of Nox4 and Nox2 in hyperoxia-induced reactive oxygen species generation and migration of human lung endothelial cells. *Antioxidants & redox signaling*. 2009;11:747-764.
46. Pendyala S, Moitra J, Kalari S, Kleeberger SR, Zhao Y, Reddy SP, Garcia JG and Natarajan V. Nrf2 regulates hyperoxia-induced Nox4 expression in human lung endothelium: identification of functional antioxidant response elements on the Nox4 promoter. *Free Radical Biology and Medicine*. 2011;50:1749-1759.
47. D'Auréaux B and Toledano MB. ROS as signalling molecules: mechanisms that generate specificity in ROS homeostasis. *Nat Rev Mol Cell Biol*. 2007;8:813-24.
48. Gough DR and Cotter TG. Hydrogen peroxide: a Jekyll and Hyde signalling molecule. *Cell Death Dis*. 2011;2:e213.

49. Nowicki P, Flavahan S, Hassanain H, Mitra S, Holland S, Goldschmidt-Clermont P and Flavahan N. Redox signaling of the arteriolar myogenic response. *Circulation research*. 2001;89:114-116.
50. De Gaetano G, Donati MB and Cerletti C. Prevention of thrombosis and vascular inflammation: benefits and limitations of selective or combined COX-1, COX-2 and 5-LOX inhibitors. *Trends in pharmacological sciences*. 2003;24:245-252.
51. Hemler ME, Cook HW and Lands WE. Prostaglandin biosynthesis can be triggered by lipid peroxides. *Archives of biochemistry and biophysics*. 1979;193:340-345.
52. Cseko C, Bagi Z and Koller A. Biphasic effect of hydrogen peroxide on skeletal muscle arteriolar tone via activation of endothelial and smooth muscle signaling pathways. *J Appl Physiol (1985)*. 2004;97:1130-7.
53. Ray R, Murdoch CE, Wang M, Santos CX, Zhang M, Alom-Ruiz S, Anilkumar N, Ouattara A, Cave AC and Walker SJ. Endothelial Nox4 NADPH oxidase enhances vasodilatation and reduces blood pressure in vivo. *Arteriosclerosis, thrombosis, and vascular biology*. 2011;31:1368-1376.
54. Caterina MJ, Schumacher MA, Tominaga M, Rosen TA, Levine JD and Julius D. The capsaicin receptor: a heat-activated ion channel in the pain pathway. *Nature*. 1997;389:816-824.
55. Miyake T, Shirakawa H, Nakagawa T and Kaneko S. Activation of mitochondrial transient receptor potential vanilloid 1 channel contributes to microglial migration. *Glia*. 2015;63:1870-1882.
56. Beyer EC and Berthoud VM. Gap junction gene and protein families: Connexins, innexins, and pannexins. *Biochimica et Biophysica Acta (BBA)-Biomembranes*. 2018;1860:5-8.
57. Bruzzone R, Hormuzdi SG, Barbe MT, Herb A and Monyer H. Pannexins, a family of gap junction proteins expressed in brain. *Proceedings of the national academy of sciences*. 2003;100:13644-13649.
58. Penuela S, Bhalla R, Gong X-Q, Cowan KN, Celetti SJ, Cowan BJ, Bai D, Shao Q and Laird DW. Pannexin 1 and pannexin 3 are glycoproteins that exhibit many distinct characteristics from the connexin family of gap junction proteins. *Journal of Cell Science*. 2007;120:3772-3783.
59. Penuela S, Celetti SJ, Bhalla R, Shao Q and Laird DW. Diverse subcellular distribution profiles of pannexin1 and pannexin3. *Cell communication & adhesion*. 2008;15:133-142.
60. Penuela S, Bhalla R, Nag K and Laird DW. Glycosylation regulates pannexin intermixing and cellular localization. *Mol Biol Cell*. 2009;20:4313-23.
61. Boassa D, Qiu F, Dahl G and Sosinsky G. Trafficking dynamics of glycosylated pannexin1 proteins. *Cell communication & adhesion*. 2008;15:119-132.
62. Sahu G, Sukumaran S and Bera AK. Pannexins form gap junctions with electrophysiological and pharmacological properties distinct from connexins. *Scientific reports*. 2014;4:1-9.
63. Lohman AW, Leskov IL, Butcher JT, Johnstone SR, Stokes TA, Begandt D, DeLalio LJ, Best AK, Penuela S, Leitinger N, Ravichandran KS, Stokes KY and Isakson BE. Pannexin 1 channels regulate leukocyte emigration through the venous endothelium during acute inflammation. *Nat Commun*. 2015;6:7965.
64. Boyce AK, Kim MS, Wicki-Stordeur LE and Swayne LA. ATP stimulates pannexin 1 internalization to endosomal compartments. *Biochemical Journal*. 2015;470:319-330.
65. Lai C, Bechberger J and Naus C. Pannexin2 as a novel growth regulator in C6 glioma cells. *Oncogene*. 2009;28:4402-4408.

66. Swayne LA, Sorbara CD and Bennett SA. Pannexin 2 is expressed by postnatal hippocampal neural progenitors and modulates neuronal commitment. *Journal of Biological Chemistry*. 2010;285:24977-24986.
67. Ambrosi C, Gassmann O, Pranskevich JN, Boassa D, Smock A, Wang J, Dahl G, Steinem C and Sosinsky GE. Pannexin1 and Pannexin2 channels show quaternary similarities to connexons and different oligomerization numbers from each other. *Journal of Biological Chemistry*. 2010;285:24420-24431.
68. Iwamoto T, Nakamura T, Doyle A, Ishikawa M, de Vega S, Fukumoto S and Yamada Y. Pannexin 3 regulates intracellular ATP/cAMP levels and promotes chondrocyte differentiation. *J Biol Chem*. 2010;285:18948-58.
69. Iwamoto T, Nakamura T, Ishikawa M, Yoshizaki K, Sugimoto A, Ida-Yonemochi H, Ohshima H, Saito M, Yamada Y and Fukumoto S. Pannexin 3 regulates proliferation and differentiation of odontoblasts via its hemichannel activities. *PLoS One*. 2017;12:e0177557.
70. Michalski K, Syrjanen JL, Henze E, Kumpf J, Furukawa H and Kawate T. The Cryo-EM structure of pannexin 1 reveals unique motifs for ion selection and inhibition. *Elife*. 2020;9.
71. Zhang P, Ishikawa M, Doyle A, Nakamura T, He B and Yamada Y. Pannexin 3 regulates skin development via Epiprofin. *Scientific reports*. 2021;11:1-16.
72. The Human Protein Atlas. 2020:ENSG00000113916-BCL6/cell.
73. Ishikawa M, Williams G, Forcinito P, Ishikawa M, Petrie RJ, Saito K, Fukumoto S and Yamada Y. Pannexin 3 ER Ca²⁺ channel gating is regulated by phosphorylation at the Serine 68 residue in osteoblast differentiation. *Scientific reports*. 2019;9:1-14.
74. Langlois S, Xiang X, Young K, Cowan BJ, Penuela S and Cowan KN. Pannexin 1 and pannexin 3 channels regulate skeletal muscle myoblast proliferation and differentiation. *Journal of Biological Chemistry*. 2014;289:30717-30731.
75. Bhalla-Gehi R, Penuela S, Churko JM, Shao Q and Laird DW. Pannexin1 and pannexin3 delivery, cell surface dynamics, and cytoskeletal interactions. *J Biol Chem*. 2010;285:9147-60.
76. Pham TL, St-Pierre ME, Ravel-Chapuis A, Parks TE, Langlois S, Penuela S, Jasmin BJ and Cowan KN. Expression of Pannexin 1 and Pannexin 3 during skeletal muscle development, regeneration, and Duchenne muscular dystrophy. *Journal of Cellular Physiology*. 2018;233:7057-7070.
77. Song F, Sun H, Huang L, Fu D and Huang C. The role of pannexin3-modified human dental pulp-derived mesenchymal stromal cells in repairing rat cranial critical-sized bone defects. *Cellular Physiology and Biochemistry*. 2017;44:2174-2188.
78. Whyte-Fagundes P, Kurtenbach S, Zoidl C, Shestopalov VI, Carlen PL and Zoidl G. A potential compensatory role of Panx3 in the VNO of a Panx1 knock out mouse model. *Frontiers in molecular neuroscience*. 2018;11:135.
79. Cowan KN, Langlois S, Penuela S, Cowan BJ and Laird DW. Pannexin1 and Pannexin3 exhibit distinct localization patterns in human skin appendages and are regulated during keratinocyte differentiation and carcinogenesis. *Cell communication & adhesion*. 2012;19:45-53.
80. Hanson CA, Drake KR, Baird MA, Han B, Kraft LJ, Davidson MW and Kenworthy AK. Overexpression of caveolin-1 is sufficient to phenocopy the behavior of a disease-associated mutant. *Traffic*. 2013;14:663-677.

81. Kubo A, Ueda S, Yamane A, Wada-Kakuda S, Narita M, Matsuyama M, Nomori A, Takashima A, Kato T and Onodera O. Ectopic expression induces abnormal somatodendritic distribution of tau in the mouse brain. *Journal of Neuroscience*. 2019;39:6781-6797.
82. Lisenbee CS, Karnik SK and Trelease RN. Overexpression and mislocalization of a Tail-Anchored GFP redefines the identity of peroxisomal ER. *Traffic*. 2003;4:491-501.
83. Han B, Tiwari A and Kenworthy AK. Tagging strategies strongly affect the fate of overexpressed caveolin-1. *Traffic*. 2015;16:417-438.
84. Boassa D, Ambrosi C, Qiu F, Dahl G, Gaietta G and Sosinsky G. Pannexin1 channels contain a glycosylation site that targets the hexamer to the plasma membrane. *Journal of Biological Chemistry*. 2007;282:31733-31743.
85. Deng Z, He Z, Makshev G, Bitter RM, Rau M, Fitzpatrick JA and Yuan P. Cryo-EM structures of the ATP release channel pannexin 1. *Nature Structural & Molecular Biology*. 2020;27:373-381.
86. Jin Q, Zhang B, Zheng X, Li N, Xu L, Xie Y, Song F, Bhat EA, Chen Y and Gao N. Cryo-EM structures of human pannexin 1 channel. *Cell research*. 2020;30:449-451.
87. Qu R, Dong L, Zhang J, Yu X, Wang L and Zhu S. Cryo-EM structure of human heptameric Pannexin 1 channel. *Cell research*. 2020;30:446-448.
88. Ruan Z, Orozco IJ, Du J and Lü W. Structures of human pannexin 1 reveal ion pathways and mechanism of gating. *Nature*. 2020;584:646-651.
89. Drożdżyk K, Sawicka M, Bahamonde-Santos M-I, Jonas Z, Deneka D, Albrecht C and Dutzler R. Cryo-EM structures and functional properties of CALHM channels of the human placenta. *Elife*. 2020;9:e55853.
90. Pillon NJ, Li YE, Fink LN, Brozinick JT, Nikolayev A, Kuo M-S, Bilan PJ and Klip A. Nucleotides released from palmitate-challenged muscle cells through pannexin-3 attract monocytes. *Diabetes*. 2014;63:3815-3826.
91. Ishikawa M, Iwamoto T, Nakamura T, Doyle A, Fukumoto S and Yamada Y. Pannexin 3 functions as an ER Ca(2+) channel, hemichannel, and gap junction to promote osteoblast differentiation. *J Cell Biol*. 2011;193:1257-74.
92. Ishikawa M, Williams GL, Ikeuchi T, Sakai K, Fukumoto S and Yamada Y. Pannexin 3 and connexin 43 modulate skeletal development through their distinct functions and expression patterns. *J Cell Sci*. 2016;129:1018-30.
93. Fu D, Song F, Sun H, Pei D, Wang Y, Lei J and Huang C. Expression of Pannexin3 in human odontoblast-like cells and its hemichannel function in mediating ATP release. *Archives of Oral Biology*. 2015;60:1510-1516.
94. Ma D, Feng L, Cheng Y, Xin M, You J, Yin X, Hao Y, Cui L and Feng J. Astrocytic gap junction inhibition by carbenoxolone enhances the protective effects of ischemic preconditioning following cerebral ischemia. *Journal of neuroinflammation*. 2018;15:1-12.
95. Vessey JP, Lalonde MR, Mizan HA, Welch NC, Kelly ME and Barnes S. Carbenoxolone inhibition of voltage-gated Ca channels and synaptic transmission in the retina. *Journal of neurophysiology*. 2004;92:1252-1256.
96. Zhou Q, Zhang Z, Nagasawa T and Hiai S. The structure activity relationship of saikosaponins and glycyrrhizin derivatives for Na⁺, K⁺-ATPase inhibiting action. *Yao xue xue bao = Acta Pharmaceutica Sinica*. 1996;31:496-501.
97. Michalski K and Kawate T. Carbenoxolone inhibits Pannexin1 channels through interactions in the first extracellular loop. *Journal of General Physiology*. 2016;147:165-174.

98. White TW, Goodenough DA and Paul DL. Targeted ablation of connexin50 in mice results in microphthalmia and zonular pulverulent cataracts. *The Journal of cell biology*. 1998;143:815-825.
99. Rong P, Wang X, Niesman I, Wu Y, Benedetti LE, Dunia I, Levy E and Gong X. Disruption of Gja8 ($\alpha 8$ connexin) in mice leads to microphthalmia associated with retardation of lens growth and lens fiber maturation. 2002.
100. Dunia I, Cibert C, Gong X, Xia C-h, Recouvreur M, Levy E, Kumar N, Bloemendal H and Benedetti EL. Structural and immunocytochemical alterations in eye lens fiber cells from Cx46 and Cx50 knockout mice. *European journal of cell biology*. 2006;85:729-752.
101. Sellitto C, Li L and White TW. Connexin50 is essential for normal postnatal lens cell proliferation. *Investigative ophthalmology & visual science*. 2004;45:3196-3202.
102. Banks EA, Yu XS, Shi Q and Jiang JX. Promotion of lens epithelial-fiber differentiation by the C-terminus of connexin 45.6—a role independent of gap junction communication. *Journal of cell science*. 2007;120:3602-3612.
103. Shi Q, Gu S, Yu XS, White TW, Banks EA and Jiang JX. Connexin controls cell-cycle exit and cell differentiation by directly promoting cytosolic localization and degradation of E3 ligase Skp2. *Developmental cell*. 2015;35:483-496.
104. Shi Q, Banks EA, Yu XS, Gu S, Lauer J, Fields GB and Jiang JX. Amino acid residue Val362 plays a critical role in maintaining the structure of C terminus of connexin 50 and in lens epithelial-fiber differentiation. *Journal of Biological Chemistry*. 2010;285:18415-18422.
105. Xiang X, Langlois S, St-Pierre M-E, Barré JF, Grynspan D, Purgina B and Cowan KN. Pannexin 1 inhibits rhabdomyosarcoma progression through a mechanism independent of its canonical channel function. *Oncogenesis*. 2018;7:1-16.
106. Xiang X, Langlois S, St-Pierre M-E, Blinder A, Charron P, Graber TE, Fowler SL, Baird SD, Bennett SA and Alain T. Identification of pannexin 1-regulated genes, interactome, and pathways in rhabdomyosarcoma and its tumor inhibitory interaction with AHNAK. *Oncogene*. 2021;40:1868-1883.
107. Lu H, Shamanna RA, de Freitas JK, Okur M, Khadka P, Kulikowicz T, Holland PP, Tian J, Croteau DL and Davis AJ. Cell cycle-dependent phosphorylation regulates RECQL4 pathway choice and ubiquitination in DNA double-strand break repair. *Nature communications*. 2017;8:1-14.
108. Miles RR, Crockett DK, Lim MS and Elenitoba-Johnson KS. Analysis of BCL6-interacting proteins by tandem mass spectrometry. *Mol Cell Proteomics*. 2005;4:1898-909.
109. Luck K, Kim D-K, Lambourne L, Spirohn K, Begg BE, Bian W, Brignall R, Cafarelli T, Campos-Laborie FJ and Charlotheaux B. A reference map of the human binary protein interactome. *Nature*. 2020;580:402-408.
110. Yachie N, Petsalaki E, Mellor JC, Weile J, Jacob Y, Verby M, Ozturk SB, Li S, Cote AG and Mosca R. Pooled-matrix protein interaction screens using Barcode Fusion Genetics. *Molecular systems biology*. 2016;12:863.
111. Baron BW, Nucifora G, McCabe N, Espinosa 3rd R, Le Beau MM and McKeithan TW. Identification of the gene associated with the recurring chromosomal translocations t(3;14)(q27;q32) and t(3;22)(q27;q11) in B-cell lymphomas. *Proceedings of the National Academy of Sciences*. 1993;90:5262-5266.

112. Kerckaert J-P, Deweindt C, Tilly H, Quief S, Lecocq G and Bastard C. LAZ3, a novel zinc-finger encoding gene, is disrupted by recurring chromosome 3q27 translocations in human lymphomas. *Nature genetics*. 1993;5:66-70.
113. Ye BH, Lista F, Lo Coco F, Knowles DM, Offit K, Chaganti R and Dalla-Favera R. Alterations of a zinc finger-encoding gene, BCL-6, in diffuse large-cell lymphoma. *Science*. 1993;262:747-750.
114. Albagli-Curiel O. Ambivalent role of BCL6 in cell survival and transformation. *Oncogene*. 2003;22:507-516.
115. Hatzi K and Melnick A. Breaking bad in the germinal center: how deregulation of BCL6 contributes to lymphomagenesis. *Trends Mol Med*. 2014;20:343-52.
116. Basso K and Dalla-Favera R. BCL6: master regulator of the germinal center reaction and key oncogene in B cell lymphomagenesis. *Advances in immunology*. 2010;105:193-210.
117. Duy C, Yu JJ, Nahar R, Swaminathan S, Kweon S-M, Polo JM, Valls E, Klemm L, Shojaee S and Cerchietti L. BCL6 is critical for the development of a diverse primary B cell repertoire. *Journal of Experimental Medicine*. 2010;207:1209-1221.
118. Huang C, Gonzalez DG, Cote CM, Jiang Y, Hatzi K, Teater M, Dai K, Hla T, Haberman AM and Melnick A. The BCL6 RD2 domain governs commitment of activated B cells to form germinal centers. *Cell Rep*. 2014;8:1497-508.
119. Phan RT, Saito M, Kitagawa Y, Means AR and Dalla-Favera R. Genotoxic stress regulates expression of the proto-oncogene Bcl6 in germinal center B cells. *Nat Immunol*. 2007;8:1132-9.
120. Iqbal J, Greiner TC, Patel K, Dave BJ, Smith L, Ji J, Wright G, Sanger W, Pickering D and Jain S. Distinctive patterns of BCL6 molecular alterations and their functional consequences in different subgroups of diffuse large B-cell lymphoma. *Leukemia*. 2007;21:2332-2343.
121. Ye BH, Cattoretti G, Shen Q, Zhang J, Hawe N, Waard Rd, Leung C, Nouri-Shirazi M, Orazi A and Chaganti R. The BCL-6 proto-oncogene controls germinal-centre formation and Th2-type inflammation. *Nature genetics*. 1997;16:161-170.
122. Buchberger E, Payrhuber D, El Harchi M, Zagraban B, Scheuba K, Zommer A, Bugyik E, Dome B, Kral JB and Schrottmaier WC. Inhibition of the transcriptional repressor complex Bcl-6/BCoR induces endothelial sprouting but does not promote tumor growth. *Oncotarget*. 2017;8:552.
123. Chen YL, Baker TM, Lee F, Shui B, Lee JC, Tvrdik P, Kotlikoff MI and Sonkusare SK. Calcium signal profiles in vascular endothelium from Cdh5-GCaMP8 and Cx40-GCaMP2 mice. *Journal of vascular research*. 2021;58:159-171.
124. Duan S, Cermak L, Pagan JK, Rossi M, Martinengo C, di Celle PF, Chapuy B, Shipp M, Chiarle R and Pagano M. FBXO11 targets BCL6 for degradation and is inactivated in diffuse large B-cell lymphomas. *Nature*. 2012;481:90-3.
125. Okabe S, Fukuda T, Ishibashi K, Kojima S, Okada S, Hatano M, Ebara M, Saisho H and Tokuhisa T. BAZF, a novel Bcl6 homolog, functions as a transcriptional repressor. *Molecular and cellular biology*. 1998;18:4235-4244.
126. Sakashita C, Fukuda T, Okabe S, Kobayashi H, Hirosawa S, Tokuhisa T, Miyasaka N, Miura O and Miki T. Cloning and characterization of the human BAZF gene, a homologue of the BCL6 oncogene. *Biochemical and biophysical research communications*. 2002;291:567-573.
127. Takenaga M, Hatano M, Takamori M, Yamashita Y, Okada S, Kuroda Y and Tokuhisa T. Bcl6-dependent transcriptional repression by BAZF. *Biochemical and biophysical research communications*. 2003;303:600-608.

128. Ohnuki H, Inoue H, Takemori N, Nakayama H, Sakaue T, Fukuda S, Miwa D, Nishiwaki E, Hatano M and Tokuhisa T. BAZF, a novel component of cullin3-based E3 ligase complex, mediates VEGFR and Notch cross-signaling in angiogenesis. *Blood, The Journal of the American Society of Hematology*. 2012;119:2688-2698.
129. Fan Y, Wang Y, Tang Z, Zhang H, Qin X, Zhu Y, Guan Y, Wang X, Staels B and Chien S. Suppression of pro-inflammatory adhesion molecules by PPAR- δ in human vascular endothelial cells. *Arteriosclerosis, thrombosis, and vascular biology*. 2008;28:315-321.
130. Dent AL, Vasanwala FH and Toney LM. Regulation of gene expression by the proto-oncogene BCL-6. *Critical reviews in oncology/hematology*. 2002;41:1-9.
131. Bereshchenko OR, Gu W and Dalla-Favera R. Acetylation inactivates the transcriptional repressor BCL6. *Nature genetics*. 2002;32:606-613.
132. Chang CC, Ye BH, Chaganti RS and Dalla-Favera R. BCL-6, a POZ/zinc-finger protein, is a sequence-specific transcriptional repressor. *Proc Natl Acad Sci U S A*. 1996;93:6947-52.
133. Seyfert VL, Allman D, He Y and Staudt LM. Transcriptional repression by the proto-oncogene BCL-6. *Oncogene*. 1996;12:2331-42.
134. Dhordain P, Albagli O, Lin RJ, Ansieau S, Quief S, Leutz A, Kerckaert JP, Evans RM and LePrince D. Corepressor SMRT binds the BTB/POZ repressing domain of the LAZ3/BCL6 oncoprotein. *Proc Natl Acad Sci U S A*. 1997;94:10762-7.
135. Dhordain P, Lin RJ, Quief S, Lantoine D, Kerckaert JP, Evans RM and Albagli O. The LAZ3(BCL-6) oncoprotein recruits a SMRT/mSIN3A/histone deacetylase containing complex to mediate transcriptional repression. *Nucleic Acids Res*. 1998;26:4645-51.
136. Huynh KD and Bardwell VJ. The BCL-6 POZ domain and other POZ domains interact with the co-repressors N-CoR and SMRT. *Oncogene*. 1998;17:2473-2484.
137. Wong C-W and Privalsky ML. Components of the SMRT corepressor complex exhibit distinctive interactions with the POZ domain oncoproteins PLZF, PLZF-RAR α , and BCL-6. *Journal of Biological Chemistry*. 1998;273:27695-27702.
138. Huynh KD, Fischle W, Verdin E and Bardwell VJ. BCoR, a novel corepressor involved in BCL-6 repression. *Genes & development*. 2000;14:1810-1823.
139. Niu H, Ye BH and Dalla-Favera R. Antigen receptor signaling induces MAP kinase-mediated phosphorylation and degradation of the BCL-6 transcription factor. *Genes Dev*. 1998;12:1953-61.
140. Perez-Rosado A, Artiga M, Vargiu P, Sanchez-Aguilera A, Alvarez-Barrientos A and Piris M. BCL6 represses NFkappaB activity in diffuse large B-cell lymphomas. *J Pathol*. 2008;214:498-507.
141. Barish GD, Yu RT, Karunasiri M, Ocampo CB, Dixon J, Benner C, Dent AL, Tangirala RK and Evans RM. Bcl-6 and NF-kappaB cisomes mediate opposing regulation of the innate immune response. *Genes Dev*. 2010;24:2760-5.
142. Barish GD, Ruth TY, Karunasiri MS, Becerra D, Kim J, Tseng TW, Tai L-J, LeBlanc M, Diehl C and Cerchietti L. The Bcl6-SMRT/NCoR cisome represses inflammation to attenuate atherosclerosis. *Cell metabolism*. 2012;15:554-562.
143. Moon PM, Penuela S, Barr K, Khan S, Pin CL, Welch I, Attur M, Abramson SB, Laird DW and Beier F. Deletion of Panx3 Prevents the Development of Surgically Induced Osteoarthritis. *J Mol Med (Berl)*. 2015;93:845-56.
144. O'Donnell BL and Penuela S. Pannexin 3 channels in health and disease. *Purinergic Signalling*. 2021;17:577-589.

145. Billaud M, Chiu YH, Lohman AW, Parpaite T, Butcher JT, Mutchler SM, DeLalio LJ, Artamonov MV, Sandilos JK, Best AK, Somlyo AV, Thompson RJ, Le TH, Ravichandran KS, Bayliss DA and Isakson BE. A molecular signature in the pannexin1 intracellular loop confers channel activation by the α 1 adrenoceptor in smooth muscle cells. *Sci Signal*. 2015;8:ra17.
146. Denzel A, Maus UA, Rodriguez Gomez M, Moll C, Niedermeier M, Winter C, Maus R, Hollingshead S, Briles DE, Kunz-Schughart LA, Talke Y and Mack M. Basophils enhance immunological memory responses. *Nat Immunol*. 2008;9:733-42.
147. Ohmori K, Luo Y, Jia Y, Nishida J, Wang Z, Bunting KD, Wang D and Huang H. IL-3 induces basophil expansion in vivo by directing granulocyte-monocyte progenitors to differentiate into basophil lineage-restricted progenitors in the bone marrow and by increasing the number of basophil/mast cell progenitors in the spleen. *J Immunol*. 2009;182:2835-41.
148. Good ME, Chiu YH, Poon IKH, Medina CB, Butcher JT, Mendu SK, DeLalio LJ, Lohman AW, Leitinger N, Barrett E, Lorenz UM, Desai BN, Jaffe IZ, Bayliss DA, Isakson BE and Ravichandran KS. Pannexin 1 Channels as an Unexpected New Target of the Anti-Hypertensive Drug Spironolactone. *Circ Res*. 2018;122:606-615.
149. DeLalio LJ, Keller AS, Chen J, Boyce AKJ, Artamonov MV, Askew-Page HR, Keller TCSt, Johnstone SR, Weaver RB, Good ME, Murphy SA, Best AK, Mintz EL, Penuela S, Greenwood IA, Machado RF, Somlyo AV, Swayne LA, Minshall RD and Isakson BE. Interaction Between Pannexin 1 and Caveolin-1 in Smooth Muscle Can Regulate Blood Pressure. *Arterioscler Thromb Vasc Biol*. 2018;38:2065-2078.
150. DeLalio LJ, Billaud M, Ruddiman CA, Johnstone SR, Butcher JT, Wolpe AG, Jin X, Keller TCSt, Keller AS, Rivière T, Good ME, Best AK, Lohman AW, Swayne LA, Penuela S, Thompson RJ, Lampe PD, Yeager M and Isakson BE. Constitutive SRC-mediated phosphorylation of pannexin 1 at tyrosine 198 occurs at the plasma membrane. *J Biol Chem*. 2019;294:6940-6956.
151. Billaud M, Lohman AW, Straub AC, Looft-Wilson R, Johnstone SR, Araj CA, Best AK, Chekeni FB, Ravichandran KS, Penuela S, Laird DW and Isakson BE. Pannexin1 regulates α 1-adrenergic receptor-mediated vasoconstriction. *Circ Res*. 2011;109:80-5.
152. Yu CH, Redemann S, Wu HY, Kiewisz R, Yoo TY, Conway W, Farhadifar R, Müller-Reichert T and Needleman D. Central-spindle microtubules are strongly coupled to chromosomes during both anaphase A and anaphase B. *Mol Biol Cell*. 2019;30:2503-2514.
153. Redemann S, Lantsch I, Lindow N, Prohaska S, Srayko M and Müller-Reichert T. A Switch in Microtubule Orientation during *C. elegans* Meiosis. *Curr Biol*. 2018;28:2991-2997.e2.
154. Chen Y-L, Daneva Z, Kuppusamy M, Ottolini M, Baker TM, Klimentova E, Shah SA, Sokolowski JD, Park MS and Sonkusare SK. Novel smooth muscle Ca²⁺-signaling nanodomains in blood pressure regulation. *Circulation*. 2022;146:548-564.
155. Mirdita M, Schütze K, Moriwaki Y, Heo L, Ovchinnikov S and Steinegger M. ColabFold: making protein folding accessible to all. *Nature Methods*. 2022:1-4.
156. Roel-Touris J, Jiménez-García B and Bonvin AM. Integrative modeling of membrane-associated protein assemblies. *Nature communications*. 2020;11:1-11.
157. Cheng TMK, Blundell TL and Fernandez-Recio J. pyDock: electrostatics and desolvation for effective scoring of rigid-body protein-protein docking. *Proteins: Structure, Function, and Bioinformatics*. 2007;68:503-515.

158. Williams CJ, Headd JJ, Moriarty NW, Prisant MG, Videau LL, Deis LN, Verma V, Keedy DA, Hintze BJ and Chen VB. MolProbity: More and better reference data for improved all-atom structure validation. *Protein Science*. 2018;27:293-315.
159. Weighill D, Guebila MB, Glass K, Quackenbush J and Platig J. Predicting genotype-specific gene regulatory networks. *Genome Research*. 2022;32:524-533.
160. Bailey TL, Johnson J, Grant CE and Noble WS. The MEME suite. *Nucleic acids research*. 2015;43:W39-W49.
161. Liu X, Lu H, Chen T, Nallaparaju KC, Yan X, Tanaka S, Ichiyama K, Zhang X, Zhang L and Wen X. Genome-wide analysis identifies Bcl6-controlled regulatory networks during T follicular helper cell differentiation. *Cell reports*. 2016;14:1735-1747.
162. Sommars MA, Ramachandran K, Senagolage MD, Futtner CR, Germain DM, Allred AL, Omura Y, Bederian IR and Barish GD. Dynamic repression by BCL6 controls the genome-wide liver response to fasting and steatosis. *Elife*. 2019;8:e43922.
163. Liu Y, Li H, Bubolz AH, Zhang DX and Gutterman DD. Endothelial cytoskeletal elements are critical for flow-mediated dilation in human coronary arterioles. *Medical & biological engineering & computing*. 2008;46:469-478.
164. Liu Y, Zhao H, Li H, Kalyanaraman B, Nicolosi AC and Gutterman DD. Mitochondrial sources of H₂O₂ generation play a key role in flow-mediated dilation in human coronary resistance arteries. *Circulation research*. 2003;93:573-580.
165. Judkins CP, Diep H, Broughton BR, Mast AE, Hooker EU, Miller AA, Selemidis S, Dusting GJ, Sobey CG and Drummond GR. Direct evidence of a role for Nox2 in superoxide production, reduced nitric oxide bioavailability, and early atherosclerotic plaque formation in ApoE^{-/-} mice. *American Journal of Physiology-Heart and Circulatory Physiology*. 2010;298:H24-H32.
166. Jung O, Marklund SL, Geiger H, Pedrazzini T, Busse R and Brandes RP. Extracellular superoxide dismutase is a major determinant of nitric oxide bioavailability: in vivo and ex vivo evidence from ecSOD-deficient mice. *Circulation research*. 2003;93:622-629.
167. Silswal N, Touchberry CD, Daniel DR, McCarthy DL, Zhang S, Andresen J, Stubbs JR and Wacker MJ. FGF23 directly impairs endothelium-dependent vasorelaxation by increasing superoxide levels and reducing nitric oxide bioavailability. *American Journal of Physiology-Endocrinology and Metabolism*. 2014;307:E426-E436.
168. Dent AL, Shaffer AL, Yu X, Allman D and Staudt LM. Control of inflammation, cytokine expression, and germinal center formation by BCL-6. *Science*. 1997;276:589-92.
169. Fukuda T, Yoshida T, Okada S, Hatano M, Miki T, Ishibashi K, Okabe S, Koseki H, Hirosawa S and Taniguchi M. Disruption of the Bcl6 gene results in an impaired germinal center formation. *The Journal of experimental medicine*. 1997;186:439-448.
170. Nakagawa R, Toboso-Navasa A, Schips M, Young G, Bhaw-Rosun L, Llorian-Sopena M, Chakravarty P, Sesay AK, Kassiotis G and Meyer-Hermann M. Permissive selection followed by affinity-based proliferation of GC light zone B cells dictates cell fate and ensures clonal breadth. *Proceedings of the National Academy of Sciences*. 2021;118:e2016425118.
171. Kurosu T, Fukuda T, Miki T and Miura O. BCL6 overexpression prevents increase in reactive oxygen species and inhibits apoptosis induced by chemotherapeutic reagents in B-cell lymphoma cells. *Oncogene*. 2003;22:4459-68.
172. Sewastianik T, Szydłowski M, Jabłonska E, Białopiotrowicz E, Kiliszek P, Gorniak P, Polak A, Prochorec-Sobieszek M, Szumera-Cieckiewicz A and Kaminski T. FOXO1 is a TXN-and p300-

dependent sensor and effector of oxidative stress in diffuse large B-cell lymphomas characterized by increased oxidative metabolism. *Oncogene*. 2016;35:5989-6000.

173. Billaud M, Chiu Y-H, Lohman AW, Parpaite T, Butcher JT, Mutchler SM, DeLalio LJ, Artamonov MV, Sandilos JK and Best AK. A molecular signature in the pannexin1 intracellular loop confers channel activation by the α 1 adrenoreceptor in smooth muscle cells. *Science signaling*. 2015;8:ra17-ra17.

174. Chekeni FB, Elliott MR, Sandilos JK, Walk SF, Kinchen JM, Lazarowski ER, Armstrong AJ, Penuela S, Laird DW, Salvesen GS, Isakson BE, Bayliss DA and Ravichandran KS. Pannexin 1 channels mediate 'find-me' signal release and membrane permeability during apoptosis. *Nature*. 2010;467:863-7.

175. DeLalio LJ, Masati E, Mendu S, Ruddiman CA, Yang Y, Johnstone SR, Milstein JA, Keller IV TS, Weaver RB and Guagliardo NA. Pannexin 1 channels in renin-expressing cells influence renin secretion and blood pressure homeostasis. *Kidney international*. 2020;98:630-644.

176. Yang Y, Delalio LJ, Best AK, Macal E, Milstein J, Donnelly I, Miller AM, McBride M, Shu X, Koval M, Isakson BE and Johnstone SR. Endothelial Pannexin 1 Channels Control Inflammation by Regulating Intracellular Calcium. *J Immunol*. 2020;204:2995-3007.

177. Khan S, Taverna F, Rohlenova K, Treps L, Geldhof V, de Rooij L, Sokol L, Pircher A, Conradi LC, Kalucka J, Schoonjans L, Eelen G, Dewerchin M, Karakach T, Li X, Goveia J and Carmeliet P. EndoDB: a database of endothelial cell transcriptomics data. *Nucleic Acids Res*. 2019;47:D736-d744.

178. Celetti SJ, Cowan KN, Penuela S, Shao Q, Churko J and Laird DW. Implications of pannexin 1 and pannexin 3 for keratinocyte differentiation. *J Cell Sci*. 2010;123:1363-72.

179. Moon PM, Penuela S, Barr K, Khan S, Pin CL, Welch I, Attur M, Abramson SB, Laird DW and Beier F. Deletion of Panx3 prevents the development of surgically induced osteoarthritis. *Journal of molecular medicine*. 2015;93:845-856.

180. Wakefield CB, Lee VR, Johnston D, Boroumand P, Pillon NJ, Sayedyahosseini S, O'Donnell BL, Tang J, Sanchez-Pupo RE and Barr KJ. Pannexin 3 deletion reduces fat accumulation and inflammation in a sex-specific manner. *International Journal of Obesity*. 2022;46:726-738.

181. Halliwill KD, Quigley DA, Kang HC, Del Rosario R, Ginzinger D and Balmain A. Panx3 links body mass index and tumorigenesis in a genetically heterogeneous mouse model of carcinogen-induced cancer. *Genome medicine*. 2016;8:1-17.

182. Axelsson MA, Karlsson NG, Steel DM, Ouwendijk J, Nilsson T and Hansson GC. Neutralization of pH in the Golgi apparatus causes redistribution of glycosyltransferases and changes in the O-glycosylation of mucins. *Glycobiology*. 2001;11:633-644.

183. Bachert C, Lee TH and Linstedt AD. Luminal endosomal and Golgi-retrieval determinants involved in pH-sensitive targeting of an early Golgi protein. *Molecular biology of the cell*. 2001;12:3152-3160.

184. Rivinoja A, Hassinen A, Kokkonen N, Kauppila A and Kellokumpu S. Elevated Golgi pH impairs terminal N-glycosylation by inducing mislocalization of Golgi glycosyltransferases. *Journal of cellular physiology*. 2009;220:144-154.

185. Kim J, Seo M, Kim SK and Bae YS. Flagellin-induced NADPH oxidase 4 activation is involved in atherosclerosis. *Scientific reports*. 2016;6:1-16.

186. Kim J, Yoo J-Y, Suh JM, Park S, Kang D, Jo H and Bae YS. The flagellin-TLR5-Nox4 axis promotes the migration of smooth muscle cells in atherosclerosis. *Experimental & molecular medicine*. 2019;51:1-13.
187. Kumar SK and Mani KP. Endocan alters nitric oxide production in endothelial cells by targeting AKT/eNOS and NFkB/iNOS signaling. *Nitric Oxide*. 2021;117:26-33.
188. Manea A, Manea SA, Gafencu AV, Raicu M and Simionescu M. AP-1–Dependent transcriptional regulation of NADPH oxidase in human aortic smooth muscle cells: role of p22phox subunit. *Arteriosclerosis, thrombosis, and vascular biology*. 2008;28:878-885.
189. Nisimoto Y, Jackson HM, Ogawa H, Kawahara T and Lambeth JD. Constitutive NADPH-dependent electron transferase activity of the Nox4 dehydrogenase domain. *Biochemistry*. 2010;49:2433-2442.
190. Shiose A, Kuroda J, Tsuruya K, Hirai M, Hirakata H, Naito S, Hattori M, Sakaki Y and Sumimoto H. A novel superoxide-producing NAD (P) H oxidase in kidney. *Journal of Biological Chemistry*. 2001;276:1417-1423.
191. Cox AG, Winterbourn CC and Hampton MB. Measuring the redox state of cellular peroxiredoxins by immunoblotting *Methods in enzymology*: Elsevier; 2010(474): 51-66.
192. Piovesan D, Necci M, Escobedo N, Monzon AM, Hatos A, Mičetić I, Quaglia F, Paladin L, Ramasamy P and Dosztányi Z. MobiDB: intrinsically disordered proteins in 2021. *Nucleic acids research*. 2021;49:D361-D367.
193. Mena EL, Kjolby RA, Saxton RA, Werner A, Lew BG, Boyle JM, Harland R and Rape M. Dimerization quality control ensures neuronal development and survival. *Science*. 2018;362:eaap8236.
194. Huttlin EL, Jedrychowski MP, Elias JE, Goswami T, Rad R, Beausoleil SA, Villén J, Haas W, Sowa ME and Gygi SP. A tissue-specific atlas of mouse protein phosphorylation and expression. *Cell*. 2010;143:1174-1189.
195. Mascle X, Albagli O and Lemerrier C. Point mutations in BCL6 DNA-binding domain reveal distinct roles for the six zinc fingers. *Biochemical and biophysical research communications*. 2003;300:391-396.
196. Dikalova AE, Bikineyeva AT, Budzyn K, Nazarewicz RR, McCann L, Lewis W, Harrison DG and Dikalov SI. Therapeutic targeting of mitochondrial superoxide in hypertension. *Circulation research*. 2010;107:106-116.
197. Somers MJ, Mavromatis K, Galis ZS and Harrison DG. Vascular superoxide production and vasomotor function in hypertension induced by deoxycorticosterone acetate–salt. *Circulation*. 2000;101:1722-1728.
198. Vendrov AE, Hakim ZS, Madamanchi NR, Rojas M, Madamanchi C and Runge MS. Atherosclerosis is attenuated by limiting superoxide generation in both macrophages and vessel wall cells. *Arteriosclerosis, thrombosis, and vascular biology*. 2007;27:2714-2721.
199. Sorescu D, Weiss D, Lassègue B, Clempus RE, Szöcs K, Sorescu GP, Valppu L, Quinn MT, Lambeth JD and Vega JD. Superoxide production and expression of nox family proteins in human atherosclerosis. *Circulation*. 2002;105:1429-1435.
200. Chouchani ET, Pell VR, James AM, Work LM, Saeb-Parsy K, Frezza C, Krieg T and Murphy MP. A unifying mechanism for mitochondrial superoxide production during ischemia-reperfusion injury. *Cell metabolism*. 2016;23:254-263.

201. Huk I, Nanobashvili J, Neumayer C, Punz A, Mueller M, Afkhampour K, Mittlboeck M, Losert U, Polterauer P and Roth E. L-arginine treatment alters the kinetics of nitric oxide and superoxide release and reduces ischemia/reperfusion injury in skeletal muscle. *Circulation*. 1997;96:667-675.
202. Prabha PS, Das U, Koratkar R, Sagar PS and Ramesh G. Free radical generation, lipid peroxidation and essential fatty acids in uncontrolled essential hypertension. *Prostaglandins, leukotrienes and essential fatty acids*. 1990;41:27-33.
203. Forman HJ. Use and abuse of exogenous H₂O₂ in studies of signal transduction. *Free Radical Biology and Medicine*. 2007;42:926-932.
204. Gao YJ, Hirota S, Zhang DW, Janssen LJ and Lee RM. Mechanisms of hydrogen-peroxide-induced biphasic response in rat mesenteric artery. *British journal of pharmacology*. 2003;138:1085-1092.
205. Lucchesi PA, Belmadani S and Matrougui K. Hydrogen peroxide acts as both vasodilator and vasoconstrictor in the control of perfused mouse mesenteric resistance arteries. *J Hypertens*. 2005;23:571-9.
206. Santiago E, Contreras C, García-Sacristán A, Sánchez A, Rivera L, Climent B and Prieto D. Signaling pathways involved in the H₂O₂-induced vasoconstriction of rat coronary arteries. *Free Radic Biol Med*. 2013;60:136-46.
207. Saravi SSS, Eroglu E, Waldeck-Weiermair M, Sorrentino A, Steinhorn B, Belousov V and Michel T. Differential endothelial signaling responses elicited by chemogenetic H₂O₂ synthesis. *Redox biology*. 2020;36:101605.
208. Yamaguchi K, Asano K, Mori M, Takasugi T, Fujita H, Suzuki Y and Kawashiro T. Constriction and dilatation of pulmonary arterial ring by hydrogen peroxide-importance of prostanoids *Oxygen Transport to Tissue XVI*: Springer; 1994: 457-463.
209. Grzelak A, Balcerczyk A, Mateja A and Bartosz G. Hemoglobin can nitrate itself and other proteins. *Biochimica et Biophysica Acta (BBA)-General Subjects*. 2001;1528:97-100.
210. Straub AC, Lohman AW, Billaud M, Johnstone SR, Dwyer ST, Lee MY, Bortz PS, Best AK, Columbus L and Gaston B. Endothelial cell expression of haemoglobin α regulates nitric oxide signalling. *Nature*. 2012;491:473-477.
211. Keller TCSt, Lechavue C, Keller AS, Broseghini-Filho GB, Butcher JT, Page HRA, A. I, Y. TZ, DeLalio LJ, Brooks S, Sharma P, Hong K, Xu W, Padilha AS, Ruddiman CA, Best AK, Macal E, Kim-Shapiro DB, Christ G, Yan Z, Cortese-Krott MM, Ricart K, Patel RK, Bender TP, Sonkusare SK, Weiss MJ, Auckerman H, Columbus L and Isakson BE. Endothelial alpha globin is a nitrite reductase. *Nature Communications*. 2022.
212. Larsen BT, Gutterman DD, Sato A, Toyama K, Campbell WB, Zeldin DC, Manthathi VL, Falck JR and Miura H. Hydrogen peroxide inhibits cytochrome p450 epoxygenases: interaction between two endothelium-derived hyperpolarizing factors. *Circulation research*. 2008;102:59-67.
213. Liu Y, Bubolz AH, Mendoza S, Zhang DX and Gutterman DD. H₂O₂ is the transferrable factor mediating flow-induced dilation in human coronary arterioles. *Circulation research*. 2011;108:566-573.
214. Matoba T and Shimokawa H. Hydrogen peroxide is an endothelium-derived hyperpolarizing factor in animals and humans. *Journal of pharmacological sciences*. 2003;92:1-6.

215. Matoba T, Shimokawa H, Nakashima M, Hirakawa Y, Mukai Y, Hirano K, Kanaide H and Takeshita A. Hydrogen peroxide is an endothelium-derived hyperpolarizing factor in mice. *The Journal of clinical investigation*. 2000;106:1521-1530.
216. Muñoz M, López-Oliva ME, Pinilla E, Martínez MP, Sánchez A, Rodríguez C, García-Sacristán A, Hernández M, Rivera L and Prieto D. CYP epoxygenase-derived H₂O₂ is involved in the endothelium-derived hyperpolarization (EDH) and relaxation of intrarenal arteries. *Free Radical Biology and Medicine*. 2017;106:168-183.
217. Yada T, Shimokawa H, Hiramatsu O, Kajita T, Shigeto F, Goto M, Ogasawara Y and Kajiya F. Hydrogen peroxide, an endogenous endothelium-derived hyperpolarizing factor, plays an important role in coronary autoregulation in vivo. *Circulation*. 2003;107:1040-1045.
218. Cao S, Anishkin A, Zinkevich NS, Nishijima Y, Korishettar A, Wang Z, Fang J, Wilcox DA and Zhang DX. Transient receptor potential vanilloid 4 (TRPV4) activation by arachidonic acid requires protein kinase A-mediated phosphorylation. *Journal of Biological Chemistry*. 2018;293:5307-5322.
219. Wegierski T, Lewandrowski U, Müller B, Sickmann A and Walz G. Tyrosine phosphorylation modulates the activity of TRPV4 in response to defined stimuli. *Journal of Biological Chemistry*. 2009;284:2923-2933.
220. Suresh K, Servinsky L, Reyes J, Baksh S, Udem C, Caterina M, Pearse DB and Shimoda LA. Hydrogen peroxide-induced calcium influx in lung microvascular endothelial cells involves TRPV4. *American Journal of Physiology-Lung Cellular and Molecular Physiology*. 2015;309:L1467-L1477.
221. Behringer EJ, Shaw RL, Westcott EB, Socha MJ and Segal SS. Aging impairs electrical conduction along endothelium of resistance arteries through enhanced Ca²⁺-activated K⁺ channel activation. *Arteriosclerosis, thrombosis, and vascular biology*. 2013;33:1892-1901.
222. Edwards DH, Li Y and Griffith TM. Hydrogen peroxide potentiates the EDHF phenomenon by promoting endothelial Ca²⁺ mobilization. *Arteriosclerosis, thrombosis, and vascular biology*. 2008;28:1774-1781.
223. Mattson DL. Immune mechanisms of salt-sensitive hypertension and renal end-organ damage. *Nature Reviews Nephrology*. 2019;15:290-300.
224. Norlander AE, Madhur MS and Harrison DG. The immunology of hypertension. *Journal of Experimental Medicine*. 2018;215:21-33.
225. Rodríguez-Iturbe B, Pons H and Johnson RJ. Role of the immune system in hypertension. *Physiological reviews*. 2017;97:1127-1164.
226. Kirabo A, Fontana V, De Faria AP, Loperena R, Galindo CL, Wu J, Bikineyeva AT, Dikalov S, Xiao L and Chen W. DC isoketal-modified proteins activate T cells and promote hypertension. *The Journal of clinical investigation*. 2014;124:4642-4656.
227. Miguel CD, Guo C, Lund H, Feng D and Mattson DL. Infiltrating T lymphocytes in the kidney increase oxidative stress and participate in the development of hypertension and renal disease. *American Journal of Physiology-Renal Physiology*. 2011;300:F734-F742.
228. Bravo Y, Quiroz Y, Ferrebuz A, Vaziri ND and Rodríguez-Iturbe B. Mycophenolate mofetil administration reduces renal inflammation, oxidative stress, and arterial pressure in rats with lead-induced hypertension. *American Journal of Physiology-Renal Physiology*. 2007;293:F616-F623.

229. O'Leary R, Penrose H, Miyata K and Satou R. Macrophage-derived IL-6 contributes to ANG II-mediated angiotensinogen stimulation in renal proximal tubular cells. *American Journal of Physiology-Renal Physiology*. 2016;310:F1000-F1007.
230. Kamat NV, Thabet SR, Xiao L, Saleh MA, Kirabo A, Madhur MS, Delpire E, Harrison DG and McDonough AA. Renal transporter activation during angiotensin-II hypertension is blunted in interferon- γ -/- and interleukin-17A-/- mice. *Hypertension*. 2015;65:569-576.
231. Kasal DA, Barhoumi T, Li MW, Yamamoto N, Zdanovich E, Rehman A, Neves MF, Laurant P, Paradis P and Schiffrin EL. T regulatory lymphocytes prevent aldosterone-induced vascular injury. *Hypertension*. 2012;59:324-330.
232. Moriyama M, Yamochi T, Semba K, Akiyama T and Mori S. BCL-6 is phosphorylated at multiple sites in its serine- and proline-clustered region by mitogen-activated protein kinase (MAPK) in vivo. *Oncogene*. 1997;14:2465-74.
233. Chen D, Zang Y-H, Qiu Y, Zhang F, Chen A-D, Wang J-J, Chen Q, Li Y-H, Kang Y-M and Zhu G-Q. BCL6 attenuates proliferation and oxidative stress of vascular smooth muscle cells in hypertension. *Oxidative medicine and cellular longevity*. 2019;2019.
234. Crespin S, Bechberger J, Mesnil M, Naus CC and Sin WC. The carboxy-terminal tail of connexin43 gap junction protein is sufficient to mediate cytoskeleton changes in human glioma cells. *J Cell Biochem*. 2010;110:589-97.
235. Johnstone SR, Best AK, Wright CS, Isakson BE, Errington RJ and Martin PE. Enhanced connexin 43 expression delays intra-mitotic duration and cell cycle traverse independently of gap junction channel function. *J Cell Biochem*. 2010;110:772-82.
236. Johnstone SR, Kroncke BM, Straub AC, Best AK, Dunn CA, Mitchell LA, Peskova Y, Nakamoto RK, Koval M, Lo CW, Lampe PD, Columbus L and Isakson BE. MAPK phosphorylation of connexin 43 promotes binding of cyclin E and smooth muscle cell proliferation. *Circ Res*. 2012;111:201-11.
237. Miao G, Godt D and Montell DJ. Integration of Migratory Cells into a New Site In Vivo Requires Channel-Independent Functions of Innexins on Microtubules. *Dev Cell*. 2020;54:501-515.e9.
238. Zucker SN, Bancroft TA, Place DE, Des Soye B, Bagati A and Berezney R. A dominant negative Cx43 mutant differentially affects tumorigenic and invasive properties in human metastatic melanoma cells. *J Cell Physiol*. 2013;228:853-9.
239. Nielsen BS, Toft-Bertelsen TL, Lolansen SD, Anderson CL, Nielsen MS, Thompson RJ and MacAulay N. Pannexin 1 activation and inhibition is permeant-selective. *J Physiol*. 2020;598:361-379.
240. Ohnmacht C and Voehringer D. Basophil effector function and homeostasis during helminth infection. *Blood, The Journal of the American Society of Hematology*. 2009;113:2816-2825.
241. Kay AB. Paul Ehrlich and the early history of granulocytes. *Microbiology spectrum*. 2016;4:4.4. 62.
242. Crivellato E and Ribatti D. The mast cell: an evolutionary perspective. *Biological Reviews*. 2010;85:347-360.
243. de Barros CM, Andrade LR, Allodi S, Viskov C, Mourier PA, Cavalcante MsC, Straus AH, Takahashi HK, Pomin VH and Carvalho VF. The hemolymph of the ascidian *Styela plicata*

(Chordata-Tunicata) contains heparin inside basophil-like cells and a unique sulfated galactoglucan in the plasma. *Journal of Biological Chemistry*. 2007;282:1615-1626.

244. Gilfillan AM and Beaven MA. Regulation of mast cell responses in health and disease. *Critical Reviews™ in Immunology*. 2011;31.

245. Holgate ST. The role of mast cells and basophils in inflammation. *Clin Exp Allergy*. 2000;30 Suppl 1:28-32.

246. Sawaguchi M, Tanaka S, Nakatani Y, Harada Y, Mukai K, Matsunaga Y, Ishiwata K, Oboki K, Kambayashi T, Watanabe N, Karasuyama H, Nakae S, Inoue H and Kubo M. Role of mast cells and basophils in IgE responses and in allergic airway hyperresponsiveness. *J Immunol*. 2012;188:1809-18.

247. Voehringer D. Protective and pathological roles of mast cells and basophils. *Nature Reviews Immunology*. 2013;13:362-375.

248. Padawer J. Mast cells: extended lifespan and lack of granule turnover under normal in vivo conditions. *Experimental and molecular pathology*. 1974;20:269-280.

249. Dvorak AM. Ultrastructural studies of human basophils and mast cells. *Journal of Histochemistry & Cytochemistry*. 2005;53:1043-1070.

250. Galli SJ, Nakae S and Tsai M. Mast cells in the development of adaptive immune responses. *Nature immunology*. 2005;6:135-142.

251. Schneider E, Thieblemont N, De Moraes ML and Dy M. Basophils: new players in the cytokine network. *European cytokine network*. 2010;21:142-153.

252. Voehringer D, Shinkai K and Locksley RM. Type 2 immunity reflects orchestrated recruitment of cells committed to IL-4 production. *Immunity*. 2004;20:267-277.

253. Huang H and Li Y. Mechanisms controlling mast cell and basophil lineage decisions. *Current allergy and asthma reports*. 2014;14:1-6.

254. Sokol CL, Barton GM, Farr AG and Medzhitov R. A mechanism for the initiation of allergen-induced T helper type 2 responses. *Nat Immunol*. 2008;9:310-8.

255. Cohen M, Giladi A, Gorki A-D, Solodkin DG, Zada M, Hladik A, Miklosi A, Salame T-M, Halpern KB and David E. Lung single-cell signaling interaction map reveals basophil role in macrophage imprinting. *Cell*. 2018;175:1031-1044. e18.

256. Schramm G, Mohrs K, Wodrich M, Doenhoff MJ, Pearce EJ, Haas H and Mohrs M. Cutting edge: IPSE/alpha-1, a glycoprotein from *Schistosoma mansoni* eggs, induces IgE-dependent, antigen-independent IL-4 production by murine basophils in vivo. *The Journal of Immunology*. 2007;178:6023-6027.

257. Schramm G, Falcone FH, Gronow A, Haisch K, Mamat U, Doenhoff MJ, Oliveira G, Galle Jr, Dahinden CA and Haas H. Molecular characterization of an interleukin-4-inducing factor from *Schistosoma mansoni* eggs. *Journal of Biological Chemistry*. 2003;278:18384-18392.

258. Sicklinger F, Meyer IS, Li X, Radtke D, Dicks S, Kornadt MP, Mertens C, Meier JK, Lavine KJ and Zhang Y. Basophils balance healing after myocardial infarction via IL-4/IL-13. *Journal of Clinical Investigation*. 2021;131:e136778.

259. Piliponsky AM, Shubin NJ, Lahiri AK, Truong P, Clauson M, Niino K, Tsuha AL, Nedospasov SA, Karasuyama H and Reber LL. Basophil-derived tumor necrosis factor can enhance survival in a sepsis model in mice. *Nature immunology*. 2019;20:129-140.

260. Cheng LE, Sullivan BM, Retana LE, Allen CD, Liang H-E and Locksley RM. IgE-activated basophils regulate eosinophil tissue entry by modulating endothelial function. *Journal of Experimental Medicine*. 2015;212:513-524.
261. Salter BM, Oliveria JP, Nusca G, Smith SG, Tworek D, Mitchell PD, Watson RM, Sehmi R and Gauvreau GM. IL-25 and IL-33 induce Type 2 inflammation in basophils from subjects with allergic asthma. *Respiratory research*. 2016;17:1-13.
262. Min B, Prout M, Hu-Li J, Zhu J, Jankovic D, Morgan ES, Urban Jr JF, Dvorak AM, Finkelman FD and LeGros G. Basophils produce IL-4 and accumulate in tissues after infection with a Th2-inducing parasite. *The Journal of experimental medicine*. 2004;200:507-517.
263. Chevrier S, Kratina T, Emslie D, Tarlinton DM and Corcoran LM. IL4 and IL21 cooperate to induce the high Bcl6 protein level required for germinal center formation. *Immunol Cell Biol*. 2017;95:925-932.
264. Karasuyama H, Mukai K, Tsujimura Y and Obata K. Newly discovered roles for basophils: a neglected minority gains new respect. *Nature Reviews Immunology*. 2009;9:9-13.
265. Obata K, Mukai K, Tsujimura Y, Ishiwata K, Kawano Y, Minegishi Y, Watanabe N and Karasuyama H. Basophils are essential initiators of a novel type of chronic allergic inflammation. *Blood*. 2007;110:913-20.
266. Siracusa MC, Kim BS, Spergel JM and Artis D. Basophils and allergic inflammation. *J Allergy Clin Immunol*. 2013;132:789-801; quiz 788.
267. Pecaric-Petkovic T, Didichenko SA, Kaempfer S, Spiegl N and Dahinden CA. Human basophils and eosinophils are the direct target leukocytes of the novel IL-1 family member IL-33. *Blood, The Journal of the American Society of Hematology*. 2009;113:1526-1534.
268. Jackson-Jones LH, Rückerl D, Svedberg F, Duncan S, Maizels RM, Sutherland TE, Jenkins SJ, McSorley HJ, Bénézech C and MacDonald AS. IL-33 delivery induces serous cavity macrophage proliferation independent of interleukin-4 receptor alpha. *European journal of immunology*. 2016;46:2311-2321.
269. Li J, Razumilava N, Gores GJ, Walters S, Mizuochi T, Mourya R, Bessho K, Wang Y-H, Glaser SS and Shivakumar P. Biliary repair and carcinogenesis are mediated by IL-33-dependent cholangiocyte proliferation. *The Journal of clinical investigation*. 2014;124:3241-3251.
270. Schiering C, Krausgruber T, Chomka A, Fröhlich A, Adelman K, Wohlfert EA, Pott J, Griseri T, Bollrath J and Hegazy AN. The alarmin IL-33 promotes regulatory T-cell function in the intestine. *Nature*. 2014;513:564-568.
271. Yin X, Cao H, Wei Y and Li H-H. Alteration of the IL-33-sST2 pathway in hypertensive patients and a mouse model. *Hypertension Research*. 2019;42:1664-1671.
272. Steer CA, Mathä L, Shim H and Takei F. Lung group 2 innate lymphoid cells are trained by endogenous IL-33 in the neonatal period. *JCI insight*. 2020;5.
273. Shinohara A, Imai Y, Nakagawa M, Takahashi T, Ichikawa M and Kurokawa M. Intracellular reactive oxygen species mark and influence the megakaryocyte-erythrocyte progenitor fate of common myeloid progenitors. *Stem Cells*. 2014;32:548-57.
274. Siracusa MC, Saenz SA, Hill DA, Kim BS, Headley MB, Doering TA, Wherry EJ, Jessup HK, Siegel LA and Kambayashi T. TSLP promotes interleukin-3-independent basophil haematopoiesis and type 2 inflammation. *Nature*. 2011;477:229-233.
275. Voehringer D. Regulation of type 2 immunity by basophils. *Adv Exp Med Biol*. 2013;785:37-41.

276. Oh K, Shen T, Le Gros G and Min B. Induction of Th2 type immunity in a mouse system reveals a novel immunoregulatory role of basophils. *Blood*. 2007;109:2921-7.
277. Mohrs M, Shinkai K, Mohrs K and Locksley RM. Analysis of type 2 immunity in vivo with a bicistronic IL-4 reporter. *Immunity*. 2001;15:303-311.
278. Kassem KM, Ali M and Rhaleb NE. Interleukin 4: Its Role in Hypertension, Atherosclerosis, Valvular, and Nonvalvular Cardiovascular Diseases. *J Cardiovasc Pharmacol Ther*. 2020;25:7-14.
279. Roselló-Lletí E, Rivera M, Bertomeu V, Cortés R, Jordán A and González-Molina A. [Interleukin-4 and cardiac fibrosis in patients with heart failure]. *Rev Esp Cardiol*. 2007;60:777-80.
280. Cottrell JN, Amaral LM, Harmon A, Cornelius DC, Cunningham MW, Jr., Vaka VR, Ibrahim T, Herse F, Wallukat G, Dechend R and LaMarca B. Interleukin-4 supplementation improves the pathophysiology of hypertension in response to placental ischemia in RUPP rats. *Am J Physiol Regul Integr Comp Physiol*. 2019;316:R165-r171.
281. van Heuven-Nolsen D, De Kimpe SJ, Muis T, van Ark I, Savelkoul H, Beems RB, van Oosterhout AJ and Nijkamp FP. Opposite role of interferon-gamma and interleukin-4 on the regulation of blood pressure in mice. *Biochem Biophys Res Commun*. 1999;254:816-20.
282. Cao X, Kozak CA, Liu YJ, Noguchi M, O'Connell E and Leonard WJ. Characterization of cDNAs encoding the murine interleukin 2 receptor (IL-2R) gamma chain: chromosomal mapping and tissue specificity of IL-2R gamma chain expression. *Proc Natl Acad Sci U S A*. 1993;90:8464-8.
283. Takeshita T, Asao H, Ohtani K, Ishii N, Kumaki S, Tanaka N, Munakata H, Nakamura M and Sugamura K. Cloning of the gamma chain of the human IL-2 receptor. *Science*. 1992;257:379-82.
284. Gauchat JF, Schlagenhaut E, Feng NP, Moser R, Yamage M, Jeannin P, Alouani S, Elson G, Notarangelo LD and Wells T. A novel 4-kb interleukin-13 receptor α mRNA expressed in human B, T, and endothelial cells encoding an alternate type-II interleukin-4/interleukin-13 receptor. *European journal of immunology*. 1997;27:971-978.
285. Schnyder B, Lugli S, Feng N, Etter H, Lutz RA, Ryffel B, Sugamura K, Wunderli-Allenspach H and Moser R. Interleukin-4 (IL-4) and IL-13 bind to a shared heterodimeric complex on endothelial cells mediating vascular cell adhesion molecule-1 induction in the absence of the common gamma chain. 1996.
286. Graber P, Gretener D, Herren S, Aubry JP, Elson G, Poudrier J, Lecoanet-Henchoz S, Alouani S, Losberger C, Bonnefoy JY, Kosco-Vilbois MH and Gauchat JF. The distribution of IL-13 receptor alpha1 expression on B cells, T cells and monocytes and its regulation by IL-13 and IL-4. *Eur J Immunol*. 1998;28:4286-98.
287. Luzina IG, Keegan AD, Heller NM, Rook GA, Shea-Donohue T and Atamas SP. Regulation of inflammation by interleukin-4: a review of "alternatives". *J Leukoc Biol*. 2012;92:753-64.
288. Silva-Filho JL, Caruso-Neves C and Pinheiro AAS. IL-4: an important cytokine in determining the fate of T cells. *Biophys Rev*. 2014;6:111-118.
289. Kotowicz K, Callard RE, Friedrich K, Matthews DJ and Klein N. Biological activity of IL-4 and IL-13 on human endothelial cells: functional evidence that both cytokines act through the same receptor. *Int Immunol*. 1996;8:1915-25.
290. Lohman AW, Billaud M, Straub AC, Johnstone SR, Best AK, Lee M, Barr K, Penuela S, Laird DW and Isakson BE. Expression of pannexin isoforms in the systemic murine arterial network. *J Vasc Res*. 2012;49:405-16.

291. Good ME, Eucker SA, Li J, Bacon HM, Lang SM, Butcher JT, Johnson TJ, Gaykema RP, Patel MK and Zuo Z. Endothelial cell Pannexin1 modulates severity of ischemic stroke by regulating cerebral inflammation and myogenic tone. *JCI insight*. 2018;3.
292. Daneva Z, Ottolini M, Chen YL, Klimentova E, Kuppusamy M, Shah SA, Minshall RD, Seye CI, Laubach VE and Isakson BE. Endothelial pannexin 1–TRPV4 channel signaling lowers pulmonary arterial pressure in mice. *Elife*. 2021;10:e67777.
293. Blanco R and Gerhardt H. VEGF and Notch in tip and stalk cell selection. *Cold Spring Harbor perspectives in medicine*. 2013;3:a006569.
294. Chavkin NW, Genet G, Poulet M, Jeffery ED, Marziano C, Genet N, Vasavada H, Nelson EA, Acharya BR and Kour A. Endothelial cell cycle state determines propensity for arterial-venous fate. *Nature Communications*. 2022;13:5891.
295. Alinikula J, Nera KP, Junntila S and Lassila O. Alternate pathways for Bcl6-mediated regulation of B cell to plasma cell differentiation. *European journal of immunology*. 2011;41:2404-2413.
296. Misawa T, SoRelle JA, Choi JH, Yue T, Wang K-w, McAlpine W, Wang J, Liu A, Tabeta K and Turer EE. Mutual inhibition between Prkd2 and Bcl6 controls T follicular helper cell differentiation. *Science immunology*. 2020;5:eaaz0085.
297. Nurieva RI, Chung Y, Martinez GJ, Yang XO, Tanaka S, Matskevitch TD, Wang Y-H and Dong C. Bcl6 mediates the development of T follicular helper cells. *Science*. 2009;325:1001-1005.
298. Stahl A, Connor KM, Sapienza P, Chen J, Dennison RJ, Krah NM, Seaward MR, Willett KL, Aderman CM and Guerin KI. The mouse retina as an angiogenesis model. *Investigative ophthalmology & visual science*. 2010;51:2813-2826.
299. Hosokawa Y, Maeda Y and Seto M. Target genes downregulated by the BCL-6/LAZ3 oncoprotein in mouse Ba/F3 cells. *Biochemical and biophysical research communications*. 2001;283:563-568.
300. Choi J and Crotty S. Bcl6-mediated transcriptional regulation of follicular helper T cells (TFH). *Trends in immunology*. 2021;42:336-349.
301. Li Q, Zhou L, Wang L, Li S, Xu G, Gu H, Li D, Liu M, Fang L and Wang Z. Bcl6 modulates innate immunity by controlling macrophage activity and plays critical role in experimental autoimmune encephalomyelitis. *European Journal of Immunology*. 2020;50:525-536.
302. Venkatadri R, Sabapathy V, Dogan M, Mohammad S, Harvey SE, Simpson SR, Grayson JM, Yan N, Perrino FW and Sharma R. Targeting Bcl6 in the TREX1 D18N murine model ameliorates autoimmunity by modulating T-follicular helper cells and germinal center B cells. *European Journal of Immunology*. 2022.
303. Cardenas MG, Yu W, Beguelin W, Teater MR, Geng H, Goldstein RL, Oswald E, Hatzi K, Yang S-N and Cohen J. Rationally designed BCL6 inhibitors target activated B cell diffuse large B cell lymphoma. *The Journal of clinical investigation*. 2016;126:3351-3362.
304. Krull JE, Wenzl K, Hartert KT, Manske MK, Sarangi V, Maurer MJ, Larson MC, Nowakowski GS, Ansell SM and McPhail E. Somatic copy number gains in MYC, BCL2, and BCL6 identifies a subset of aggressive alternative-DH/TH DLBCL patients. *Blood cancer journal*. 2020;10:1-8.
305. Polo JM, Juszczynski P, Monti S, Cerchiatti L, Ye K, Grealley JM, Shipp M and Melnick A. Transcriptional signature with differential expression of BCL6 target genes accurately identifies BCL6-dependent diffuse large B cell lymphomas. *Proceedings of the National Academy of Sciences*. 2007;104:3207-3212.

306. Geng H, Brennan S, Milne TA, Chen W-Y, Li Y, Hurtz C, Kweon S-M, Zickl L, Shojaee S and Neuberg D. Integrative epigenomic analysis identifies biomarkers and therapeutic targets in adult B-acute lymphoblastic leukemia. *Cancer discovery*. 2012;2:1004-1023.
307. Hurtz C, Chan LN, Geng H, Ballabio E, Xiao G, Deb G, Khoury H, Chen C-W, Armstrong SA and Chen J. Rationale for targeting BCL6 in MLL-rearranged acute lymphoblastic leukemia. *Genes & development*. 2019;33:1265-1279.
308. Hurtz C, Hatzi K, Cerchietti L, Braig M, Park E, Kim Y-m, Herzog S, Ramezani-Rad P, Jumaa H and Müller MC. BCL6-mediated repression of p53 is critical for leukemia stem cell survival in chronic myeloid leukemia. *Journal of Experimental Medicine*. 2011;208:2163-2174.
309. Madapura H, Nagy N, Ujvari D, Kallas T, Kröhnke M, Amu S, Björkholm M, Stenke L, Mandal P and McMurray J. Interferon γ is a STAT1-dependent direct inducer of BCL6 expression in imatinib-treated chronic myeloid leukemia cells. *Oncogene*. 2017;36:4619-4628.
310. Sultan M, Nearing JT, Brown JM, Huynh TT, Cruickshank BM, Lamoureaux E, Vidovic D, Dahn ML, Fernando W and Coyle KM. An in vivo genome-wide shRNA screen identifies BCL6 as a targetable biomarker of paclitaxel resistance in breast cancer. *Molecular Oncology*. 2021;15:2046-2064.
311. Walker SR, Liu S, Xiang M, Nicolais M, Hatzi K, Giannopoulou E, Elemento O, Cerchietti L, Melnick A and Frank DA. The transcriptional modulator BCL6 as a molecular target for breast cancer therapy. *Oncogene*. 2015;34:1073-1082.
312. Deb D, Rajaram S, Larsen JE, Dospoy PD, Marullo R, Li LS, Avila K, Xue F, Cerchietti L and Minna JD. Combination therapy targeting BCL6 and phospho-STAT3 defeats intratumor heterogeneity in a subset of non-small cell lung cancers. *Cancer research*. 2017;77:3070-3081.
313. Marullo R, Ahn H, Cardenas M, Melnick A, Xue F and Cerchietti L. The transcription factor BCL6 is a rational target in non-small cell lung cancer (NSCLC). 2016.
314. Xu L, Chen Y, Dutra-Clarke M, Mayakonda A, Hazawa M, Savinoff SE, Doan N, Said JW, Yong WH and Watkins A. BCL6 promotes glioma and serves as a therapeutic target. *Proceedings of the National Academy of Sciences*. 2017;114:3981-3986.
315. Cerchietti LC, Ghetu AF, Zhu X, Da Silva GF, Zhong S, Matthews M, Bunting KL, Polo JM, Farès C, Arrowsmith CH, Yang SN, Garcia M, Coop A, Mackerell AD, Jr., Privé GG and Melnick A. A small-molecule inhibitor of BCL6 kills DLBCL cells in vitro and in vivo. *Cancer Cell*. 2010;17:400-11.
316. Heink S, Yogev N, Garbers C, Herwerth M, Aly L, Gasperi C, Husterer V, Croxford AL, Möller-Hackbarth K and Bartsch HS. Trans-presentation of IL-6 by dendritic cells is required for the priming of pathogenic TH 17 cells. *Nature immunology*. 2017;18:74-85.
317. Bocharnikov AV, Keegan J, Wacleche VS, Cao Y, Fonseka CY, Wang G, Muise ES, Zhang KX, Arazi A and Keras G. PD-1hiCXCR5-T peripheral helper cells promote B cell responses in lupus via MAF and IL-21. *JCI insight*. 2019;4.
318. Gensous N, Schmitt N, Richez C, Ueno H and Blanco P. T follicular helper cells, interleukin-21 and systemic lupus erythematosus. *Rheumatology*. 2017;56:516-523.
319. Quentmeier H, Pommerenke C, Dirks WG, Eberth S, Koeppel M, MacLeod RA, Nagel S, Steube K, Uphoff CC and Drexler HG. The LL-100 panel: 100 cell lines for blood cancer studies. *Scientific Reports*. 2019;9:8218.

320. Burns MB, Lackey L, Carpenter MA, Rathore A, Land AM, Leonard B, Refsland EW, Kotandeniya D, Tretyakova N and Nikas JB. APOBEC3B is an enzymatic source of mutation in breast cancer. *Nature*. 2013;494:366-370.
321. Zisi A, Kanellis DC, Moussaud S, Karlsson I, Carén H, Bräutigam L, Bartek J and Lindström MS. Small Molecule-mediated Disruption of Ribosome Biogenesis Synergizes With FGFR Inhibitors to Suppress Glioma Cell Growth. *Neuro-oncology*. 2022.
322. Coan DE, Wechezak AR, Viggers RF and Sauvage LR. Effect of shear stress upon localization of the Golgi apparatus and microtubule organizing center in isolated cultured endothelial cells. *Journal of Cell Science*. 1993;104:1145-1153.
323. Lipowsky HH, Kovalcheck S and Zweifach BW. The distribution of blood rheological parameters in the microvasculature of cat mesentery. *Circ Res*. 1978;43:738-49.
324. Lipowsky HH, Usami S and Chien S. In vivo measurements of "apparent viscosity" and microvessel hematocrit in the mesentery of the cat. *Microvasc Res*. 1980;19:297-319.
325. Rogers KA, McKee NH and Kalnins VI. Preferential orientation of centrioles toward the heart in endothelial cells of major blood vessels is reestablished after reversal of a segment. *Proc Natl Acad Sci U S A*. 1985;82:3272-6.
326. Kwon H-B, Wang S, Helker CS, Rasouli SJ, Maischein H-M, Offermanns S, Herzog W and Stainier DY. In vivo modulation of endothelial polarization by Apelin receptor signalling. *Nature communications*. 2016;7:11805.
327. Joberty G, Petersen C, Gao L and Macara IG. The cell-polarity protein Par6 links Par3 and atypical protein kinase C to Cdc42. *Nature cell biology*. 2000;2:531-539.
328. Lin D, Edwards AS, Fawcett JP, Mbamalu G, Scott JD and Pawson T. A mammalian PAR-3–PAR-6 complex implicated in Cdc42/Rac1 and aPKC signalling and cell polarity. *Nature cell biology*. 2000;2:540-547.
329. Palazzo AF, Joseph HL, Chen Y-J, Dujardin DL, Alberts AS, Pfister KK, Vallee RB and Gundersen GG. Cdc42, dynein, and dynactin regulate MTOC reorientation independent of Rho-regulated microtubule stabilization. *Current Biology*. 2001;11:1536-1541.
330. Orlofsky A. Positioning of the centrosome and golgi complex. *The Golgi Apparatus and Centriole: Functions, Interactions and Role in Disease*. 2019:127-200.
331. Yadav S and Linstedt AD. Golgi positioning. *Cold Spring Harbor perspectives in biology*. 2011;3:a005322.
332. Deakin NO and Turner CE. Paxillin inhibits HDAC6 to regulate microtubule acetylation, Golgi structure, and polarized migration. *Journal of Cell Biology*. 2014;206:395-413.
333. Dubois F, Alpha K and Turner CE. Paxillin regulates cell polarization and anterograde vesicle trafficking during cell migration. *Molecular Biology of the Cell*. 2017;28:3815-3831.
334. Matsuyama A, Shimazu T, Sumida Y, Saito A, Yoshimatsu Y, Seigneurin-Berny D, Osada H, Komatsu Y, Nishino N and Khochbin S. In vivo destabilization of dynamic microtubules by HDAC6-mediated deacetylation. *The EMBO journal*. 2002;21:6820-6831.
335. Weigel AV, Chang C-L, Shtengel G, Xu CS, Hoffman DP, Freeman M, Iyer N, Aaron J, Khuon S and Bogovic J. ER-to-Golgi protein delivery through an interwoven, tubular network extending from ER. *Cell*. 2021;184:2412-2429. e16.
336. Aridor M, Fish KN, Bannykh S, Weissman J, Roberts TH, Lippincott-Schwartz J and Balch WE. The Sar1 GTPase coordinates biosynthetic cargo selection with endoplasmic reticulum export site assembly. *The Journal of cell biology*. 2001;152:213-230.

337. Giraudo CG and Maccioni HJ. Endoplasmic reticulum export of glycosyltransferases depends on interaction of a cytoplasmic dibasic motif with Sar1. *Molecular biology of the Cell*. 2003;14:3753-3766.
338. Barlowe C, Orci L, Yeung T, Hosobuchi M, Hamamoto S, Salama N, Rexach MF, Ravazzola M, Amherdt M and Schekman R. COPII: a membrane coat formed by Sec proteins that drive vesicle budding from the endoplasmic reticulum. *Cell*. 1994;77:895-907.
339. Appenzeller-Herzog C and Hauri H-P. The ER-Golgi intermediate compartment (ERGIC): in search of its identity and function. *Journal of cell science*. 2006;119:2173-2183.
340. Aridor M, Bannykh SI, Rowe T and Balch WE. Sequential coupling between COPII and COPI vesicle coats in endoplasmic reticulum to Golgi transport. *The Journal of cell biology*. 1995;131:875-893.
341. Mancias JD and Goldberg J. Structural basis of cargo membrane protein discrimination by the human COPII coat machinery. *The EMBO journal*. 2008;27:2918-2928.
342. Pagano A, Letourneur F, Garcia-Estefania D, Carpentier J-L, Orci L and Paccaud J-P. Sec24 proteins and sorting at the endoplasmic reticulum. *Journal of Biological Chemistry*. 1999;274:7833-7840.
343. Tang BL, Kausalya J, Low DY, Lock ML and Hong W. A family of mammalian proteins homologous to yeast Sec24p. *Biochemical and biophysical research communications*. 1999;258:679-684.
344. Adolf F, Rhiel M, Hessling B, Gao Q, Hellwig A, Béthune J and Wieland FT. Proteomic profiling of mammalian COPII and COPI vesicles. *Cell reports*. 2019;26:250-265. e5.
345. Adolf F, Rhiel M, Reckmann I and Wieland FT. Sec24C/D-isoform-specific sorting of the preassembled ER-Golgi Q-SNARE complex. *Molecular biology of the cell*. 2016;27:2697-2707.
346. Béthune J, Kol M, Hoffmann J, Reckmann I, Brügger B and Wieland F. Coatomer, the coat protein of COPI transport vesicles, discriminates endoplasmic reticulum residents from p24 proteins. *Molecular and cellular biology*. 2006;26:8011-8021.
347. Eugster A, Frigerio G, Dale M and Duden R. The α - and β' -COP WD40 domains mediate cargo-selective interactions with distinct di-lysine motifs. *Molecular biology of the cell*. 2004;15:1011-1023.
348. Zhang G, Xu R, Heinemann SH and Hoshi T. Cysteine oxidation and rundown of large-conductance Ca²⁺-dependent K⁺ channels. *Biochemical and biophysical research communications*. 2006;342:1389-1395.
349. Tang XD, Daggett H, Hanner M, Garcia ML, McManus OB, Brot N, Weissbach H, Heinemann SH and Hoshi T. Oxidative regulation of large conductance calcium-activated potassium channels. *The Journal of general physiology*. 2001;117:253-274.
350. Belousov VV, Fradkov AF, Lukyanov KA, Staroverov DB, Shakhbazov KS, Terskikh AV and Lukyanov S. Genetically encoded fluorescent indicator for intracellular hydrogen peroxide. *Nature methods*. 2006;3:281-286.
351. Waldeck-Weiermair M, Yadav S, Spyropoulos F, Krüger C, Pandey AK and Michel T. Dissecting in vivo and in vitro redox responses using chemogenetics. *Free Radical Biology and Medicine*. 2021;177:360-369.
352. Steinhorn B, Sorrentino A, Badole S, Bogdanova Y, Belousov V and Michel T. Chemogenetic generation of hydrogen peroxide in the heart induces severe cardiac dysfunction. *Nature communications*. 2018;9:1-10.

353. Sorrentino A, Steinhorn B, Troncione L, Saravi SSS, Badole S, Eroglu E, Kijewski MF, Divakaran S, Di Carli M and Michel T. Reversal of heart failure in a chemogenetic model of persistent cardiac redox stress. *American Journal of Physiology-Heart and Circulatory Physiology*. 2019;317:H617-H626.